PROCESSES CONTROLLING THE FATE AND TRANSPORT OF TRACE METALS IN THE SUBSURFACE DURING CHANGING REDOX POTENTIAL

Thesis by

Claire Farnsworth

In Partial Fulfillment of the Requirements

for the Degree of

Doctor of Philosophy

CALIFORNIA INSTITUTE OF TECHNOLOGY

Pasadena, California

2011

(Defended May 10, 2011)

Acknowledgements

First and foremost, I must thank Janet Hering, my advisor. I'm especially grateful for her editorial standards, financial and personal support, career guidance, and her invitation to move to Eawag. I attribute much of my personal growth over the course of my graduate work either directly or indirectly to Janet.

Jess Adkins, Michael Hoffmann, and Victoria Orphan have been supportive committee members from afar. Jim Morgan pointed me in the right direction towards some key papers and concepts early in my graduate work.

Rich Wildman became my unofficial graduate school mentor. From the shores of Lake Powell to the shores of Greifensee, Rich's enthusiasm and unwavering support gave me confidence and kept me going in the tough times. I thank both Rich and his wife, Zena Harris, for being my "training wheels" in Zürich. Vanessa Sternitzke listened to far more details of uncooperative Mn-oxidizing bacteria than any person should have to and made sure that I saw a bit of Switzerland as long as I was there. I would not have survived this Ph.D. without her patient friendship and our hiking adventures. Kate Campbell introduced me to gels and manganese in the lab. The consummate professional, it took me a couple of months to realize that she didn't already know the results of my doped-gel experiments.

I must acknowledge technical support from Nathan Dalleska at Caltech and Thomas Ruettimann, Caroline Stengel, Hermann Moench, Lisa Salhi, and Brian Sinnet at Eawag. Ich danke der Hydrogeologie-Gruppe des Freie Universität Berlins, namentlich Gudrun Massmann, Christian Menz, und Thomas Taute, für die gute Zusammenarbeit

beim Tegeler See. Sarah Griffis worked hard and asked good questions, besides getting in Lake Tegel on a cold day in July. I'm grateful to my microbiologist collaborators: Dianne Newman's group at Caltech, especially Alexa Price-Whelan and Yun Wang; Colleen Hansel's group at Harvard, especially Derek Learman and Cara Santelli; and Frederik Hammes, Hans-Ulrich Weilenmann, Karin Lautenschlager, and Johannes Wolf at Eawag. Andreas Voegelin performed all XAS sampling and analysis, and maintained good spirits throughout the long hours at the beamline.

Stephan Hug kindly let me be an unofficial member of his research group at Eawag. Edi Hoehn spent a full morning discussing bank filtration with me at the original Glattfelden site, and suggested collaboration with Gudrun Massmann. Peggy O'Day, Lars Maechler, and Matthias Brennwald had some key input in the initial design of my column experiments. Linda Roberts, Helen Rowland, Benoit Pernet-Codrier, Lenny Winkel, and Christine Wenk offered helpful discussions and friendship at Eawag. Megan Ferguson, Arthur Fitzmaurice, Azra Bilgin, Tom He, Diana Stefanescu, and Tao Cheng created a pleasant working group at Caltech. Maria Luisa Ruiz-Ripoll, Cristina Mojica, Yvonne Chen, and Katie Cychosz have provided six years' worth of graduate school sympathy and career advice. I'm grateful for Kathleen Wyss-Shore's professional guidance when I most needed it.

I credit Dan Giammar and Liyun Xie of the Aquatic Chemistry Lab at Washington University in St. Louis with teaching me good basic laboratory skills and making my enthusiasm for science productive. Jeanne Dalton taught me redox chemistry at St. Pius X Catholic High School, and her A.P. chemistry course, which presented us

with general hypotheses to be tested rather than explicit laboratory instructions, gave me my first taste in designing and executing chemistry experiments.

Finally, I would like to thank my parents, who have supported my intellectual pursuits, even as they take me further and further from home, and my siblings, who never cease to find ways to humble me, often in song. I must especially thank my grandparents, Sam and Carolyn Magruder, whose financial support during my Bachelor's studies started me on this path. I hope you agree it was a pretty good investment.

Abstract

This study investigated the cycling of Mn and Fe as oxic surface water entered shallow sediments and was reduced, and as reduced groundwater became exposed to oxygen and was oxidized. A Mn-oxide doped gel probe sampler was developed to study *in situ* rates of reductive dissolution and was validated with laboratory studies with ascorbic acid and *Shewanella oneidensis* MR-1 as model reductants. The sampler was deployed in the bank sediments of Lake Tegel, Berlin, Germany. Modeling of the diffusion-controlled reaction converted the mass loss from the gels in the sampler to a profile of pseudo-first-order rate constants as a function of depth. The rate constants were highest at depths with high dissolved Fe and low operationally defined fractions of reducible oxides of Fe and Mn in the sediments.

A laboratory column experiment showed that 1.3-m water table fluctuations, as observed in bank filtration sites around Berlin, were able to provide sufficient dissolved oxygen delivery for *Pseudomonas putida* GB-1, an obligate aerobe, to oxidize Mn(II) *in situ*. Accumulation of Mn on the quartz sand in the column at the end of the experiment was limited to the top 60 cm, as measured with X-ray fluorescence (XRF), and X-ray absorption spectroscopy (XAS) analysis confirmed that the solid formed was a Mn(IV) oxide characteristic of biogenic origin. After a period of "filter ripening" in the column, rates of *in situ* oxidation were still lower than rates in engineered aerated sand filters.

Adjacent to a production well with a water table that fluctuates up to 7 m annually at Lake Tegel, however, sediments collected from a borehole did not show any significant accumulation of Mn or Fe with depth, as measured by XRF; analysis of the

speciation of Mn and Fe in the solid phase by XAS suggested a slight increase in the proportions of total Mn as Mn(II) and of total Fe as Fe(II) with depth. At this location, vertical zonation of groundwater may preclude the co-occurrence of reduced Mn and Fe with dissolved oxygen entrapped by water table fluctuations. Whether groundwater changes from oxidizing to reducing conditions or vice versa, the behavior of Mn and Fe reflects a complex interaction between sediments, solutes, microbial activity, and hydrology.

TABLE OF CONTENTS

Acknowledgements iii
Abstract vi
Table of Contents viii
List of Figures x
List of Tables xiii

Chapter 1: Introduction 1-1

Chapter 2: Inorganic Geochemistry and Redox Dynamics in Bank Filtration Settings 2-1
Abstract 2-1
Introduction 2-2
Geochemistry of Bank Filtration 2-6
Reduction near the bank 2-9
Oxidation near the production well 2-12
Dissolution of carbonate minerals in the aquifer 2-15
Sorption in the aquifer 2-19

Chapter 3: A Hydrous Manganese Oxide Doped Gel Probe Sampler for Measuring *In Situ* Reductive Dissolution Rates: I. Laboratory Development 3-1
Abstract 3-1
Introduction 3-2
Experimental Section 3-4
Results 3-11
Discussion 3-16
Acknowledgements 3-21

Chapter 4: A Hydrous Manganese Oxide Doped Gel Probe Sampler for Measuring *In Situ* Reductive Dissolution Rates: II. Field Deployment 4-1
Abstract 4-1
Introduction 4-2
Materials and Methods 4-4
Results 4-10
Discussion 4-15
Acknowledgements 4-21

Chapter 5: Manganese Oxidation Induced by Water Table Fluctuations in a Sand Column 5-1
Abstract 5-1

Introduction 5-2
Experimental Section 5-3
Results and Discussion 5-10
Acknowledgements 5-21

Chapter 6: Mn and Fe Dynamics in the Shallow Groundwater Adjacent to Lake Tegel, Berlin, Germany 6-1
Abstract 6-1
Introduction 6-2
Experimental Section 6-3
Results and Discussion 6-6
Acknowledgements 6-15

Chapter 7: Conclusions 7-1
Summary 7-1
In Situ Rates of Reductive Dissolution 7-1
Oxidizing Conditions Induced by Water Table Oscillations 7-5
Field Conditions Necessary for *In Situ* Mn and Fe Oxidation 7-6
Future Research in Inorganic Geochemistry Relevant to Bank Filtration 7-7
Wider Implications 7-11

Appendix A: Supporting Information for Chapter 3 ..... A-1
Appendix B: Supporting Information for Chapter 4 ..... B-1
Appendix C: Supporting Information for Chapter 5 ..... C-1
References R-1

LIST OF FIGURES

Figure ***Page Number***

2.1 Schematics of various types of managed aquifer recharge 2-4

2.2 Profile of geochemical changes along a natural and bank filtration flow path 2-7

2.3 pe-pH predominance plot for Fe and Mn under typical pH and redox conditions for groundwater 2-9

2.4 Soluble metal concentrations in equilibrium with calcite and metal carbonates 2-18

3.1 Integrated expression for the rate of Mn release as a function of time at pH 8.0 3-13

3.2 1-D model output of Mn(II) accumulation in the bulk solution 3-16

4.1 Location of sampling site at Lake Tegel 4-5

4.2 Porewater concentrations of dissolved Mn and Fe and apparent pseudo-first-order rate coefficient k′ 4-12

4.3 Total extracted Mn and Fe from sediment cores in sequential extraction 4-13

4.4 Mn and Fe concentrations measured in sediments, expressed as percentage of the total elemental concentration recovered in all 5 sequential extraction steps 4-14

5.1 Changes in the visible water level in the column, the effluent dissolved oxygen, and filtered relative effluent concentrations of Mn and Zn over time 5-11

5.2 XRF profile of Mn and Zn along the column at the end of the experiment..... 5-15

6.1 Map of sampling locations and bank filtration well galleries at Lake Tegel 6-4

6.2 XRF concentrations of Mn and Fe as a function of depth in the aquifer 6-8

6.3 Mn sorption isotherm on aquifer sediments 6-9

6.4 Mn K-edge XANES spectra of Lake Tegel aquifer samples from different depths compared to reference spectra 6-11

6.5 Fe K-edge XANES and EXAFS spectra of Lake Tegel aquifer samples from different depths compared to reference spectra 6-12

A.1 X-ray diffractogram for synthesized HMO A-2

A.2 AQUASIM model output for the reaction of ascorbate and HMO-doped gels in gels A-7

A.3 AQUASIM model output for the reaction of ascorbate and HMO-doped gels in a miniprobe A-8

A.4 AQUASIM model output for the reaction of *S. oneidensis* MR-1 and HMO-doped gels in solution A-9

A.5 AQUASIM model output for the reaction of *S. oneidensis* MR-1 and HMO-doped gels in a miniprobe A-10

A.6 Theoretical behavior of Mn reduction in an HMO-doped gel, in the absence of diffusion A-11

A.7 Rate estimates as a function of time for the reaction of *S. oneidensis* MR-1 and HMO-doped gels in miniprobes A-12

A.8 Comparison of Mn concentrations measured in clear gels deployed in the same probe as HMO-doped gels and in a separate gel probe 85 cm away A-13

B.1 Moles of HMO lost in each gel per s of deployment time B-4

B.2 Extracted Mn and Fe concentrations per kg dry sediment, as determined by sequential extraction B-5

B.3 Particle size in Lake Tegel shoreline sediment B-5

B.4 Dissolved Mn and Mn oxide inside of a gel, as calculated by the Matlab m-file “ksolver” B-10

B.5 Apparent pseudo-first-order rate coefficient k′ from HMO-doped gel probe deployed 20 m from the shoreline of Lake Tegel, Berlin, Germany B-11

B.6 Apparent pseudo-first-order rate coefficient k′ from HMO-doped gel probe deployed at Laguna Figueroa salt flats, Baja California, Mexico B-12

C.1 Schematic and photo of the column set up C-2

C.2 Filtered relative effluent concentrations of Br C-4

C.3 Mn XANES and EXAFS spectra at the top of the sand column C-5

C.4 XRF profile of P at the end of the experiment C-7

C.5 Mass balance for unreacted gels and batches at the end of the reduction assay C-8

C.6 Effluent pH measured directly at the base of the column C-9

LIST OF TABLES

Table ***Page Number***

3.1 Summary of linear regression data for laboratory-measured rates of reductive dissolution 3-14

3.2 Summary of literature values for Mn oxide reduction by *S. oneidensis* MR-1 3-19

4.1 Experimental conditions for sequential extraction 4-10

4.2 Surface-area-normalized Mn reduction rates from field studies 4-17

4.3 Summary of literature values for Mn oxide reduction rate coefficients 4-19

5.1 Mn removal parameters for each water table oscillation 5-12

5.2 Potential rates of Mn oxidation and reduction in the column 5-18

6.1 Composition of artificial groundwater for sorption experiments 6-6

6.2 Average groundwater composition in production well 18 6-10

A.1 Final mass balance in abiotic miniprobe reductive dissolution experiments A-2

A.2 Basic components of MR-1 minimal medium A-3

A.3 Parameters input to or solved by AQUASIM model A-4

A.4 AQUASIM mass balance at steady state A-5

A.5 [Mn(II)] release over time A-6

A.6 Bias of clear gels co-located in the same miniprobe as HMO-doped gels A-13

B.1 Lake Tegel sediment characterization B-3

B.2 Porewater concentrations of detectable trace elements B-4

B.3 Calculation of surface-area-normalized Mn reduction rates from field studies B-6

B.4 Gel probe data input to Matlab m-file “ksolver” and output k′ values B-13

B.5 Sequential extraction fractions of Mn (mg kg^{-1}) B-14

B.6 Sequential extraction fractions of Fe (mg kg^{-1}) B-14

C.1 Results of oxidation assays at the end of the column experiment.....C-2

C.2 Linear combination fit results for Mn XANES and EXAFS spectra at the top of the sand column C-6

C.3 Pseudo-first-order rate coefficients for Mn oxide reduction and OD_{600} during the reduction assay C-7

C.4 Observed levels of water table during experiment C-12

C.5 Dissolved oxygen concentrations in the column effluent C-13

C.6 pH values in the column effluent C-14

C.7 Mn C/C_0 values in the column effluent C-15

C.8 Zn C/C_0 values in the column effluent C-16

C.9 XRF concentrations of Mn and Zn in the column at the end of the experiment C-17

Chapter 1

Introduction

Population growth and expansion of irrigated agriculture put increasing demands on current water resources management. Combined with anticipated increases in the frequency and intensity of drought and precipitation due to climate change, these pressures may render existing surface water storage insufficient (Barnett and Pierce 2008), if not impractical in arid and semi-arid areas subject to lower streamflows and excessive evaporation (Gleick 2002, Brikowski 2008). Alternative water resources management, if able to take advantage of water reuse and to reduce the capital- and energy-intensity of water treatment, promises to improve sustainability and reliability in light of these pressures.

One form of alternative water resources management with a long history in Europe is bank filtration. In this system, groundwater is extracted from a well adjacent to a river or lake, thereby inducing infiltration from the surface water body into the shallow groundwater. The natural processes along the infiltration flow path lead to nutrient, organic carbon, and pathogen removal, thereby improving the quality of the water recovered (Schwarzenbach et al. 1983, Dillon 2005). Active in some locations for more than 100 years (Eckert and Irmscher 2006), current estimates suggest that 27 million people, approximately 23% of the population, in Slovakia, Hungary, Germany,

Switzerland, and the Netherlands rely on bank filtration for their drinking water supply (Hiscock and Grischek 2002).

An operational limitation of bank filtration is the release of iron (Fe) and manganese (Mn) as the infiltrating water passes from oxic to reducing conditions in the river- or lake-bank. High concentrations of Fe and/or Mn often necessitate post-extraction treatment in bank filtration sites in Germany (Massmann et al. 2008b), the Netherlands (de Vet et al. 2010), and Canada (Petrunic et al. 2005). However, re-introduction of dissolved oxygen to the shallow groundwater along the infiltration path could potentially precipitate Fe and Mn oxides *in situ*. Furthermore, the stability of Fe and Mn oxides is known to control the release of other trace metals in groundwater (Davranche and Bollinger 2000). A bank filtration site in Berlin, Germany, with Fe and Mn concentrations above WHO guidelines (5 μM and 2 μM, respectively) was selected to study the processes controlling these two key trace metals in further detail.

Scope and Objectives

The objective of this research is to quantify the rates and mechanisms controlling Fe and Mn behavior in bank filtration systems. Specifically, it will address the following questions:

- How do the rates of reductive dissolution, the predominant mobilization pathway for Fe and Mn, vary with depth in the bank sediments?
- Do water table fluctuations in the vicinity of the production wells provide sufficient dissolved oxygen to enable *in situ* Mn oxidation?

- What ambient conditions lead to the presence or absence of significant *in situ* Mn and Fe oxidation?

A critical review of the inorganic geochemistry of bank filtration systems, in light of the relevant physical and transport processes, is presented in Chapter 2. This chapter, along with an additional section in Chapter 7 on future research needs, has been submitted to *Environmental Science and Technology* for publication. A Mn-oxide-doped gel probe sampler was developed to measure *in situ* rates of reductive dissolution in shallow (< 50 cm) sediments. The laboratory development of this method, including experiments with model reductants (ascorbic acid and *Shewanella oneidensis* MR-1) and modeling to account for diffusion, is presented in Chapter 3. Gel probes were deployed in the sediments of Lake Tegel (Berlin, Germany) in July, and in Chapter 4, the subsequent reductive dissolution rates were paired with sequential extraction of nearby sediment cores to understand the relevant diagenetic processes in this setting. Chapters 3 and 4 were published as companion papers in *Environmental Science and Technology* in January 2010.

Anoxic microbial medium was flowed through a quartz-sand-filled column inoculated with *Pseudomonas putida* GB-1 (a well-characterized Mn oxidizing bacterium) and subjected to 1.3 m water level changes every 30–50 h for 600 h. The frequency and amplitude of the water level fluctuations, as well as the flow conditions, were designed to simulate the conditions present in the shallow groundwater at the Lake Tegel bank filtration site. Analysis of the Mn removal rates in the column and the solid-phase Mn at the end of the experiment are detailed in Chapter 5. Aquifer sediments up to 25 m depth were collected during the drilling of a borehole 3 m away from a production well at Lake

Tegel. In Chapter 6, the results the solid-phase characterization for Mn and Fe are discussed in terms of the general conditions necessary for *in situ* Mn and Fe accumulations in bank filtration settings. Chapter 7 presents the conclusions of this work, including further commentary on Chapters 3 and 4 in light of more recent publications, and a section on future research needs in bank filtration settings. Additional field and experimental data can be found in the appendices; data are organized such that Appendices A, B, and C provide supporting information for Chapters 3, 4, and 5, respectively.

Chapter 2

Inorganic Geochemistry and Redox Dynamics in Bank Filtration Settings

Abstract

Bank filtration induces flow of surface water through a hydraulically connected aquifer by excess pumping from a production well in the aquifer. This chapter presents the four main geochemical processes relevant for inorganic geochemistry, with a focus on iron (Fe) and manganese (Mn), during bank filtration: reduction near the bank, oxidation near the production well, carbonate dissolution, and sorption to aquifer materials. Physical and transport processes affect these geochemical processes and influence the redox state of the infiltrate. The presence of Fe and Mn in bank infiltrate is directly related to its redox status and can necessitate drinking water treatment after extraction. Long-term, *in situ* sequestration of Fe and Mn requires precipitation of oxide or carbonate solids, since a sorption front can break through at the production well.

Introduction

Anthropogenic pressure on existing water resources management is growing due to population growth and the expansion of irrigated agriculture and may be exacerbated by climate change. The frequency and intensity of both drought and precipitation are anticipated to increase as a result of climate change; glaciers are already retreating. In the western U.S., observations over the past 50 years include more winter precipitation falling as rain instead of snow, earlier snow melt, and associated changes in river flow, as well as drier summer conditions due to regional warming (Barnett et al. 2008). Major Asian river basins that depend on glacial melt water are also susceptible to altered, and eventually decreased, flows as glaciers retreat and disappear (Immerzeel et al. 2010). Episodic groundwater recharge may also be significantly impacted by changes in precipitation events (Eckhardt and Ulbrich 2003, Ng et al. 2010). Population growth continues in areas of limited water resources (NRC 2008, Vorosmarty et al. 2010), and overdraft of groundwater, both seasonal and year-round, is a more and more common problem (Wada et al. 2010). In some coastal areas, existing use of groundwater resources has had to be curtailed or modified due to saltwater intrusion (Jha and Peiffer 2005, Brown and Misut 2010). Expansion of irrigated agriculture to feed burgeoning populations will further stress limited water resources; northern China, for example, contains 65% of the country's arable land, but only 18% of its water resources (Piao et al. 2010).

As a result of these pressures, water shortage is forecast for 36% of the global population by 2050 under a climate change and population growth scenario (Rockström et al. 2009). Moreover, 80% of the world's population would currently be exposed to

high levels of threat to water security if not for massive investments in water infrastructure in developed countries (Vorosmarty et al. 2010). The lower Colorado River basin may already be in overdraft, as inflows have decreased to Lakes Powell and Mead while outflows from Glen Canyon and Hoover Dams continue at legally mandated rates (Barnett and Pierce 2008). Indeed, surface water storage may become impractical in arid and semi-arid areas due to lower streamflows and excessive evaporation (Bouwer 2002, Brikowski 2008). In addition, it is estimated that 1 billion people still lack access to safe drinking water, and in the developing world, the cost of building and maintaining conventional water and wastewater treatment can be prohibitive (Buros and Pyne 1994). Clearly, demand exists for more water management in the coming decades, but existing large-scale dam and irrigation projects may be unable to provide adequate water resources under the increasing anthropogenic pressure (Gleick 2002). Therefore, alternate water management schemes are necessary to take increasing advantage of water reuse and to reduce the capital- and energy-intensity of water treatment systems.

Many of these alternate management schemes fall under heading of "managed aquifer recharge" (MAR) or "managed underground storage". Forms of MAR involve engineered delivery of water into the subsurface, which is later recovered after some storage and passage through aquifer material (Figure 2.1). Delivery modes can range from direct injection to passive spreading ponds, and the quality of the water delivered to the recharge systems can range from ambient surface water to wastewater treatment plant effluent (Bouwer 2002). Aquifer storage and recovery (ASR) and aquifer storage transfer and recovery (ASTR) inject water directly into an aquifer for storage. In ASR, essentially the same parcel is later recovered from the injection well itself. In ASTR, water is

recovered from a down-gradient well and can, at early recovery times, include a substantial component of the native groundwater. Infiltration ponds are usually constructed off-stream where surface water is diverted and allowed to infiltrate (generally through an unsaturated zone) to an underlying unconfined aquifer. In soil-aquifer treatment (SAT), treated sewage effluent, or reclaimed water, is infiltrated intermittently through infiltration ponds to facilitate nutrient and pathogen removal in passage through the unsaturated zone for recovery by wells after residence in the aquifer. Bank filtration refers to extraction of groundwater from a well or caisson near or under a river or lake, which induces infiltration from the surface water body, thereby improving and making more consistent the quality of water recovered (NRC 2008).

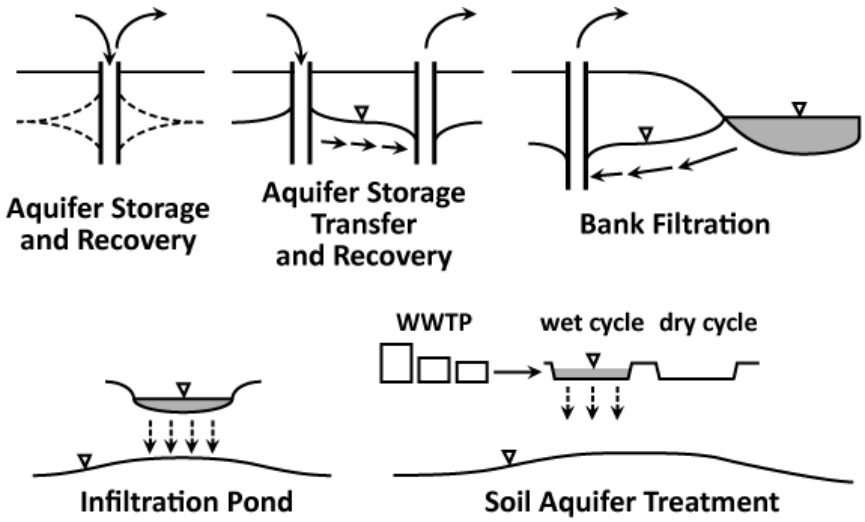

Figure 2.1. Schematics of various types of managed aquifer recharge. Adapted from Dillon (2005). WWTP denotes a wastewater treatment plant.

In contrast with some MAR schemes, bank filtration has a long history in Europe, with some sites in use for more than 130 years in Germany (Ziegler 2001, Eckert and Irmscher 2006). Bank filtration relies upon natural processes to remove nutrients,

organic carbon, and microbes, especially pathogens, present in the source water (Schwarzenbach et al. 1983). Recent research in bank filtration settings has focused extensively on understanding the processes behind effective pathogen removal (Castro and Tufenkji 2008, Metge et al. 2010, Toze et al. 2010) and on quantifying the removal of persistent organic micropollutants (Massmann et al. 2008a, Hoppe-Jones et al. 2010), both of which are critical to determine the post-extraction treatment required for bank filtrate to meet water quality standards. The effects of inorganic geochemical processes along the infiltration flow path on the quality of extracted bank filtrate have received much less attention, despite the observed exceedance of WHO drinking water guidelines for iron (Fe) of 0.3 mg l^{-1} or 5 μM and manganese (Mn) of 0.1 mg l^{-1} or 2 μM at various well fields in Canada (Thomas et al. 1994), Germany (Hässelbarth and Lüdemann 1972), and the Netherlands (de Vet et al. 2010). Although the treatment to remove Fe and Mn is relatively simple in practice (often aeration and sand filtration (de Vet et al. 2010)), the presence of these elements can lead to well screen clogging (van Beek 1984, van Beek et al. 2009) and can also indicate conditions where trace metals associated with Fe and Mn oxide solids are released along the flow path (von Gunten and Kull 1986). Thus, *in situ* sequestration of Fe and Mn could potentially decrease both the risk of breakthrough of Fe, Mn, and any associated trace metals at the extraction well and the need for post-extraction treatment. If the sequestration occurs at some distance from the well screen, this could also decrease the likelihood of well clogging.

Both reductive dissolution of Fe and Mn oxides and subsequent sequestration of dissolved Fe and Mn in bank filtration are dependent upon the spatial and temporal variation of the redox state along the flow path. Furthermore, transient redox conditions

can be significant for inorganic geochemistry and pathogen and organic micropollutant removal alike (von Gunten et al. 1991, Castro and Tufenkji 2008, Massmann et al. 2008b). This review presents the fundamental geochemical processes of bank filtration systems, with a focus on Fe and Mn, in light of relevant physical and transport processes.

Geochemistry of Bank Filtration

The evolution of groundwater along the infiltration flow path in bank filtration involves four key geochemical processes that can affect the efficiency of the system as well as the quality of the extracted water: reduction near the bank, oxidation near the production well, dissolution of carbonate minerals in the aquifer, and sorption-desorption to the aquifer material (Figure 2.2). These processes are also relevant in other MAR schemes, but specific aspects of other forms of MAR are not considered here.

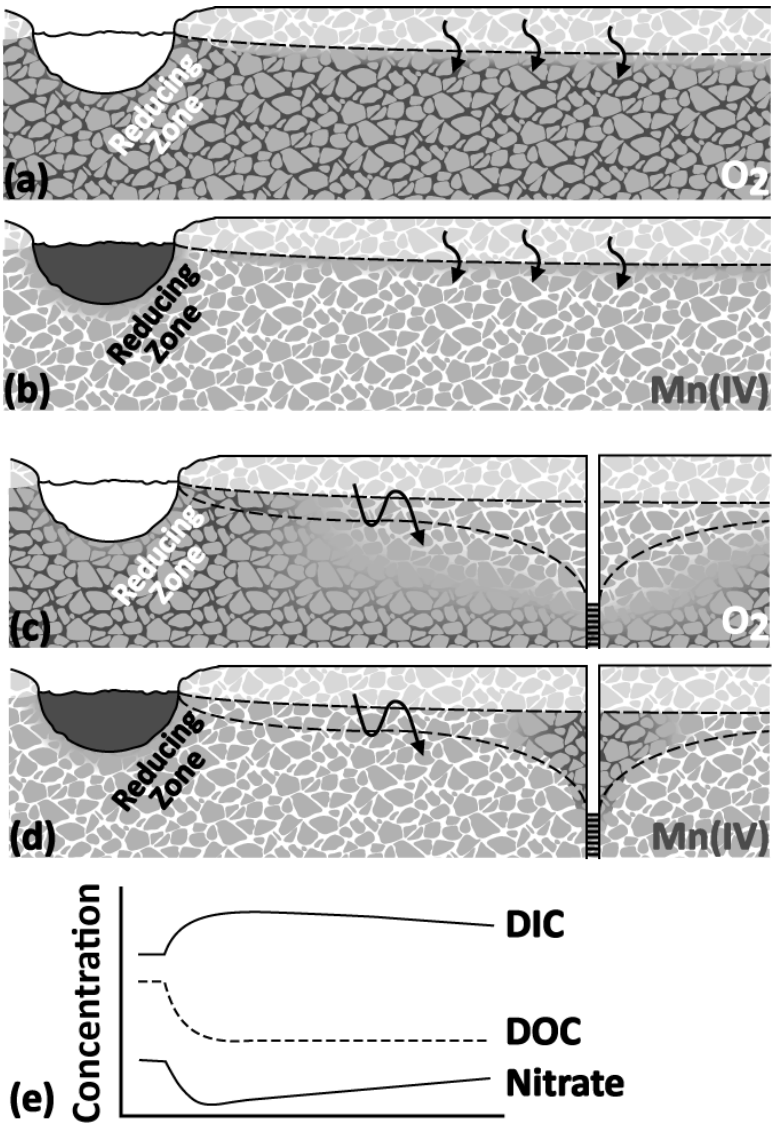

Figure 2.2. Profile of geochemical changes along a natural (a,b) and bank filtration (c,d) flow path. Dissolved oxygen levels are indicated by white (a,c), and oxidized Mn by dark grey (b,d). Arrows indicate the dominant mechanisms of reaeration: diffusion and rain infiltration under natural conditions and water table oscillations during bank filtration. The relative concentration profiles of dissolved inorganic carbon (DIC), dissolved organic carbon (DOC), and nitrate in bank filtration are shown in (e) after Bourg and Bertin (1993).

Bank filtration settings generally have different flow conditions than natural riverbank settings. A natural riverbank may be gaining or losing, relative to the adjacent aquifer, but bank filtration induces losing conditions. Furthermore, a bank filtration

well's cone of depression draws down the water table, sometimes as far as to the bank itself (Massmann and Sültenfuß 2008), and on-off cycles of the production well cause oscillations of the water table (Figure 2.2), which affects oxygen delivery to the infiltrate (Kohfahl et al. 2009). Bank filtration wells may additionally induce native groundwater, which would not normally interact with surface water, to mix with infiltrate in or near the production well. This can help dilute and buffer concentrations in the infiltrate (Schubert 2002), or it can lead to undesirable geochemical processes such as Fe or Mn precipitation in production well screens (van Beek et al. 2009).

Fe and Mn are used to illustrate the geochemical processes below. Briefly, Mn has three common oxidation states in the environment (+II, +III, and +IV), and Fe has two (+II and +III) (Figure 2.3). Fe(II) and Mn(II) are soluble at low-to-neutral pH, and precipitate as $Fe(OH)_2$ (s) and $Mn(OH)_2$ (s), respectively, at very alkaline pH values (e.g., higher than pH 9 in Figure 2.3). Depending on the carbonate concentrations, which can be elevated in the subsurface, Fe(II) and Mn(II) can precipitate as siderite ($FeCO_3$) and rhodochrosite ($MnCO_3$). Mn(III) and Mn(IV) are largely insoluble, found most frequently in Mn oxides and oxyhydroxides such as birnessite ($K(Mn^{3+},Mn^{4+})_2O_4 \cdot 1.5H_2O$), pyrolusite ($MnO_2$), hausmannite ($Mn_3O_4$), and manganite (MnOOH) (Post 1999). Fe(III) is also largely found in insoluble oxides and oxyhydroxides, which are stable under more reducing conditions than those of Mn(III/IV) (Figure 2.3). Reductive dissolution of Fe and Mn oxides is largely microbially mediated (Lovley 1991, Lloyd 2003), and oxidative precipitation of Fe(II) and Mn(II) can be as well (Corstjens et al. 1992, Tebo et al. 2004). Although kinetics of abiotic Fe(II) oxidation by oxygen are relatively rapid at circumneutral pH, Mn oxidation is slow below

pH 9 (Morgan 2005), with abiotic Mn oxidation orders of magnitude slower than microbially Mn oxidation (Hastings and Emerson 1986, Davies and Morgan 1989, Luther 2005). Recent studies of microbially-mediated Mn oxidation have suggested that the majority of naturally-occurring environmental Mn oxides are derived either from direct biogenic Mn(II) oxidation or from the subsequent alteration of biogenic oxides (Tebo et al. 2004).

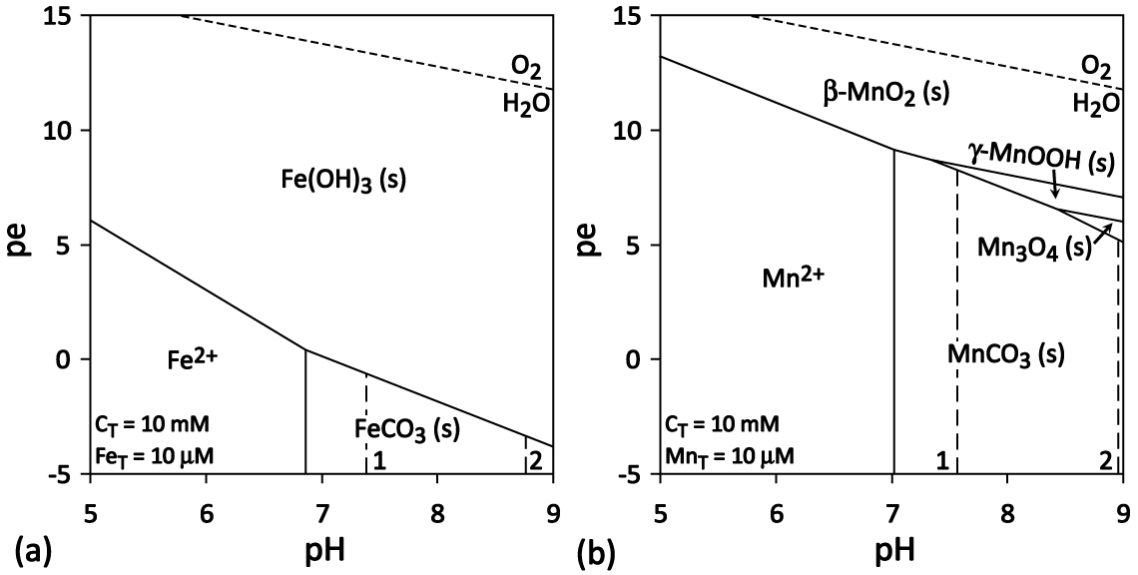

Figure 2.3. pe-pH predominance plot for (a) Fe (total = 10 µM) and (b) Mn (total = 10 µM) under typical pH and redox conditions for groundwater (C_T = 10 mM). Dashed vertical lines show the (a) Fe^{2+}/ $FeCO_3$ (s) and (b) Mn^{2+}/ $MnCO_3$ (s) equilibria for (1) C_T = 5 mM, Mn_T = Fe_T = 5 µM, and (2) C_T = 1 mM, Mn_T = Fe_T = 1 µM. Concentration changes slightly expand the γ-MnOOH (s) and Mn_3O_4 (s) predominance areas to lower pe and pH (not shown).

Reduction near the bank

Reducing conditions near the bank have been documented in many field sites (Jacobs et al. 1988, Bourg and Bertin 1993, Thomas et al. 1994, Massmann et al. 2008b). The influx of organic carbon from the overlying body of water into shallow sediments drives

sufficient microbial activity to exhaust the supply of oxygen and often nitrate, leading to the reductive dissolution of Mn and Fe oxides (Berner 1980). Seasonal variation in the organic carbon load to the sediments correlates with the extent of reduction in the groundwater. Higher surface water temperatures in the summer lead to increased algal and phytoplankton growth, which yield higher summer loads of dissolved organic carbon. Secondary to these higher loads are increases in microbial respiration rate in the shallow sediments due to higher summer temperatures; this temperature signal is, however, damped as the infiltrate travels along the flow path (Greskowiak et al. 2006). These seasonal effects lead to a greater extent of reducing conditions as compared to the winter (von Gunten and Kull 1986, von Gunten et al. 1991, Bourg and Richard-Raymond 1994, Hoffmann and Gunkel 2011a). Solid organic carbon in the aquifer sediments can additionally promote reduction of oxygen, nitrate, and Mn oxides further along the flow path (Kedziorek et al. 2008).

On one hand, bank filtration is effective precisely because much of the organic carbon from the surface water is oxidized in the sediments and removed from the bank filtrate. At Lake Tegel in Berlin, bank filtration eliminates 20–45% of the dissolved organic carbon present in the surface water (Ziegler 2001, Hoffmann and Gunkel 2011a). Included in the dissolved organic carbon load are trace organic pollutants that persist through upstream wastewater treatment. Removal of any of these trace compounds in bank filtration is an added benefit. On the other hand, some trace organic compounds are only minimally removed under reducing conditions. Organic micropollutant removal at bank filtration sites has been studied extensively elsewhere (Schwarzenbach et al. 1983, Massmann et al. 2006, Massmann et al. 2008a, Hoppe-Jones et al. 2010).

The increase of the biomass of microbes that actively oxidize organic carbon can negatively impact the hydrologic properties of a bank filtration system. Microbial overgrowth leads to a clogged layer, especially in settings that are relatively stagnant compared to riverbanks. The development of a clogged layer at the bottom of an artificial recharge pond in Berlin caused a decrease in infiltration rate of one order of magnitude, at which point the layer was mechanically removed (Greskowiak et al. 2005). In a more natural lake bank filtration setting, the clogging layer cannot be removed. At Lake Tegel in Berlin, long-term pore water velocities were the same order of magnitude as the minimum at the above artificial recharge pond (Hoffmann and Gunkel 2011b). A significant portion of the pore volume of the shallow sediments was filled with algae, which occurred at concentrations nearly 1000× that in the overlying lake water (Gunkel and Hoffmann 2005). Nevertheless, transport through the clogged sands at the lake margins accounts for the majority of the bank filtrate in this site, so this issue is not likely to be prohibitive.

The other half of the redox reactions is also significant. Coupled to the oxidation of organic carbon, microbial reduction of nitrate in bank filtration systems is a distinct asset, whereas reduction of Mn and Fe oxides can be problematic. Nitrate reduction to N_2 (the most common end product) decreases the nutrient load in the infiltrate (Doussan et al. 1997, Doussan et al. 1998). Mn- and Fe-oxide reduction result instead from interactions between microbes and the native sediments at the site (Lovley 1991, Lloyd 2003). Significant overlap in enzymatic activities exists within microbial populations such that microbes able to reduce Mn oxides are often also capable of Fe oxide reduction (Beliaev and Saffarini 1998), and those rates of reduction are quite comparable (Blakeney

et al. 2000, Ruebush et al. 2006). Mineralogy plays a key role in both the reactivity (Burdige et al. 1992, Ruebush et al. 2006) and the sorption capacity (Post 1999) of Fe and Mn oxides; more crystalline solids are less reactive and have lower sorption capacities.

When solid-phase oxides in the sediments are reductively dissolved, Fe and Mn are released to sediment porewater. High levels of dissolved Fe and Mn in bank filtrate can be problematic in and of themselves (Thomas et al. 1994, Petrunic et al. 2005), but both Mn and Fe oxides are major sinks for trace metals (Lovley 1991), and sorbed metals are released to solution during their reduction (Davranche and Bollinger 2000). This was observed for Cd, Cr, Cu, Pb, U, and Zn, as well as phosphate, at the Glatt River site (von Gunten and Kull 1986, Jacobs et al. 1988, von Gunten et al. 1991, Lienert et al. 1994). Subsequent reduction in the P concentration in sewage effluent, as required by regulations, resulted in lower levels of eutrophication in the surface water of the Glatt, effectively decreasing the organic carbon load in both the river and the bank filtrate. The decreased organic carbon load no longer supported extensive Fe- and Mn-oxide reduction, and dissolved metal concentrations were no longer elevated (Lienert et al. 1994), which illustrates the direct and indirect impacts of the reductive dissolution of Fe and Mn oxides on the quality of bank filtrate.

Oxidation near the production well

Along the flow path from the reducing zone near the bank to the production well, air reenters the water and can restore oxic conditions in the shallow infiltrate. Three main pathways for oxygen entry to the shallow groundwater are often considered: diffusive flux from the overlying unsaturated zone, vertical infiltration of oxic rain water, and gas

entrapment due to water table oscillations (i.e., induced by intermittent production-well use). Modeling at Lake Wann (Berlin, Germany) clearly indicated that the dominant reaeration pathway was gas entrapment due to water table oscillations, once oscillations were greater than 0.5 m (Kohfahl et al. 2009). Laboratory studies predict dissolved gas saturation in excess of air equilibrium when gas bubbles are entrapped and collapse under sufficient water pressure; subsequent water table oscillations induce downward propagation of this "excess air" (Williams and Oostrom 2000). Excess air has been observed in the shallow groundwater of Berlin's bank filtration sites (Massmann and Sültenfuß 2008), in support of the laboratory and model results. The generalized dissolved oxygen profile for bank filtration sites in Figure 2.2c reflects the reaeration of bank filtrate as the production well is turned on and off, especially in the vicinity of the cone of depression. In the winter, lateral infiltration of oxic surface water through the banks is an additional reaeration pathway as the extent of the near-bank reducing zone is limited by lower organic carbon loads and lower microbial respiration rates and dissolved oxygen solubility is higher (von Gunten et al. 1991, Massmann et al. 2008b). Thus, reaeration of the infiltrate is heavily influenced by the production well pump operation, seasonal nutrient loads, and temperature.

The oxic zone near to the production well has significant implications. Dissolved Mn and Fe from the reducing zone may precipitate as oxides in the presence of oxygen. In Figure 2.2, the spatial extent of Fe oxidation would be expected to align more closely with the oxygen profile (Figure 2.2c) rather than the Mn profile (Figure 2.2d) due to the rapid oxidation kinetics of Fe(II) (Luther 2005) and its potential (microbially-mediated) oxidation by nitrate (Senn and Hemond 2002). Mn oxidation only occurs in the presence

of oxygen (Boogerd and de Vrind 1987, Morgan 2005), and can be assumed to be microbially mediated based upon the relative rates of abiotic and microbial oxidation (Morgan 2000). Despite its slow oxidation kinetics, dissolved Mn at the Lot River (France) displayed an inverse trend with dissolved oxygen in the wells along the flow path (Bourg and Bertin 1993, Bourg and Bertin 2002). However, breakthrough of elevated, dissolved Mn at an oxic production well could occur either because of slow oxidation kinetics or a nearby reduction hotspot (Bourg and Richard-Raymond 1994). Attempts to use E_h-based measurements or thermodynamic calculations to predict locations susceptible to elevated Mn have been very limited in their success (Kedziorek and Bourg 2009).

Similar processes can influence Fe, Mn, and other trace metals; for oxidative processes, Mn may be more significant than Fe either because Mn(III/IV) oxides can directly oxidize reduced species such as As(III) (Manning et al. 2002) or because metals such as Co(II) and Cr(III) can be indirectly oxidized by Mn(II)-oxidizing microbes (Murray et al. 2007). Field studies of streambed sediments downstream of acid mine drainage showed Co, Ni, and Zn sequestration concomitant with Mn and Fe oxidation at circumneutral pH, rather than with upstream Fe oxidation at more acidic pH (Gandy et al. 2007). The Glatt River bank filtration site (Switzerland) experienced seasonal changes in dissolved oxygen (due to surface water organic carbon loads discussed above), which affected the stability of Fe and Mn oxides. Reduction of Fe and Mn corresponded with seasonal release of trace metals, whereas winter Mn oxide formation in observation wells corresponded with seasonal sequestration of trace metals (von Gunten and Kull 1986).

The location and extent of reaeration can significantly affect the water quality at production wells and their flow rates as a result of clogging. In one site at the Seine River (France), a thick clayey sand layer inhibited the reaeration of the bank filtrate, and the prolonged reducing conditions generated elevated ammonium concentrations in the production well (Doussan et al. 1998). Dutch well fields often clog due to well-screen mixing of mildly oxic shallow groundwater and anoxic deep groundwater with elevated dissolved iron (van Beek et al. 2009). Iron oxidation is not generally observed far from the production wells in these well fields, which suggests that the infiltrate is not as readily reaerated along the flow path as other sites, given the fast kinetics (Luther 2005) of iron oxide precipitation. Many wells across Germany also clog with microbial Fe and Mn oxide encrustations, which require regular removal to maintain well yield (Hässelbarth and Lüdemann 1972). Bank filtration adjacent to polder settings in both Germany (Massmann et al. 2004) and the Netherlands (de Vet et al. 2010) is susceptible to elevated concentrations of sulfide, ammonium, and methane in the infiltrate, which tends to require post-extraction treatment for drinking water purposes. As polders are typically clay and peat soils reclaimed via extensive groundwater pumping and/or levees, their low hydraulic conductivity, long residence times, and sustained anoxic conditions are unsurprising (Massmann et al. 2004).

Dissolution of carbonate minerals in the aquifer

Disequilibrium between the bank filtrate and the native aquifer can lead to mineral dissolution and/or precipitation during the water's passage. Other than redox-sensitive minerals as described above, carbonate minerals (e.g., $CaCO_3$, $MgCO_3$) are most

susceptible to dissolution during bank filtration. Silicate mineral dissolution tends to be less extensive than carbonate mineral dissolution (Bourg and Bertin 1993, Bourg and Richard-Raymond 1994, NRC 2008). Sulfide mineral dissolution is often considered in deep-well ASR and ASTR (Herczeg et al. 2004), but significant sulfide mineral abundances or dissolved sulfide concentrations are atypical in the shallow alluvial aquifers targeted for bank filtration. Polder settings are an exception, as they can result in anoxic groundwater with enough sulfide to precipitate sulfide minerals (Massmann et al. 2003).

Infiltrate with lower alkalinity and/or pH than the ambient groundwater has been observed to promote calcite ($CaCO_3$) dissolution in many field sites (von Gunten et al. 1991, Bourg and Bertin 1993, van Breukelen et al. 1998, Petkewich et al. 2004, Greskowiak et al. 2005) and some laboratory studies (Rinck-Pfeiffer et al. 2000, Patterson et al. 2010). Even if the infiltrate is chemically similar to the ambient groundwater, CO_2 and H^+ generated by oxidation of organic carbon in the bank can push the infiltrate to disequilibrium with the local aquifer (Bourg and Richard-Raymond 1994, van Breukelen et al. 1998, Rinck-Pfeiffer et al. 2000). Since only low levels of trace elements are typically affiliated with calcite (Morel and Hering 1993), its dissolution has different implications than the dissolution of Fe or Mn oxides. Increases in dissolved Ca and Mg from carbonate dissolution contribute to water hardness, but changes in hardness have been negligible in field and lab studies (Bourg and Bertin 1993, Johnson et al. 1999, Patterson et al. 2010). In one column study, calcite dissolution contributed to a locally higher hydraulic conductivity (Rinck-Pfeiffer et al. 2000). There is some concern that overly aggressive water could dissolve enough calcite grains so as to destabilize the soil,

especially with reverse-osmosis-treated water in SAT sites (Johnson et al. 1999), but it is unlikely that natural surface water would threaten an aquifer's structural stability during bank filtration.

Past the reducing zone near the bank, reprecipitation of calcite can sometimes be anticipated based upon geochemical transport models (van Breukelen et al. 1998, Petkewich et al. 2004) and laboratory studies (Rinck-Pfeiffer et al. 2000). Many field studies do not explicitly consider reprecipitation, but if enough calcite has been dissolved, significant amounts of reprecipitated calcite could clog the pores of the aquifer, as has been observed in column studies (Rinck-Pfeiffer et al. 2000). Field-scale geochemical transport models nevertheless suggest that the reprecipitated quantities of calcite should not affect the aquifer's porosity (van Breukelen et al. 1998, Petkewich et al. 2004).

Although carbonates are not major sinks for trace elements, in locations with sufficiently high alkalinity, carbonate minerals can control dissolved Fe, Mn, and other trace cation concentrations (Tessier et al. 1979). The carbonate solids of Fe (siderite) and Mn (rhodochrosite) are more soluble than those with most other trace metals. The potential control on dissolved trace metal concentrations by carbonate precipitation is illustrated in Figure 2.4 (in which equilibrium with calcite is assumed). Besides metal-carbonates, some trace metals can form even less soluble mixed hydroxycarbonates or co-precipitate in calcite (Rimstidt et al. 1998), so the concentrations in Figure 2.4 can be considered an upper bound of the solid-phase-controlled equilibrium concentrations expected for the given conditions. One caveat to this approach is that the kinetics of precipitation could be slow, as suspensions of bentonite precipitation seeds,

supersaturated in calcite and rhodochrosite or siderite, took more than 100 d to reach steady state (Jensen et al. 2002).

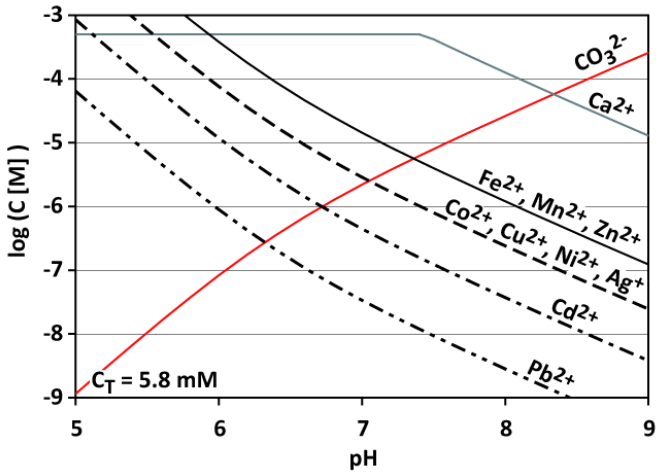

Figure 2.4. Soluble metal concentrations in equilibrium with calcite and metal carbonates (C_T = 5.8 mM; Ca_T = 0.5 mM, the average value for North American fresh water (Morel and Hering 1993)). Solubility products (in the form MCO_3 except Ag_2CO_3) taken from the MINTEQa2 database (2006). For simplicity, concentrations have been plotted with one line for each cluster of solubility products labeled on the figure (log K_{sp} within 0.5 units).

Multiple field sites have significant fractions of carbonate-bound Mn and Fe. In a polder setting in eastern Germany, dissolved Mn in groundwater was controlled by a combination of Mn and Ca carbonates (Massmann et al. 2004). Similarly, in an *in situ* groundwater treatment plant in Switzerland, short residence time in an aerated aquifer with high calcite abundance precluded the formation of Mn oxides. Dissolved Mn down-gradient of aeration wells was controlled by Mn- and Ca-carbonates with no evidence of Mn oxide accumulation (Mettler et al. 2001). At the same site, Fe oxides were associated with calcite, suggesting that Fe(II)-calcite interaction led to preferential oxidation sites during aeration (Mettler et al. 2001). Vernal calcite dissolution due to microbial

respiration in the Glatt riverbank released significant Mn and Fe, suggesting both were carbonate-bound (von Gunten et al. 1994). Trace cations have also been released during calcite dissolution, e.g., Zn, Co, Cd, Ni, and Pb in batch incubations of aquifer sediments (Descourvières et al. 2009), and sequestered via carbonate preciptitation, e.g., Cd at the Glatt river site (von Gunten et al. 1991).

Sorption in the aquifer

Sorption and ion exchange also occur because of disequilibrium between the bank filtrate and the native aquifer. Surface-associated ions of the aquifer material desorb, while ions from the bank filtrate adsorb, during infiltration. Significant desorption from contaminated aquifer sediments would render the bank filtrate unusable without substantial post-treatment, and therefore such sites are avoided for bank filtration. In bank filtration settings, major ions dominate any ion exchange process, and as such, ion exchange rarely affects the quality of the bank filtrate. At one ASR site, exchange of carbonate for chloride in sediments did increase the chloride concentration beyond drinking water standards, and exchange of sodium in aquifer clays may have caused clay expansion and subsequent decreased permeability (Mirecki et al. 1998, Parkhurst and Petkewich 2002).

In contrast, sorption is the main retardation process for dissolved components during infiltration, especially for trace elements released to the bank filtrate in the reducing zone. Net sorption of dissolved components can enable the aquifer sediments to "buffer" the composition of the bank filtrate (Bourg and Darmendrail 1992). Trace cations such as Cd and Zn were released in the reducing zone, then sequestered via

sorption at sites in Switzerland and France (von Gunten et al. 1991, Bourg and Darmendrail 1992, Bourg and Bertin 1993). Copper, often bound to organic matter, was not as readily adsorbed as Cd and Zn (von Gunten et al. 1991). Similarly, ammonium generated under prolonged reducing conditions at the Seine River (France) only penetrated the first 10–20 m of aquifer sediments after twenty years of passage, due to sorption (Doussan et al. 1998).

Sorption depends upon the surface area of the sorbent and the affinity of the dissolved species for the sorbent surface sites. Trace element sorption on Al, Fe(III), and Mn(III/IV) oxides has been described extensively in the literature (Gadde and Laitinen 1974, Murray 1975, Axe and Trivedi 2002, Lee et al. 2002). Field observations of Al-, Fe(III)-, and Mn(III/IV)-oxide sequestration of trace metals support a strong correlation between the sorption of Mn(II) and other trace metals (Fuller and Harvey 2000, Kay et al. 2001, Lee et al. 2002). (Iron(II) sorption on oxide surfaces is complicated by rapid surface-catalyzed oxidation in the presence of oxygen (Wehrli and Stumm 1989).) Exceptions to this trend occur in sites with high levels of organically-bound Cu and Zn (von Gunten et al. 1991, Bourg and Darmendrail 1992), which remain mobile under conditions otherwise favorable to sorption on aquifer sediments.

The limitation of sorption in long-term bank filtration (e.g., sites in Berlin have been active since the late 1800s (Ziegler 2001)) results from saturation of the surfaces of the aquifer sediments. This causes an advancing sorption front in the aquifer, which can eventually reach the production well, as has been observed for Mn in Israel (Oren et al. 2007) and modeled for P in Canada (Spiteri et al. 2007). Sorption also plays a key role in *in situ* iron removal. Injection of aerated groundwater oxidizes adsorbed Fe(II) to Fe(III)

oxides, and low-Fe groundwater is subsequently extracted, while Fe(II) adsorbs to newly formed Fe(III) oxides, until Fe(II) breaks through at the well again (Appelo et al. 1999). Dilution with native groundwater and dispersion can significantly damp any sorption front moving through an aquifer for bank filtration. For example, in the 1980s along the Rhine River, elevated surface water concentrations of As, Co, Cu, Ni, and Pb did not penetrate further than 50 m along the infiltration path (Stuyfzand et al. 2006). Similar data comparing surface water and infiltrate for a German site (Duisberg) along the Rhine have been presented as a percentage "removed" from the infiltrate (e.g., 51–93% removal of As, Cu, Ni, and Pb) (Sontheimer 1980, Schmidt et al. 2003), but this terminology should be avoided. Trace elements sequestered via sorption to Fe and Mn oxides can readily desorb (Gadde and Laitinen 1974) if the composition of the bank filtrate changes, e.g., due to seasonal changes or shock loads in the source water body. Geochemical modeling of wastewater-derived P in two Canadian aquifers suggested that a P plume would move 20 m down-gradient in 17 years, upon removal of the wastewater source (Spiteri et al. 2007). Stable, long-term sequestration thus requires more than sorption alone for trace elements. Since actual breakthrough of trace metals in bank filtration wells is rare, alternate sequestration (i.e., precipitation of oxides and interactions with carbonates), coupled with dispersion and dilution, likely occurs in long-term bank filtration sites still in use.

Chapter 3

A Hydrous Manganese Oxide Doped Gel Probe Sampler for Measuring *In Situ* Reductive Dissolution Rates: I. Laboratory Development

Abstract

Reductive dissolution of redox-sensitive minerals such as manganese (Mn) oxides in natural sediments is an important mechanism for trace element mobilization into groundwater. A gel probe sampler has been constructed to study *in situ* reductive dissolution of Mn oxides. The gel consists of a polyacrylamide polymer matrix doped with hydrous Mn oxide (HMO). Gel slabs are mounted into a probe, which is designed to be inserted into the sediments. The amount of Mn released from the gel by reductive dissolution is determined by comparing the amount of Mn initially embedded into the gel with the amount remaining in the gel after exposure to conditions in the sediments or, in laboratory studies, to reducing agents. In this laboratory study, the performance of the gel probes was examined using the model reductant ascorbate and the Mn-reducing bacteria *Shewanella oneidensis* strain MR-1. In addition, a 1-D model was used to relate the reaction rates observed for HMO embedded in gels to those for HMO in suspension. One limitation of the HMO-doped gels for assessing microbial reduction rates is that the

gels prevent direct contact between the microbes and the HMO and hence preclude enzymatic reduction at the cell surface. Nonetheless, the HMO-doped gel probes offer the possibility to establish a lower bound for Mn-reduction capacity in sediments.

Introduction

Manganese (Mn) is an important and abundant element in the aqueous environment. Mn oxide solids are well-known sinks for metals and metalloids via sorption, and microbially mediated reduction of Mn oxides has been linked to the release of metals and metalloids to porewater (Lovley 1991). Biogeochemical cycling of Mn thus has implications for the cycling of other trace elements that pose a hazard to human health.

Furthermore, Mn(III,IV) oxide formation and reductive dissolution are key processes in the redox cycling of Mn and other redox-sensitive elements in sediments. The distribution of these elements with depth in sediment porewaters reflects the intensity of chemical and biological redox reactions during early diagenesis, such as the diffusion of dissolved chemical species and the rate of sediment accumulation (Berner 1980). Microbial processes dominate Mn(II) oxidation in the environment, as biological Mn oxidation is generally fast relative to abiotic Mn oxidation processes, including surface-catalyzed reactions (Davies and Morgan 1989, Morgan 2000). On the other hand, Mn(III,IV) oxides are readily reduced by both chemicals (Stone and Morgan 1984, Burdige and Nealson 1986, de Vitre et al. 1988, Wang and Stone 2006b, 2006a) and microbes (Myers and Nealson 1988a, Burdige et al. 1992, Ruebush et al. 2006). Porewater geochemistry can be assessed through a variety of methods, but the method of diffusive equilibrium in thin films (DET) has proven to be amenable to modifications for the assessment of processes occurring in sediments (Edenborn et al. 2002, Campbell et al.

2008a). The DET method uses polyacrylamide gels placed in a plastic holder, covered with a permeable membrane, and inserted vertically into sediments. The water inside the gel is allowed to equilibrate with the surrounding porewater solution via diffusion, and the composition of the ambient porewater can be determined upon removal. The early model of this device by Davison et al. (1994) used a single polyacrylamide gel slab; a modified ladder structure has been used more recently (Fones et al. 1998, Kneebone et al. 2002, Campbell et al. 2008b).

Polyacrylamide gels doped with Fe oxides have been used to evaluate of the effect of porewater composition on *in situ* sorption (Campbell et al. 2008a, 2008b). Similar probes containing agarose gels doped with Mn oxides have been used as qualitative redox indicators (Edenborn et al. 2002). These Mn oxide-doped gels take advantage of the high redox potential for Mn oxide reduction, as well as the pronounced difference in the solubility of largely insoluble Mn(III,IV) oxides as compared with the relatively soluble Mn(II) containing solids (Morgan 2000). Thus, under reducing conditions, Mn(II) can diffuse out of gels.

The purpose of this study was to develop and validate a method to quantify *in situ* rates of reductive dissolution as a function of depth along a sediment profile by using a hydrous Mn oxide (HMO) doped gel probe sampler. Reductive dissolution of HMO is quantified by measuring Mn mass loss over the course of deployment in sediments. Laboratory validation of this method was performed using two model systems—one abiotic and one biotic. Ascorbate was used for abiotic experiments since it is an analog for some functional groups found in natural organic matter (Stone and Morgan 1984). *Shewanella oneidensis* MR-1, used in the biotic experiments, is a facultative anaerobe

with a highly versatile electron transport chain (Ruebush et al. 2006) and a single polar flagellum (Abboud et al. 2005).

Experimental Section

Reagents

All chemicals used were reagent grade (Omnipure, EM Science unless otherwise noted) and used without further purification. All water used was 18 MΩ-cm deionized water (Elix/Milli-Q, Millipore). Solutions were stored in plastic containers that had been acid-washed in 5% hydrochloric acid. All nitric acid solutions were made with trace metal grade HNO_3 (70%). All hydroxylamine solutions were made with trace metal grade hydroxylamine.

HMO synthesis

The HMO precipitate was prepared by adding 50 ml of 0.02 M $KMnO_4$ (adjusted to pH 12.5 with 1M NaOH) dropwise to a stirred solution of 100 ml of 0.03 M $MnSO_4 \cdot H_2O$ (adjusted to pH 7 with 1M NaOH), following the method of Murray (1974). The stirred suspension was allowed to equilibrate over 4 h while the pH stabilized. After 4 h, the HMO was washed 3 times with water, and the precipitate was resuspended in 200 ml of water, with a resulting concentration of approximately 40 mM Mn (3.5 g l^{-1}). This form of HMO is an abiotic analog of biogenic Mn oxide best termed "triclinic Na-birnessite" (Villalobos et al. 2003, Jurgensen et al. 2004).

X-ray diffraction (Phillips X'Pert PRO, Cu-Kα X-ray source) analysis confirmed that the HMO was largely amorphous, with slightly increasing crystallinity over two

weeks. HMO was used within two weeks of synthesis to decrease the impact of changing crystallinity over time. The specific surface area measured by BET-N_2 surface adsorption was 60 $m^2\ g^{-1}$, which declined to 38 $m^2\ g^{-1}$ after 3 weeks, consistent with that of similar amorphous Mn oxide solids (Villalobos et al. 2003, Kennedy et al. 2004). Finally, the average oxidation state of the HMO solid, measured via a modified Winkler titration (Carpenter 1965), was 3.7 ± 0.1, again consistent with the values (3.6–4.0) for similar amorphous Mn oxide solids (Villalobos et al. 2003, Jurgensen et al. 2004).

Gels and gel probes

Polyacrylamide gel slabs were made by modifying the methods of Davison et al. (1994), Kneebone et al. (2002), and Campbell et al. (2008a). Gels were made by dissolving 3.75 g acrylamide (C_3H_5NO) and 0.075 g N-N'-methylene-bis-acrylamide ($(CH_2CHCONH)_2CH_2$) in either 25 ml of water (clear gels) or 7.5 ml HMO stock diluted with 17.5 ml water (HMO-doped gels). The resulting solution was deoxygenated by bubbling with compressed argon for 30–45 minutes. The simultaneous addition of 150 µl of 100g l^{-1} sodium persulfate and 25 µl of tetramethylethylenediamine (TEMED) initiated the polymerization of the gel. The solution was mixed and quickly poured into a heated, acid-washed, glass Petri dish to increase the polymerization rate. Over 4 minutes, the gel completely solidified, upon which the dish was removed from the heat. After the gel cooled to room temperature, it was gently extracted from the Petri dish with a flexible plastic spatula and transferred directly into 1 l water, in which it hydrated for approximately 24 h.

Gel slabs were hand-cut with a plastic, acid-washed blade into the appropriate size (5 mm × 25 mm, 2 mm thick) for a ladder-style gel probe and stored in water for up

to one week to prevent dehydration. Gel probes were designed to hold the gel slabs in slots etched into a plastic holder, as described in previous work (Campbell et al. 2008b). "Mini-probes" were 4 cm long with a single column of six slots for gel slabs.

Ten gels from each batch of gel slabs were each placed in 10 ml of 0.5% hydroxylamine-HCl for ≥ 12 h to dissolve the HMO out of each gel. The supernatant was diluted and analyzed with ICP-MS to determine the total Mn in the gel, which averaged 1.50 μmol per gel, with less than 15% variation between batches of gels (some gels were excluded due to visual heterogeneity in Mn oxide distribution). Similarly, once a gel slab had reacted with a solution, the gel slab was removed and equilibrated for ≥ 12 h with 0.5% hydroxylamine-HCl, which reductively dissolved any remaining HMO solid. The equilibrating solution was diluted with 1% HNO_3 and analyzed for total dissolved Mn via ICP-MS.

Laboratory experiments

A series of laboratory-based experiments were conducted to determine the abiotic and microbially mediated rates of HMO reductive dissolution in suspension and in doped polyacrylamide gels. All laboratory experiments were conducted in triplicate.

Abiotic reduction

HMO (diluted from the 3.5 g l^{-1} stock suspension), HMO-doped gels, or HMO-doped mini-probes were added to solutions of 2 mM L-ascorbic acid (Sigma) and in 33 mM Na_2SO_4 (Fisher; I = 0.1 M) buffered to pH 8.0 with 2 mM HEPES buffer. As needed, pH was adjusted by addition of 0.1 M NaOH or H_2SO_4. The total HMO concentration in all non-mini-probe experiments was approximately 4–6 times that of the mini-probe

experiments. Over 6 h, samples were taken from the stirred bulk solution, syringe-filtered (Whatman 0.2 μm mixed cellulose ester filters), and acidified in 1% HNO_3 for analysis via ICP-MS. Because of the slow rate of Mn(II) oxidation by O_2 (Morgan 2005), the total Mn remaining in recovered gel slabs at the end of the experiments was measured to confirm the mass balance. The bulk solution, gel storage bath, and recovered gels accounted for over 95% of the total Mn (Table A.1).

Microbially mediated reduction

Experiments with *S. oneidensis* MR-1 were conducted anaerobically, either in sealed anaerobic culture bottles (HMO and HMO-doped gels) or under N_2 in a glovebox (HMO-doped mini-probes). Inocula for anaerobic cultures were grown aerobically (overnight at 30°C) in Luria Broth to stationary phase (~ 10^{12} cells l^{-1}). Cells were transferred without washing to MR-1 minimal medium (pH 8; Table A.2), containing 6 mM lactate and amended with HMO, to achieve a cell density of ~ 10^{11} cells l^{-1}. The medium contained a small amount of Mn(II), which was taken into account in subsequent Mn measurements. Culture bottles were sealed with rubber stoppers and aluminum caps and shaken at 30°C. An observed turbidity increase, indicating microbial growth over the course of the experiments, was not quantified. Samples were removed through the rubber stoppers via N_2-flushed syringes, over 8 h for HMO and over 36 h for HMO-doped gels. HMO-doped mini-probes were deployed in stirred plastic beakers at room temperature (22°C) in a glovebox. Over 63 h, these samples were removed from the bulk solution in N_2-flushed syringes. All samples were subsequently filtered and acidified as in the abiotic experiments.

Data analysis

The stoichiometry of abiotic reduction at pH 8 is shown in equation (3-1).

$$MnO_2 + C_6H_7O_6^- \rightarrow Mn(II) + C_6H_5O_6^- + 2\ OH^- \quad (3\text{-}1)$$

The rate of reductive dissolution is assumed to be equal to the rate of Mn(II) production, with a rate expression shown in equation (3-2), where the rate coefficient for the reduction of the solid MnO_2 was calculated by measuring the increase in the concentration of Mn(II) in solution as a function of time, and solving the rate expression. This expression assumes that the second e^- transfer from Mn(III) to Mn(II) is instantaneous (Stone and Morgan 1987), and that the reactivity of ascorbic acid intermediates does not affect the 1:1 stoichiometry between Mn(IV) and $C_6H_7O_6^-$ (Toner and Sposito 2005).

$$\frac{d[Mn(II)]}{dt} = k\,[C_6H_7O_6^-]_t\,[MnO_2]_t \quad (3\text{-}2)$$

Here $[MnO_2]$ represents the moles of Mn solid per volume, giving k units of $M^{-1}\ s^{-1}$. Multiplying k by the Mn oxide surface loading ($m^2\ l^{-1}$) yields the surface-area-normalized rate coefficient, k_{SA} ($m^2\ mol^{-1}\ s^{-1}$). As the reaction proceeds, the concentration of MnO_2, $[MnO_2]_t$, decreases and its value is assumed to be equal to the initial MnO_2 concentration, $[MnO_2]_0$, minus the dissolved Mn concentration, $[Mn(II)]_t$, at the sampling time (equation (3-3)).

$$[MnO_2]_t = [MnO_2]_0 - [Mn(II)]_t \quad (3\text{-}3)$$

Mn(III) produced in the course of Mn(IV) reduction is assumed either to remain in the crystal lattice or to adsorb to the oxide surface until further reduction in the absence of a strong complexing agent (Morgan 2000). The presence of excess ascorbate at this pH

should guarantee that the effect of reoxidation of any readsorbed Mn(II) on equation (3-3) is negligible (Toner and Sposito 2005).

The concentration of ascorbate, $[C_6H_7O_6^-]_t$, also decreases as the reaction proceeds, according to the stoichiometry of equation (3-1); however ascorbate concentrations were deliberately maintained in approximately tenfold excess of the total Mn in the system so that the ascorbate concentration could be assumed to be roughly constant. Thus, the rate of reductive dissolution can be expressed as in equation (3-4) below.

$$\frac{d[Mn(II)]}{dt} = k[C_6H_7O_6^-]_0([MnO_2]_0 - [Mn(II)]_t) = k'([MnO_2]_0 - [Mn(II)]_t) \quad (3\text{-}4)$$

Integrating this differential equation with respect to time yields the expression in equation (3-5).

$$\ln\left(\frac{[MnO_2]_0}{[MnO_2]_0 - [Mn(II)]_t}\right) = k't \quad (3\text{-}5)$$

Plots of the left-hand side of equation (3-5) vs. time have been fitted with linear regression (performed in Microsoft Excel). The slope of the regression line is equal to k′ (t^{-1}), and the y-intercept is theoretically 0. Statistical differences between apparent rate coefficients and between y-intercepts and zero were assessed with the t-test at a significance level of 95% in Microsoft Excel.

This approach was extended to describe microbially mediated reductive dissolution by making the simplifying assumption that this reaction occurs via a hypothetical reductant, Red, with a constant concentration (see also discussion below).

One-dimensional model

To separate the diffusion component from the chemical reduction component of the observed reaction rates, a one-dimensional diffusion-reaction model was applied to the experimental data using AQUASIM 2.1 (Reichert 1994). This model represented an HMO-doped gel as a "biofilm reactor compartment" (at zero growth rate) containing a solid matrix with well-mixed water in the pore space (92% porosity). The chemical reduction of HMO to Mn(II), whose kinetics were represented as equation (3-2) above, was limited to the pore space of this compartment. The stirred bulk solution was represented as a "mixed reactor compartment". The two compartments were connected with a "diffusive link", modeling a diffusive boundary layer for the dissolved Mn(II) and the reductant.

Initial conditions in the simulations were set to match the experimental conditions, normalized to one gel, as summarized in Table A.3. Initially, all of the Mn was confined to the gel pore space as HMO, and all of the reductant was confined to the mixed reactor. In the microbial experiments, the hypothetical reductant Red was substituted for ascorbate in equation (3-2); the diffusion coefficients for ascorbate were also used for Red. For the microbial experiments with HMO in suspension, direct (presumably enzymatic) reduction at the cell surface was incorporated as shown in equation (3-6):

$$\frac{d[Mn(II)]}{dt} = k''[MnO_2]_t \, . \qquad (3\text{-}6)$$

This mechanism, however, was excluded for HMO-doped gels (see Discussion). Simulations were performed in "Parameter Estimation" mode, which minimizes χ^2 values between the model and the experimental data to solve for a specific parameter. Sensitivity analysis determined the most useful fitting parameter for each experiment. The χ^2 values were converted to p-values, which indicate the probability that the modeled

system would generate the measured experimental data, with 100% (p-value of 1.00) being ideal goodness of fit.

Results

Laboratory experiments

Dissolved Mn was found to diffuse out of the gels in the absence of an externally added reductant. Prior to the reductive dissolution experiments, the HMO-doped gels were stored and, in the case of microbial studies, deoxygenated in Milli-Q water. It was observed that a substantial fraction of the total initial Mn (generally ≤ 20%) diffused out of the gels during deoxygenation and storage, which was attributable to desorption of Mn(II) sorbed to the HMO surface. Note that Mn(II) is present in stoichiometric excess in the synthesis method. In Milli-Q water, the rate of Mn loss was approximately 4.2×10^{-11} M s^{-1}. When the gels were transferred from Milli-Q water to the background electrolyte (2 mM HEPES in 33 mM Na_2SO_4) used for the abiotic experiments, however, negligible loss of Mn was observed over 5 d (data not shown).

Abiotic experiments with HMO in suspension proceeded quickly relative to experiments with HMO embedded in the gels; dissolution of the HMO in suspension was complete within 2 minutes. A lower bound of the surface-area-normalized rate coefficient based on this observation is k_{SA} = 5 m^2 $mol^{-1}s^{-1}$; the reported rate coefficient for this reaction at pH 7.2 is 4 m^2 $mol^{-1}s^{-1}$ (Stone and Morgan 1984).

Data from the other 7 experiments (Table A.5) were interpreted using the integrated form of the rate expression (equation (3-5)) as shown in Figure 3.1. The slopes, intercepts, and correlation coefficients from linear regression analysis are

summarized in Table 3.1. The slopes correspond to the apparent rate coefficients for each experiment. Insignificant differences in rate coefficients were obtained using Mn concentrations from syringe-filtered (0.2 μm) and unfiltered samples in abiotic experiments with HMO-doped gels; syringe-filtered Mn concentrations were > 90% of unfiltered Mn concentrations (data not shown). Likewise, the use of different membrane pore sizes in the mini-probe experiments did not affect the observed rates (Table 3.1). Overall, abiotic Mn release rates are 1–2 orders of magnitude faster than biotic rates, as represented by k′. Embedding HMO in gels and placing gels in mini-probes affects the observed apparent rate coefficients more in the abiotic experiments than in the biotic experiments. Microbial experiments with HMO suspension and mini-probes exhibited a lag phase (Figure 3.1b: 1 hour, and Figure 3.1c: 8 hours, respectively), which was only statistically significant for the mini-probes (Table 3.1, see Discussion).

One abiotic experiment was conducted with both clear and HMO-doped gels loaded in a single mini-probe sampler, in the expectation that the Mn concentrations in the clear gels would be the same as in the bulk solution. However, the Mn concentrations in the clear gels were three–twentyfold greater than that in the bulk solution. The co-location of the clear and HMO-doped gels in a single mini-probe appears to produce an artifact in which the dissolved Mn diffusing out of the HMO-doped gels perturbs the local environment sampled by the clear gels. This configuration should be avoided in applications.

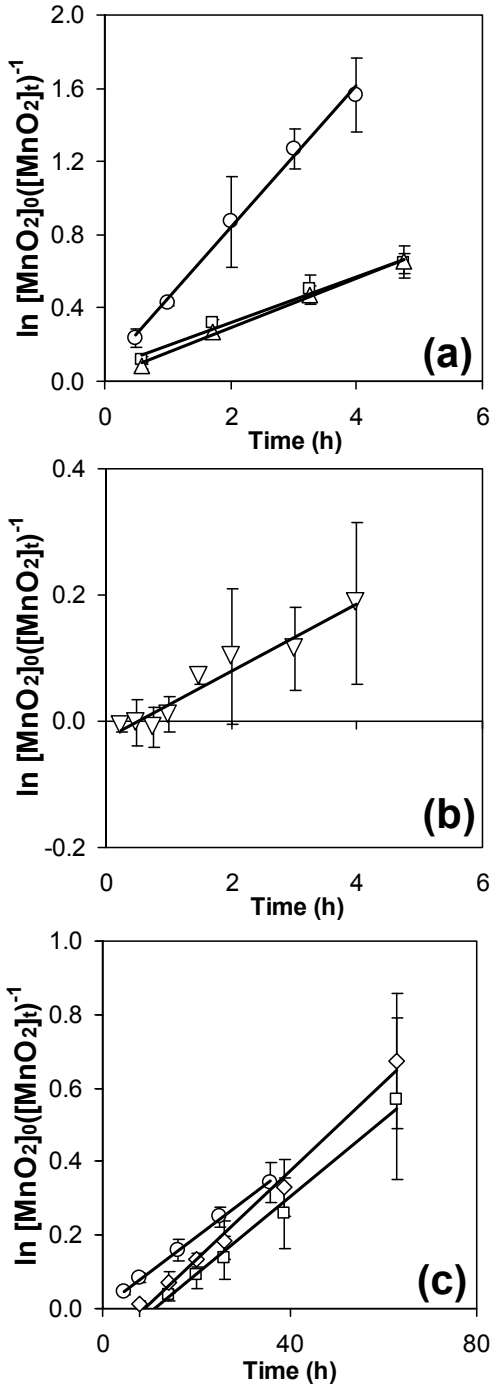

Figure 3.1. Integrated expression for the rate of Mn release, ln ($[MnO_2]_0[MnO_2]_t^{-1}$), as a function of time at pH 8.0. (a) abiotic reaction of ascorbate ($[C_6H_7O_6^-]_0$ = 2 mM) and HMO-doped gels (○; Mn_T = 184 μM) or HMO-doped gels in mini-probes with 0.45 (△; Mn_T = 52 μM) or 1.0 (□; Mn_T = 52 μM) μm membranes. (b, c) biotic reaction of *S. oneidensis* MR-1 (10^{11} cells l^{-1}) with HMO suspension (b: ▽; Mn_T = 360 μM) or (c) HMO-doped gels (○; Mn_T = 295 μM) or HMO-doped gels in mini-probes with 1.0 (□; Mn_T = 62 μM) or 5.0 (◊; Mn_T = 60 μM) μm membranes. Note difference in time axis for (c).

Table 3.1. Summary of linear regression data for laboratory-measured rates of reductive dissolution

Reductant	Oxidant	k′ (s^{-1})	±95% C.I.[a]	y-intercept	±95% C.I.	non-zero?[e]	r^2
Ascorbate	HMO[b]	5×10^{-2}	---	---	---	---	---
	HMO gels	1.0×10^{-4}	2×10^{-5}	7×10^{-2}	1×10^{-1}	no	0.99
	MP 0.45 μm[c]	3.8×10^{-5}	7×10^{-6}	2×10^{-2}	7×10^{-2}	no	1.00
	MP 1.0 μm[c]	3.5×10^{-5}	7×10^{-6}	7×10^{-2}	8×10^{-2}	yes	0.98
S. oneidensis MR-1	HMO	1.5×10^{-5}	1×10^{-5}	-3×10^{-2}	7×10^{-2}	no	0.95
	HMO gels[d]	2.7×10^{-6}	4×10^{-7}	5×10^{-3}	3×10^{-2}	no	1.00
	MP 0.45 μm[d]	2.9×10^{-6}	7×10^{-7}	-1×10^{-2}	8×10^{-2}	yes	0.99
	MP 1.0 μm[d]	3.3×10^{-6}	8×10^{-7}	-1×10^{-2}	1×10^{-1}	yes	0.99

[a] 95% confidence interval bounds for k′ (s^{-1})
[b] Rate estimated from complete dissolution in 2 minutes
[c] The rate coefficients of the two mini-probes reacted with ascorbate are not statistically different from each other.
[d] The rate coefficients of the HMO gels and the two mini-probes reduced by *S. oneidensis* MR-1 are not statistically different from each other.
[e] Is the y-intercept statistically different from zero, the initial value of ln ($[MnO_2]_0$ $[MnO_2]_t^{-1}$)?

One-dimensional model

The Mn release rates in the abiotic systems are quite different for HMO in suspension, in the gels, and in the mini-probes, even though the chemical reactants (i.e., HMO and ascorbate) are the same. This indicates that the physical properties of the systems (i.e., the embedding of the HMO in the gel and the placement of the gel in the mini-probe) must be accounted for. The AQUASIM model incorporates diffusive effects, thus allowing comparison of the different systems.

This 1-D model simulated a well-mixed bulk solution with diffusion into a gel with 92% water content, chemical reaction confined within the gel, and diffusion of the product Mn(II) into the bulk solution. Sensitivity analysis was used to identify the most useful fitting parameter for each experimental simulation: the diffusion coefficient of

ascorbate in the gel (for abiotic experiments) and the rate coefficients k″ and k′ (for the microbial experiments with HMO in suspension and in gels, respectively). Inclusion of second and third fitting parameters did not significantly improve the fit to the data.

For the two abiotic experiments, values of k derived from k′ (HMO in suspension) divided by $[C_6H_7O_6^-]_0$ (Table 3.1) were applied, and AQUASIM solved for the diffusion coefficient of ascorbate within the gel required for optimal fitting of the data (Figure 3.2). The diffusion coefficients of ascorbate in the bulk solution and Mn(II) throughout the system were adopted from literature (Yuan-Hui and Gregory 1974, Moreno et al. 2000, Nassef et al. 2007). This physical fitting parameter could account for the different Mn release rates in the two systems, so that the underlying chemical reaction rates are unaffected by the embedding of the HMO in the gel and the placement of the gel in the mini-probe.

Because the detailed mechanism in microbial reduction of metal oxides is not fully understood (Ruebush et al. 2006, O'Loughlin 2008), the AQUASIM model for microbial reduction occurred by two reactions: one with the generic reductant, Red, and the second with a surface component, k″, which required direct contact between the cells and the HMO. The surface-catalyzed reaction was therefore unavailable for HMO-doped gels and HMO-doped gels in mini-probes. For these two experiments, the model used an initial Red concentration ($[Red]_0$) fivefold greater than Mn_T for the HMO-doped gels and assigned Red the same diffusion characteristics as ascorbate in the abiotic simulations. This permitted the model to solve for k in these two experiments. AQUASIM then used the same k and $[Red]_0$ to solve for k″ in the experiment with HMO in suspension.

Chi-squared values ranged from 1.2 to 2.6 (Figure 3.2; Table A.3), which correspond with p-values greater than 0.998. Note that an 8 hour lag phase (which was not attributable to diffusion) was excluded in fitting the data from the microbial mini-probe experiment; in Figure 3.2 (right panel), time equals zero corresponds to the end of the lag period. In all cases, mass balances were satisfied for the model at steady state, with less than 1% error (Table A.4).

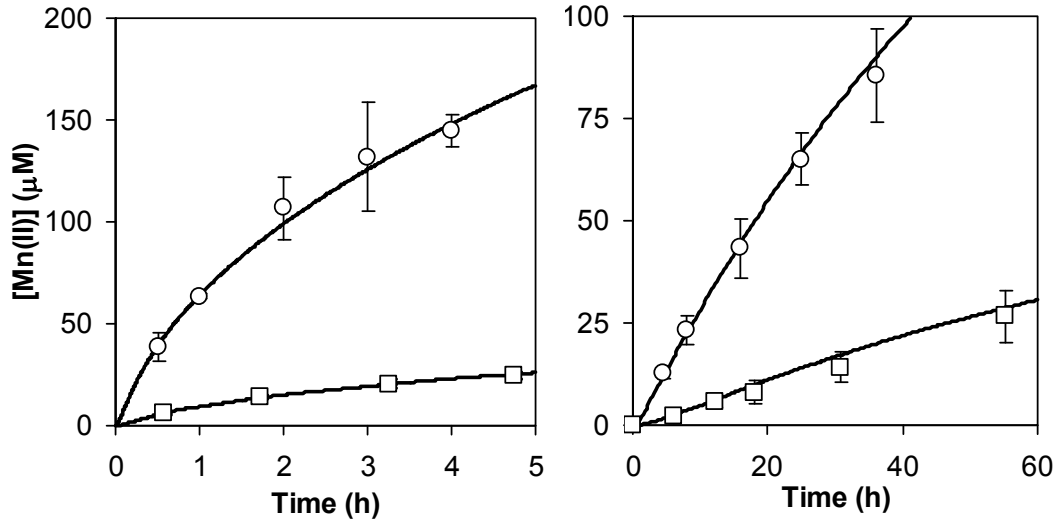

Figure 3.2. 1-D model output (lines) of Mn(II) accumulation in the bulk solution for abiotic (left) and microbially mediated (right) experiments with HMO-doped gels (○) or HMO-doped gels in mini-probes with 1.0 μm membrane (□). An 8 hour lag phase was removed from the microbial mini-probe data. Error bars are smaller than the size of the data markers in some cases. Conditions given in Figure 3.1.

Discussion

The AQUASIM modeling simulations were able to capture the physical and kinetic components of the abiotic reductive dissolution process in doped gels. The fitted value of the diffusion coefficient for ascorbate inside the gels was larger when the HMO-doped

gels were placed in the mini-probes (1.0×10^{-6} cm^2 s^{-1}) than when they were not (4.3×10^{-7} cm^2 s^{-1}). Since slower reduction was observed for HMO-doped gels in the mini-probes, this difference in the fitted diffusion coefficients can be attributed to the physical constraints of the mini-probes, which are not explicitly incorporated into the 1-D model. The bulk ascorbate diffusion coefficient is three–sevenfold larger than these gel-based diffusion coefficients, which may reflect the impact of tortuosity on diffusion in a highly porous medium (Shen and Chen 2007) or Donnan effects within the gel (Yezek and van Leeuwen 2005); both of which are presumed to be more significant for ascorbate compared to the Mn(II) ion.

The model assumed the same mechanism for microbially mediated reductive dissolution in gels: direct reduction via an external reductant (Red) diffusing into the gel. This assumption is justified because the gels and membrane prevent direct contact between *Shewanella* cells and the Mn oxide. The lack of contact is a function of dimensions: *S. oneidensis* MR-1 grown at room temperatures is approximately 0.6 μm × 3 μm in size (Abboud et al. 2005), so a membrane of pore size 0.45–5.0 μm is a strong barrier for these cells. Likewise, the largest documented pore size for polyacrylamide gels of our composition is 1.0 μm (Rüchel and Brager 1975, Chrambach 1985). Thus, cells are unlikely to enter gels, via either diffusion or chemotaxis. After 18 days of incubation, no evidence of microbial activity was found inside 3 HMO-doped gels from the sealed anaerobic culture bottles inoculated with a strain of *S. oneidensis* MR-1 that constitutively expresses a green fluorescent protein. Under a microscope (Zeiss Axioplan), the gels showed no fluorescence inside, although there was some green fluorescence at the edges of the gels (data not shown). Similarly, *Pseudomonas*

aeruginosa did not penetrate MnO_2-doped agarose gels after 1 month of incubation (Edenborn et al. 2002), so representing microbial reduction with an external reductant in the 1-D model seems appropriate.

On the other hand, the 1-D model explicitly shows that the gels do not capture all of the microbial reduction, as represented by the additional reduction mechanism required in the HMO suspension experiment. The nonzero rate coefficient k″ represents direct enzyme-catalyzed reduction at the cell surface, to which Mn oxide is inaccessible when doped in gels. In terms of the overall microbial reduction rate with HMO in suspension, k″ constitutes 65% of the total rate, whereas k′, the product of k and $[Red]_0$, constitutes the remaining 35% (Table A.3). In other words, Mn oxide-doped gels measure approximately 35% of the total reduction capacity of *S. oneidensis* MR-1.

The lower microbial reduction capacity in the gel and mini-probe model simulations could reflect either an inhibitory effect from the gel itself, or the lack of direct contact between the cells and the Mn oxide. In the former case, acrylamide is highly toxic to microorganisms (Starostina et al. 1983), and residual amounts in the polyacrylamide gels may suppress the measured reduction rates. In comparison to literature values, this study measured an HMO reduction rate of 5.4×10^{-19} mol cell^{-1} s^{-1}, which is mid-range for the values in literature (Table 3.2). Minor variations in growth medium, temperature, and Mn oxide crystallinity account for the range of over 3 orders of magnitude. The latter and more likely explanation is that prevention of direct contact between the cells and the Mn oxide in gels bypasses some portion of microbial reduction (Ruebush et al. 2006). Thus, HMO-doped gel probes only measure microbially mediated rates of reductive dissolution as generated by extracellular electron shuttles and by-

products of metabolism, rather than by direct enzymatic microbial reduction, which is a distinct artifact. These biochemical compounds are likely to be smaller than the membrane pore sizes, since like ascorbate, the pore size has no statistically significant effect on the reduction rate they produce (Table 3.1).

Table 3.2. Summary of literature values for Mn oxide reduction by *S. oneidensis* MR-1

Source	**Reported Rate (units given)**	**Growth Medium[a]**	**Mn oxide[b]**	**Rate (mol s^{-1} $cell^{-1}$)**
Burdige et al. (1992)	7.39 μM d^{-1} [c]	LO	HMO	2.14×10^{-20}
	4.65 μM d^{-1} [c]	LO	δ-MnO_2	1.35×10^{-20}
	11.8 μM d^{-1} [c]	LO	birnessite	3.43×10^{-20}
Myers and Nealson (1988a)	2.0-87×10^{-10} μmol h^{-1} $cell^{-1}$	LO	δ-MnO_2	5.6-240×10^{-20}
	1.0-4.2×10^{-8} μmol h^{-1} $cell^{-1}$	M1	δ-MnO_2	2.9-12×10^{-18}
Ruebush et al. (2006)	7.4×10^{-8} mol min^{-1} mg^{-1} [d]	M1[e]	birnessite	1.1×10^{-19}
this study	---	M1	HMO	5.4×10^{-19}

[a] LO medium is an undefined medium, whereas M1 is a defined, minimal medium.
[b] Birnessite and δ-MnO_2 are structurally similar to HMO [21].
[c] Cell number is 4×10^{6} cells ml^{-1}.
[d] Rates measured for total membrane (TM) fractions only (8.75 mg TM $cell^{-1}$)
[e] M1 medium modified with 50 mM ferric citrate (replacing fumarate), 30 mM DL-lactate, 4 mM sodium phosphate, and 10 mM HEPES

The reduction kinetics of the biochemical compounds represented by Red are much slower than the kinetics of ascorbate. The ascorbate rate coefficient is 3 orders of magnitude larger than that of Red, which is on the order of pyruvate and oxalate (Stone and Morgan 1984), but the model assumption that Red is maintained in excess of HMO is somewhat arbitrary. Instead, consider the amount of ascorbate required to generate the same reducing capacity as Red in these systems: 2.9 μM. That is, 2.9 μM ascorbate would generate the same amount of reduction as 10^{11} cells l^{-1}.

Although reduction by ascorbate is much faster than microbially mediated reduction in these laboratory studies, the experimental conditions are not likely to be representative of the environment. The concentration of abiotic reductants may be substantially lower than the ascorbate concentration used. And conversely, the cell number (10^{11} cells l^{-1}) is at the low end of the environmental range in shallow sediments of 10^{11}–10^{13} cells l^{-1} (Capone and Kiene 1988, Wellsbury et al. 1996), although metal-reducing bacteria may be only a fraction of the total biomass.

Limitations of HMO-doped gel probes

Besides the above caveat regarding microbial reduction, HMO-doped gel probes are subject to three additional considerations. First, Mn readily leaches out of the HMO-doped gels at low rates in deionized water. This method of HMO synthesis uses excess Mn(II), which results in "pre-saturated" HMO sorption sites for laboratory experiments. On one hand, saturated sorption sites could avoid the issue of reduced Mn from the solid sorbing onto the surface, making bulk solution measurements of dissolved Mn(II) more representative of the surface reduction rate. On the other hand, Mn(II) could block access of reductants to the surface of HMO, depressing the measured rates. Nevertheless, since rates of HMO reduction are comparable to those in literature for both abiotic and microbially mediated reduction, this concern is minimal. In practice, desorption rates of Mn(II) are insignificant relative to reductive dissolution rates over the course of the laboratory experiments, but non-negligible amounts of Mn may be lost to low-ionic strength storage solution prior to the start of experiments, or in transport to the field. Storage in solutions with equivalent ionic strength to the field conditions and reduction of

the storage time will minimize this effect, but failure to account for this could lead to an overestimation of the amount of Mn loss via reduction.

Second, *S. oneidensis* MR-1 exhibited an 8 h lag phase in experiments with HMO-doped gels in mini-probes. A possible consequence for field application is that microbial metabolism could require some amount of time to adjust to the newly available oxidant. For this reason, deployment times should allow for the lag time ($\leq$ 8 h) to become insignificant relative to the total deployment time.

Finally, any field application of these gel probes must consider the impact of Mn addition to sediments. In sediments with high organic carbon sediments and high microbial activity but low Mn content, Mn-reducing physiology may be prevalent (Lovley 1991) but not active under ambient conditions. The introduction of HMO-doped gels would then introduce a substrate that was not present in the sediments and the measured rate of reduction based on the HMO-doped gels would represent a potential rate of reduction (rather than the actual rate under ambient conditions). To account for this, solid phase analysis of sediment cores should accompany deployment to show definitively where Mn oxide is exhausted in the sediment. In light of this consideration, this technique may be taken to represent a lower bound (i.e., corresponding to the indirect reduction pathway only) of the potential for Mn reduction (i.e., where the solid substrate is not limiting) in a saturated environment.

Acknowledgements

We would like to thank Dianne Newman, Doug Lies, Tracy Teal, and Alexa Price-Whelan for help in the selection, cultivation, and fluorescence microscopy of *S.*

oneidensis MR-1. Peter Reichert's assistance in working with AQUASIM is also appreciated. We gratefully acknowledge funding from an NSF Graduate Research Fellowship and NSF EAR-0525387, as well as from Eawag.

Chapter 4

A Hydrous Manganese Oxide Doped Gel Probe Sampler for Measuring *In Situ* Reductive Dissolution Rates: II. Field Deployment

Abstract

In situ rates of reductive dissolution in submerged shoreline sediments at Lake Tegel (Berlin, Germany) were measured with a novel hydrous manganese (Mn) oxide-doped gel probe sampler in concert with equilibrium gel probe and sequential extraction measurements. Rates were low in the top 8 cm, then showed a peak from 8 cm to 14 cm, with a maximum at 12 cm depth. This rate corresponded with a peak in dissolved porewater iron (Fe) at 11 cm depth. Below 14 cm, the reductive dissolution rate reached an intermediate steady value. Lower rates at depth corresponded with increases in operationally defined fractions of carbonate-bound and organic- and sulfide-bound Mn and Fe as detected by sequential extraction. Observed rates of reductive dissolution, which reflect a capacity for Mn reduction rather than actual rates under ambient conditions, appear to correlate with porewater chemistry and sequential extraction fractions as expected in early sediment diagenesis, and are consistent with previous measurements of *in situ* reductive dissolution rates. Significant downward advection in

this bank filtration setting depletes the Mn and Fe oxides in the sediments and enhances the transport of dissolved Fe and Mn into the infiltrating water.

Introduction

Biogeochemical processes in lacustrine and riverine sedimentary environments can affect the quality of the neighboring groundwater (von Gunten et al. 1994). During early sediment diagenesis, microbial reactions couple the decomposition of organic matter to terminal electron accepting processes (TEAPs), typically yielding a vertical sequence progressing from high to low energy yield TEAPs with increasing sediment depth (Berner 1980). Among these TEAPs, reductive dissolution of manganese (Mn) and iron (Fe) oxides, via microbially or chemically mediated reduction (Sunda et al. 1983, Burdige and Nealson 1986, Myers and Nealson 1988a, Waite et al. 1988), releases previously bound trace elements to the sediment porewater (Murray 1974, Davranche and Bollinger 2000, Monbet et al. 2008). Nearby groundwater pumping, as in bank filtration, can sustain a flux of organic matter from overlying water into sediments, which drives TEAPs (Wellsbury et al. 1996) and transports both their by-products and released trace elements into the groundwater (von Gunten et al. 1994).

In situ rates of Mn reductive dissolution have been previously approximated with steady-state diagenetic equations coupled to expressions describing solid phase Mn with depth (Robbins and Callender 1975, Burdige and Gieskes 1983, Sundby and Silverberg 1985). The assumed Gaussian shape of the reductive dissolution rate profile in diagenetic models has never been verified with field measurements, due to the lack of an appropriate

high-resolution, *in situ* measurement technique. Otherwise, environmental Mn reductive dissolution rates have been measured in sediment incubations from sediment cores (Canfield et al. 1993) and in an *in situ* bell jar (Balzer 1982), all of whose conditions inevitably differ from or disturb the actual setting. Building on the qualitative *in situ* Mn oxide redox indicator probe developed by Edenborn and Brickett (Edenborn and Brickett 2002, Edenborn et al. 2002) and high-resolution gel-based porewater samplers (Fones et al. 1998, Campbell et al. 2008a), an Mn oxide-doped gel probe has been developed for the quantification of *in situ* reduction rates (Farnsworth and Hering 2010).

Lake Tegel is a small eutrophic lake in northwest Berlin, Germany (Schauser and Chorus 2007), used for recreation and bank filtration for municipal water supply. Wastewater effluent (after secondary treatment) is released into the upstream tributaries of Lake Tegel. Because phosphorus (P) is the limiting nutrient, its release from or retention within the lake sediments affects the water quality of the lake (Schauser et al. 2006). The water extracted from bank filtration wells requires treatment for only Fe and Mn removal currently, but algal blooms in the lake could induce break-through of organic metabolites that would require additional drinking water treatment (Massmann et al. 2007).

The purpose of this study is to evaluate the *in situ* reductive dissolution rates in shoreline sediment at Lake Tegel using a novel Mn oxide-doped gel probe sampler in concert with standard sequential extraction and equilibrium gel probe techniques. Our results will provide new insight into rates of redox processes in an environment that is relevant for both drinking water and groundwater quality in this highly-managed setting.

Materials and Methods

Site description

Lake Tegel is a small lake (mean depth 7.6 m, surface area 3.06 km^2, residence time 77 d) in northwest Berlin, Germany (Figure 4.1). The flow of the Havel River, its southwestern tributary, mostly bypasses the lake, but some local mixing occurs as the lake discharges via this river (ca. 3.5 m^3 s^{-1}) (Schauser and Chorus 2007). Most of the lake is underlain by fine-grained, organic-rich sediments with low hydraulic conductivity (lacustrine sapropel), because of which most of the infiltrating water for bank filtration travels through permeable sand at the lake margins, where water depth is < 2 m (Massmann et al. 2007). All sampling conducted in this study occurred in sands along the eastern bank of Lake Tegel.

Reagents

All chemicals used were reagent grade and used without further purification. All water used was 18 MΩ-cm deionized water (Millipore). Solutions were stored in plastic containers that had been acid-washed in 5% hydrochloric acid. All nitric acid solutions were made with trace-metal-grade HNO_3 (Merck, Suprapur, 65%). All hydroxylamine solutions were made with trace-metal-grade hydroxylamine (Fluka).

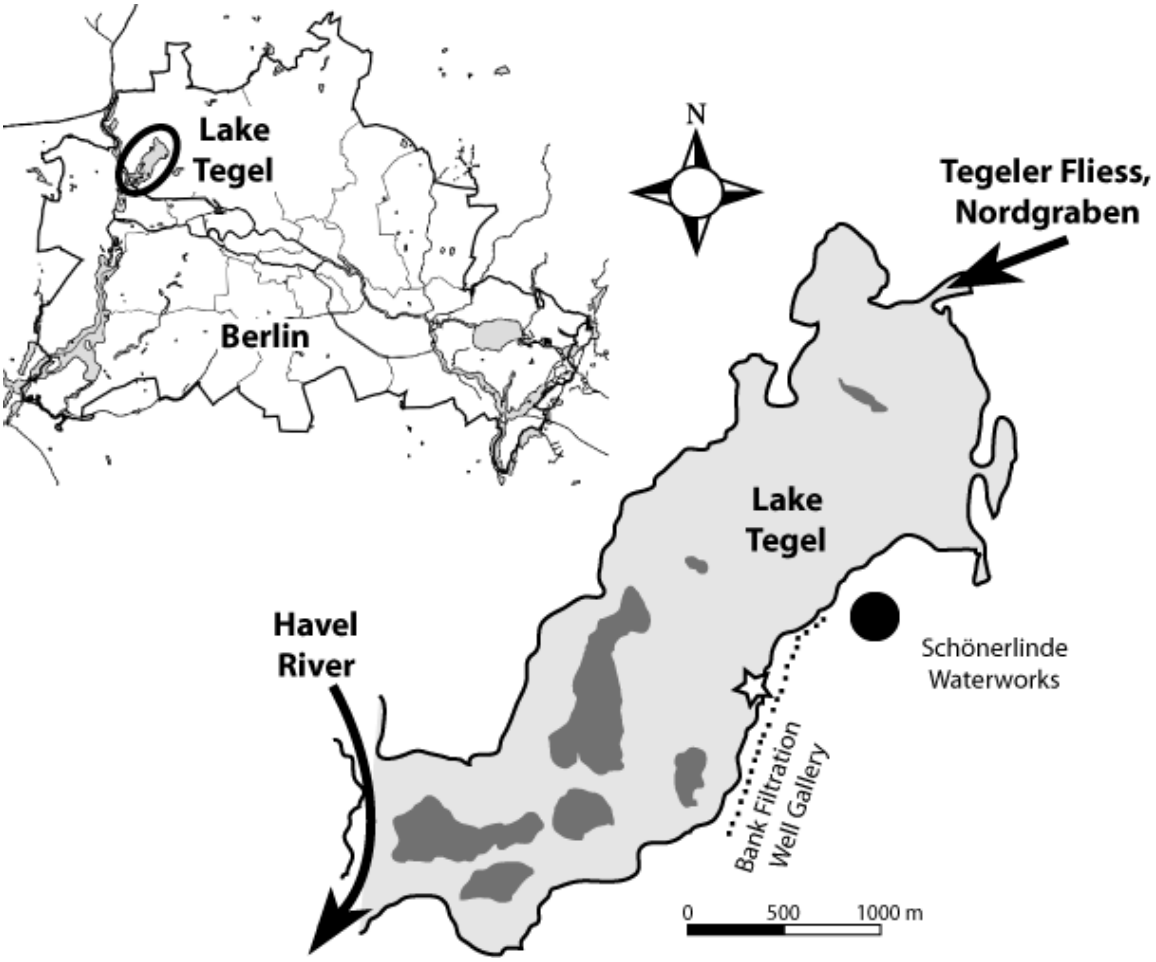

Figure 4.1. Location of Lake Tegel within Berlin city limits (upper left) and location of sampling site (star) within the lake (right; shaded regions indicate islands). Arrows indicate in- and outflows to the lake. Scale bar applies to right figure only.

Gel probe deployment

A complete description of HMO synthesis, clear and HMO-doped gel synthesis, re-equilibration, and analytical methods is provided in Part I (Farnsworth and Hering 2010). Two gel probes 35 cm long (Campbell et al. 2008b) were loaded with clear and HMO-doped gels, respectively. The gel slabs were secured with a 0.45 μm nitrocellulose membrane filter (Whatman, Protran) and held in place with a plastic face plate. The probes were placed in separate aluminum-coated O_2-impermeable polyethylene foil bags filled with deoxygenated water, bubbled with compressed N_2 gas for ≥ 24 h prior to

deployment to deoxygenate the water inside the gels, emptied of water, and welded shut for transport to the field, following Roberts et al. (2010).

The two gel probes were deployed back-to-back 3.75 m from the shore of Lake Tegel in July 2008. The foil bags were cut open on site, and the probes were inserted vertically into the sediments perpendicular to the shoreline, with several gels above the sediment-water interface (water depth 18 cm). The sandy sediments were soft up to 10 cm depth, below which they were hard; gel probes had to be hammered to the final depth of 25 cm. Wind-induced waves approximately 5 cm in height constantly propagated perpendicular to the shoreline, although no evidence of wave-driven sediment movement (e.g., ripples) was observed. Conditions during deployment were overcast, with intermittent light rain, and an average lake water temperature of 21°C (air temperature 18°C). The gel probes were allowed to interact with the sediment porewater for 48 h undisturbed before being extracted from the sediment. The gels were immediately removed from the probes and placed in individual, preweighed 2 ml tubes (Eppendorf), which were stored in ice during transport to the lab.

Upon arrival, the tubes (with gels) were weighed, and 1.25 ml 0.5% hydroxylamine HCl or 2% HNO_3 were added to the HMO-doped and clear gels, respectively. A minimum of 24 h later, these solutions were diluted for ICP-MS (Agilent 7500cx) analysis. The concentrations of Mn (or other solutes) from the gel solution was calculated as described previously (Campbell et al. 2008a).

Gel analysis

The calculation of the apparent rate coefficient for HMO reductive dissolution from HMO-doped gels is complicated by the need to account for the diffusion of dissolved Mn

out of the HMO-doped gel. A one-dimensional partial differential equation describing the dissolved Mn concentration within a gel (i.e., mol Mn per gel porewater volume) over the time of deployment was developed with Mn(II) assumed to be the only significant dissolved Mn species (Morgan 2000):

$$R = \frac{\partial}{\partial t} C_{Mn} = k' \cdot [HMO]_t - D \cdot \frac{\partial^2}{\partial x^2} [Mn(II)] \; . \qquad (4\text{-}1)$$

Here, the rate of change in Mn concentration in a gel (R, μmol ml^{-1} h^{-1}) is expressed as the difference between the rate of Mn(II) production inside the gel (i.e., reductive dissolution of HMO) and the rate of diffusion out of the gel (coefficient D, cm^2 h^{-1}). The chemical kinetics are represented as pseudo-first-order, with units of h^{-1} for k′, the apparent rate coefficient. The porewater outside a gel is considered to be an infinite sink for Mn(II), with a maximum concentration of C_{pw}, the porewater concentration measured by the clear gel at the same depth. [Mn(II)] is 0 within the gel initially, and [HMO] is initially the mean total Mn recovered from a single non-deployed gel (Mn_T), determined using 10–15 gels per batch of HMO-doped gels.

The gels give a measurement of the average rate of Mn loss over the time of probe deployment (R_{meas}): the total Mn (dissolved and solid) recovered from the gels after deployment can be subtracted from Mn_T and divided by the total time of deployment (48 h) (see Figure B.1). Iterating on k′ until the calculated R (R_{model}) is equivalent to R_{meas} gives the k′ for that gel.

A software file (see Appendix B) was developed for MATLAB to solve for k′ efficiently over an entire gel probe. Equation (4-1) was converted to the finite difference form below (equation (4-2)), which approximates the diffusion term via the central

difference theorem. The thickness of each gel (2 mm) was split into 5 equal "cells" (x-axis) for this approximation.

$$C_t^x = C_{t-1}^x + \delta t \cdot \left(k' \cdot HMO_{t-1}^x + \frac{D}{\delta x^2} \cdot \left(C_{t-1}^{x-1} - 2 \cdot C_{t-1}^x + C_{t-1}^{x+1} \right) \right) \quad (4\text{-}2)$$

$$HMO_t^x = HMO_{t-1}^x - \delta t \cdot \left(k' \cdot HMO_{t-1}^x \right) \quad (4\text{-}3)$$

$$R_{model} = \frac{Mn_T - \Sigma HMO_{48h}^x - \Sigma C_{48h}^x}{48\ h} \quad (4\text{-}4)$$

In the software code, C represents Mn(II) only, whereas HMO represents Mn(III,IV) solids, again as mol Mn per porewater volume of the gel (further description of parameters is given within code in Appendix B). In the calculation of R_{model} (equation (4-4)), HMO and C are summed over all 5 cells. The k′ for which R_{meas} - R_{model} is approximately 0 is approached with the secant method, until k'_{i+1} - k'_i = ± 0.05% k'_{i+1} or numerical precision of 3 significant digits for k′. The bounds of the 95% confidence interval for Mn_T are used to calculate error (accuracy) bounds for k′. Area-normalized rates were calculated by dividing R (mol l^{-1} h^{-1}) by the oxide surface area (m^2 g^{-1}), formula weight (g mol^{-1}), and concentration of Mn oxide per volume of porewater in the gel (mol l^{-1}).

Core processing and analysis

Two sediment cores were collected adjacent to the gel probes at the time of deployment, using 32 cm polycarbonate tubes with an internal diameter of 4.8 cm. One core was sliced immediately into 5 cm sections and stored in separate glass jars for porosity and particle-size measurements. The second core was transported on ice to the laboratory, where it was frozen until sequential extraction.

Physical parameters of sediment

Sediment sections from the first core were dried in an oven at 150°C overnight and sieved through a 500 μm sieve to remove large organic debris. Particle size and porosity measurements are detailed in Appendix B (Table B.1 and following). Hydraulic conductivity (K, expressed in cm s^{-1}) was calculated by solving

$$K = k_p \cdot \left(\frac{\rho \cdot g}{\mu} \right) \tag{4-5}$$

where k_p is intrinsic permeability (cm^2), ρ is the density of water (g cm^{-3}), g is the gravitational constant (980 cm s^{-2}), and μ is viscosity (g cm^{-1} s^{-1}). Because our sediment was reasonably well-sorted sand, we can estimate k_p with an empirical relationship presented by Bear (1972):

$$k_p = 0.617 \times 10^{-11} \cdot d \tag{4-6}$$

where d is the mean diameter of sediment particles expressed in μm.

Sequential extraction

In the laboratory, the second core was handled under N_2 in a glovebox for subsequent solid-phase extractions. The core was cut into 3 cm sections, the sediment mixed to homogenize the samples, and 3 samples taken from each section as replicates. The sequential extraction method (Table 4.1) is based upon the Peltier et al. (2005) modification of the Tessier method. The use of 20% H_2O_2, rather than 3.2 M ammonium acetate in 20% HNO_3 (Peltier et al. 2005), in step 4b and the solid-solution ratios were adapted from Ngiam and Lim (2001). For each sample, 2–3 g of wet sediment were transferred into 50 ml centrifuge tubes, followed by the reagents for each step. After each extraction step was completed, the samples were centrifuged at 1900g for 12 min,

and the resulting supernatant was filtered through a 0.45 μm cellulose acetate filter and saved for analysis. Between each reaction step (except between 4a and b), samples were rinsed with 8 ml deionized water, which was saved after a second centrifugation. All steps prior to the organic and sulfide extraction were carried out under N_2 in a glovebox, except the heating portion of step 3, which was carried out in a fume hood with minimal infiltration of O_2 into the reaction vials.

Table 4.1. Experimental conditions for modified Peltier method sequential extraction

step	extractant	target
1	8 ml 1 M MgCl, 1 h	exchangeable
2	8 ml 1 M Na-acetate, pH 5, 5 h	carbonate
3	20 ml 0.04 M hydroxylamine HCl in 25% acetic acid, 6 h at 75 °C	reducible oxides
4a	5 ml 30% H_2O_2 and 3 ml 0.02 M HNO_3, pH 2, 2 h at 75 °C	organics, sulfides
4b	3 ml 30% H_2O_2, pH 2, 2 h at 75 °C	
5	12 ml aqua regia, 24 h then 2 h at 75 °C	residual (nonsilicate)

Samples were diluted with 2% HNO_3 and analyzed by ICP-MS. Element concentrations were converted to percentages of the total amount extracted from the sample, omitting the contributions from silicate-bound minerals not extracted in this method. Concentrations were normalized to the dry weight of the sample, as measured by drying sediment from each core section in an oven for 24 h at 140°C.

Results

The porewater concentrations in Lake Tegel near-shore sediments were low in all tested trace elements except Fe and Mn (Table B.2, Figure 4.2a). Subsequent results and discussion focus on these two redox-active elements. Dissolved Fe was 1–2 orders of magnitude higher in concentration than dissolved Mn throughout the profile. Dissolved

Mn was less than 1 μM in the overlying water (-10 to 0 cm depth) and below the sediment-water interface to a depth of approximately 12 cm, below which the concentration gradually approached 5 μM. Elevated Mn concentrations were observed in two isolated samples at 20 and 22 cm depth. Dissolved Fe, on the other hand, shows a distinct peak between 4 and 18 cm depth, with a maximum of 134 μM at 11 cm. Below the peak, the Fe concentration (15 μM) is still higher than the concentrations (< 1 μM) in the overlying water and in the sediment porewater between 0 and 4 cm depth.

The profile of rate coefficients with depth (Figure 4.2b) also exhibits a distinct maximum at 12 cm. The profile reflects almost no reduction in the overlying water or between 0–1 cm depth in the sediment. The rate coefficients then gradually increase from 0.002 to 0.006 h^{-1} between 1 and 8 cm in depth ("shallow" rate coefficient), at which point a broad peak is observed, extending from 8 to 14 cm depth. The maximum rate coefficient, 0.103 h^{-1}, is two orders of magnitude faster than that at shallower depths. Below 14 cm, the rate coefficient appears to fluctuate around a lower mean of 0.031 h^{-1} ("deep" rate coefficient). Below 22 cm, the rate coefficient decreases to 0.019 h^{-1} at 24 cm depth.

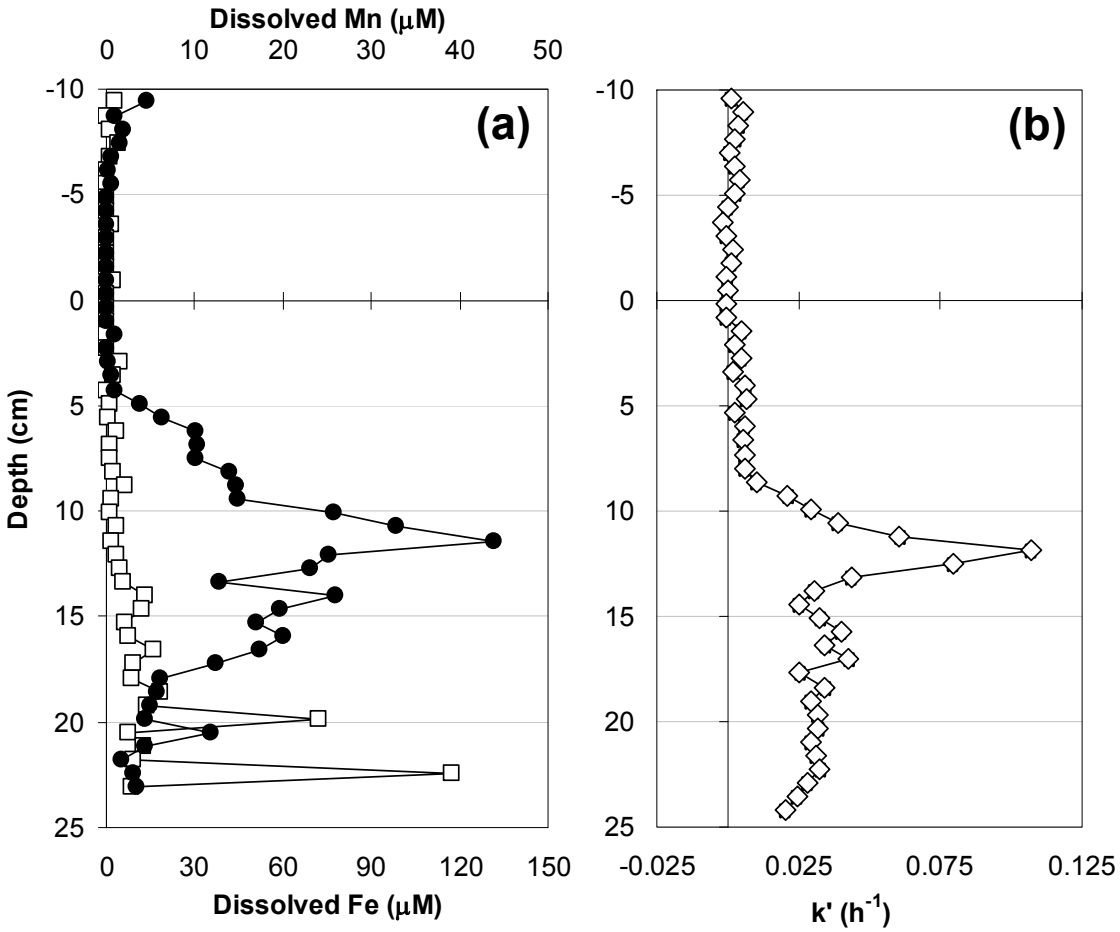

Figure 4.2. Porewater concentrations of dissolved Mn (□) and Fe (●)from clear gel probe (a), and apparent pseudo-first-order rate coefficient k′ (◇) from HMO-doped gel probe (b). Bars representing error bounds for k′ are sometimes smaller than the data markers. The probes were deployed back-to-back for 48 h in July 2008.

The sequential extraction method should recover all Fe and Mn in the sediment except for the silicate-bound fraction. Total recovered Mn ranged between 6 and 32 mg kg^{-1} over 25 cm depth (Figure 4.3). Total recovered Fe was much higher, ranging between 180 and 1100 mg kg^{-1} over the same depth. The highest amounts of both elements were recovered in the 7–10 cm section, with a decline in concentration as the depth increased, except in the 19–22 cm section.

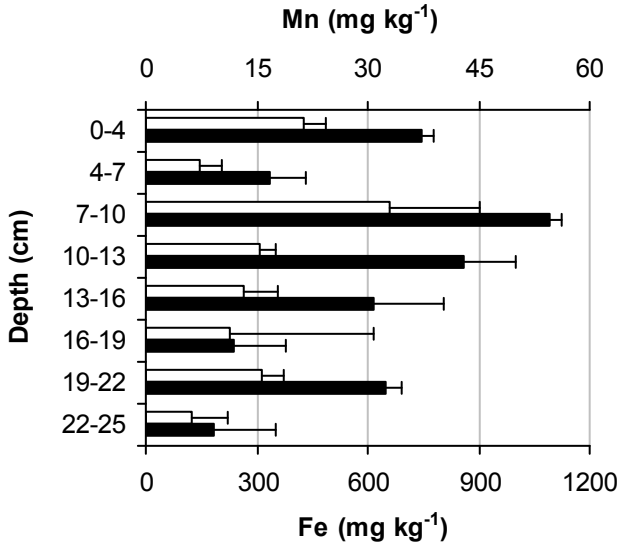

Figure 4.3. Total extracted Mn (white) and Fe (black) from sediment cores in sequential extraction. Bars are averages of 3 subsamples for each core section (standard deviation shown).

Individual, operationally defined fractions of Fe and Mn also varied with depth (Figure 4.4, Figure B.2). Manganese generally had high "exchangeable" fractions at all depths (11–55%), whereas Fe had essentially no "exchangeable" fraction (< 1%). "Carbonate-bound" Mn and Fe fractions were measured at depths greater than 16 cm, and were relatively small (4–16% Mn; < 2% Fe). "Reducible oxides" of Mn and Fe were highest at the surface-water interface, and decreased with depth. For both Fe and Mn, the fraction of "organic- and sulfide-bound" was low at the surface-water interface, increased to a maximum at 13–16 cm depth, and decreased again with depth. The "residual" fraction varied with depth, generally composing 24–78% of the total Fe and a lesser proportion of the total Mn (2–49%).

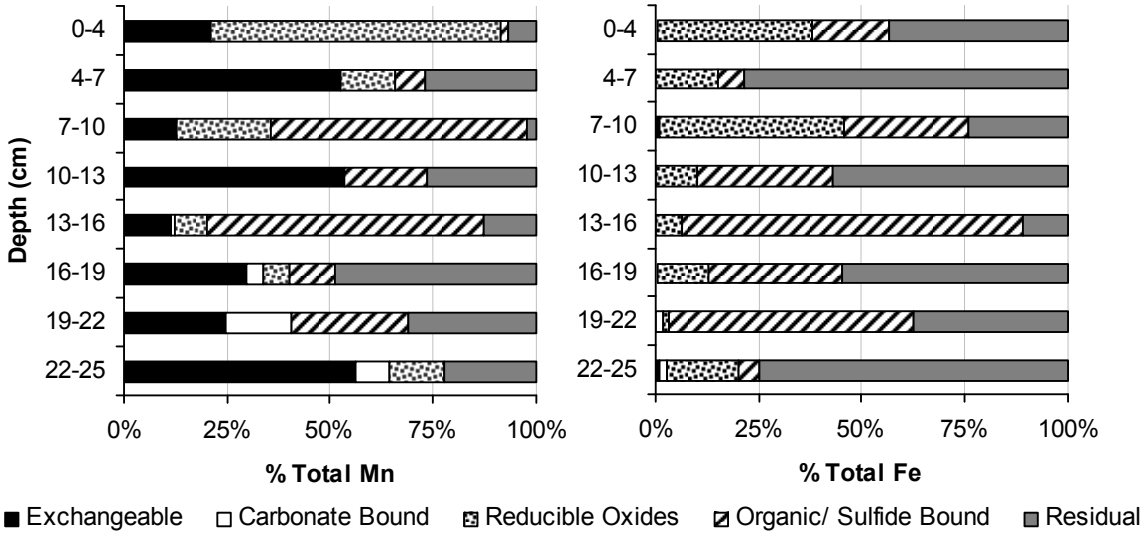

Figure 4.4. Manganese and iron concentrations measured in sediments, expressed as percentage of the total elemental concentration recovered in all 5 sequential extraction steps (given in Figure 4.3). The plotted bars are averages of 3 subsamples for each core section.

Porosity ranged from 0.41 to 0.55 (mean = 0.48) and generally increased with depth (Table B.1). Sediment was sandy, and mean particle size values were generally consistent with the trend in porosity, ranging from 215 to 332 μm (mean of all samples = 294 μm) and generally decreasing with depth, except for the deepest sample (Table B.1). Visual observations suggest that a minor peak in the particle size histograms of sediment samples from deeper core sections (Figure B.3) may result from decomposing organic matter, since varying amounts of fine, black particles were interspersed with coarse, brown sand. These black particles were more numerous in core sections that contained more large organic debris, which was partially decomposed. The temperature of the shallow groundwater sampled in this study was assumed to be equal to the measured lake water temperature, 21°C. Using this temperature, K was estimated to range from 3.90×10^{-2} to 6.71×10^{-2} cm s^{-1} (mean = 5.29×10^{-2} cm s^{-1}; Table B.2), which is similar to the range of a moderately permeable aquifer (Bear 1972).

Discussion

Trends with sediment depth

The variation of the measured reductive dissolution rate coefficients with sediment depth corresponds with indications of expected sediment diagenesis (Berner 1980). The low rates of reductive dissolution in the overlying waters and first cm of sediment likely indicate that microbial respiration is supported by more thermodynamically favorable TEAs (i.e., dissolved oxygen and/or nitrate, which are present in the overlying water at saturation (Massmann et al. 2006) and an average concentration of 280 μM (Ziegler 2001), respectively). As these TEAs are depleted in the upper sediments (i.e., 1–8 cm), dissolved Fe and Mn would then be produced by reductive dissolution. The low porewater Fe concentration above 4 cm could indicate that aerobic or anaerobic Fe oxidative precipitation occurs as the dissolved Fe produced deeper in the sediments diffuses upwards. However, low porewater Fe could also reflect downward advection in these sediments.

The peak in reductive dissolution observed with the HMO-doped gel sampler occurs at nearly the same depth as the peak in porewater Fe. Just above this, the highest amounts of sediment-bound Fe and Mn occur in the 7–10 cm section. The "reducible oxide" fraction of Mn is at a minimum at 10–13 cm, and the corresponding Fe fraction is similarly low between 10 and 16 cm depth. Active reductive dissolution of these solid fractions, as suggested by the facile reduction of introduced HMO, could explain these low fractions. Although sulfide fractions can be prematurely extracted with the "reducible oxide" fraction (Peltier et al. 2005), this artifact is less significant for Mn, because Mn is not appreciably associated with sulfide in freshwaters (Berner 1980).

"Organic- and sulfide-bound" Mn is therefore likely dominated by organic-bound Mn. In contrast, freshly formed amorphous Fe-sulfides are susceptible to premature extraction as "reducible oxides" (Peltier et al. 2005).

Decreasing porewater Fe concentrations below 12 cm indicate that dissolved Fe production is decreasing with depth, sequestration of dissolved Fe is faster than its production, or some combination thereof. The depth profile in HMO reduction (i.e., lower, relatively constant rates below 14 cm) suggests that the production of dissolved Fe may indeed decrease between 12 and 15 cm. More likely responsible for the bulk of the decreasing porewater Fe is greater dissolved Fe sequestration at depth. The appearance of "carbonate-bound" fractions below 16 cm and elevated "organic- and sulfide-bound" Fe fractions between 13 and 22 cm suggest carbonate and sulfide precipitation are prevalent at these depths. "Reducible oxide" fractions at these depths represent either more crystalline, refractory Fe and Mn oxides (Berner 1981, de Vitre et al. 1988, Burdige et al. 1992), or premature oxidation of sulfide-bound Fe (Peltier et al. 2005). Hence, the measured rates of reductive dissolution are consistent with observed sediment processes.

In situ *rates and reductants*

The range of reported Mn reductive dissolution rates is wide, and generally lower than the rates measured in these sediments (Table 4.2). Surface-area-normalized rates either measured or calculated from diagenetic models ranged from 5.4×10^{-11} mol m^{-2} h^{-1} in the equatorial Atlantic Ocean (Burdige and Gieskes 1983) to 1.9×10^{-4} mol m^{-2} h^{-1} in the Gulf of St. Lawrence (Sundby and Silverberg 1985). No clear trends with fresh or saline waters were obvious, nor were rates from diagenetic models significantly different from direct measurements. In contrast, the nutrient load in the water body seemed to be

significant; eutrophic water bodies generally had faster Mn oxide reduction rates in their sediments. The maximum rate from our study was among the faster rates in the literature, within the ranges measured in the Gulf of St. Lawrence (Sundby and Silverberg 1985) and the eastern Danish coast (Balzer 1982). The "shallow" and "deep" rates from our study were mid-range, similar in magnitude to that measured in Long Island Sound (Burdige and Gieskes 1983).

Table 4.2. Surface-area-normalized Mn reduction rates from field studies

Source	Location	Rate[a] (mol m^{-2} h^{-1})	Diagenetic Model	Eutrophic
[1]	equatorial Atlantic Ocean	5.4×10^{-11}	yes	no
	Chesapeake Bay	4.6×10^{-10}	yes	yes
[2]	AMD wetland[b]: shallow	8.4×10^{-8}	no	no
[3]	Lake Michigan	9.2×10^{-8}	yes	no
[2]	AMD wetland[b]: maximum	1.7×10^{-7}	no	no
[4]	North Sea: Skagerrak Basin	$3.2\text{-}16 \times 10^{-7}$	no	no
[1]	Long Island Sound	6.7×10^{-7}	yes	yes
This Study	Lake Tegel: shallow	9.4×10^{-7}	no	yes
	Lake Tegel: deep	7.3×10^{-6}	no	yes
	Lake Tegel: maximum	2.4×10^{-5}	no	yes
[5]	eastern Danish coast	$1.5\text{-}4.9 \times 10^{-5}$	no	yes
[6]	Gulf of St. Lawrence	$1.3\text{-}19 \times 10^{-5}$	yes	yes

[a] See Table B.3 for calculation details.
[b] Constructed wetland to treat acid mine drainage
Sources: 1 Burdige and Gieskes (1983); 2 Edenborn and Brickett (2002); 3 Robbins and Callender (1975); 4 Canfield et al. (1993); 5 Balzer (1982); 6 Sundby and Silverberg (1985)

Ideally, pseudo-first-order rate coefficients obtained in our study could be tied to experimentally derived rate coefficients in literature to help identify the possible *in situ* Mn oxide reductants. The pseudo-first-order rate coefficient (k′) should correspond to the laboratory-derived rate coefficient (k) for a given reductant (Red) as shown in Equation (4-7):

$$k' = k\,[Red] \quad (4\text{-}7)$$

where pseudo-first-order behavior is expected only for approximately constant Red concentrations. Laboratory reduction rate coefficients are available for a variety of reductants with Mn oxide in conditions similar to those at Lake Tegel (freshwater at pH ~ 8 (Massmann et al. 2006)) and are tabulated for probable environmentally relevant reductants (i.e., Fe(II), S(-II), *S. oneidensis* str. MR-1, and humic and fulvic acids) in Table 4.3. In addition, ascorbate, a strong chemical reductant for Mn oxide not anticipated to accumulate significantly in this setting, was added for comparison. Under the three distinct zones of the rate coefficient profile, shallow, maximum, and deep, the amount of Red required to generate the observed pseudo-first-order rate coefficient was calculated ($[Red]_{reqd}$).

These required reductant concentrations are uniformly lower than the measured or estimated concentrations of reductants in Lake Tegel sediments. For example, the rate coefficients for Fe(II) predict that approximately 1 μM Fe(II) could produce the observed maximum pseudo-first-order rate coefficient. However, the actual porewater Fe concentration of 134 μM suggests that the *in situ* rate should be ~ 100× faster. Discrepancies between $[Red]_{reqd}$ and the actual or estimated reductant concentrations are similarly 1–2 orders of magnitude for S(-II), *S. oneidensis* MR-1, and perhaps even humic and fulvic acid. Although preliminary work concluded that HMO-doped gels only capture 35% of microbial reduction due to the lack of direct contact between the cell wall and the Mn oxide, no incomplete measurement was observed for chemical species (Farnsworth and Hering 2010). If the measured pseudo-first-order rate coefficients are accurate, as suggested by the earlier comparison with literature *in situ* reduction rates

(Table 4.2) and preliminary work with Mn-doped gels (Farnsworth and Hering 2010), then the observed and required reductant concentrations suggest that the extrapolation from laboratory to field conditions is not valid for Lake Tegel. This could reflect a limitation of sediment microbial activity by organic carbon or a trace nutrient, as compared to laboratory media optimized for growth.

Table 4.3. Summary of literature values for Mn oxide reduction rate coefficients

Source	Red	log k [units^{-1} h^{-1}]	units	$[Red]_{reqd}$ shallow (-2.40)[a]	max (-0.99)[a]	deep (-1.51)[a]
[1]	Fe(II)	4.97	μM	0.043	1.1	0.34
[2]	Fe(II)	4.92	μM	0.048	1.2	0.37
[3]	Fe(II)	5.66	μM	0.009	0.2	0.07
	Obs rved		μM	30	134	15
[1]	S(-II)	3.66	μM	0.87	22.3	6.71
	Estimated[b]		μM			77
[4]	MR-1[c]	-12.0	cells l^{-1}	3.7×10^{9}	9.6×10^{10}	2.9×10^{10}
[2]	MR-1[c]	-11.8	cells l^{-1}	2.6×10^{9}	6.8×10^{10}	2.1×10^{10}
	Estimated[d]		cells l^{-1}	1×10^{13}	5×10^{12}	1×10^{12}
[5]	Humic Acid	-0.40	mg l^{-1}	.010	0.258	0.077
[6]	Fulvic Acid	-0.30	mg l^{-1}	0.008	0.206	0.062
[4]	Ascorbate	4.18	μM	0.267	6.9	2.07

[a] log (k′ [h^{-1}]) numbers in parentheses
[b] Estimated from maximum sulfate concentrations in Lake Tegel sediments (Schauser et al. 2006)
[c] *S. oneidensis* str. MR-1
[d] Estimated from depth profiles of total cell number in freshwater river mudbank sediment (Wellsbury et al. 1996)
Sources: 1 de Vitre et al. (1988); 2 Burdige et al. (1992); 3 Myers and Nealson (1988a); 4 Farnsworth and Hering (2010); 5 Sunda et al. (1983); 6 Waite et al. (1988)

It is, however, important to bear in mind that the introduction of the HMO-doped gel probe represents a perturbation of ambient conditions. In the case of Lake Tegel sediments, the microbial community is presented with a substrate that is relatively depleted in the ambient sediments. Although the microbial community at some depths may quickly commence Mn reduction, especially in zones of Fe reduction (Blakeney et al.

2000), the community in other zones must acclimate to the given substrate in a relatively short period of time (48 h). Thus the Mn reduction observed with the HMO-doped gel probe corresponds to a capacity for Mn reduction rather than an actual rate under ambient conditions.

Impact of field setting on rates

The sediments at the shoreline of Lake Tegel are not representative of the whole lake, although local homogeneity was observed on the scale of 5–10 m. Chemically, sediments in the lake basin were found to have 30× the Fe content of our shoreline sediments (30 mg kg^{-1} vs. > 1 mg kg^{-1}), as well as higher porewater dissolved Fe and Mn in the top 5 cm (Schauser et al. 2006). Physically, basin sediments are fine-grained lacustrine sapropel with lower hydraulic conductivity than the sandy shoreline sediment (Massmann et al. 2007), which is significant in light of the extensive groundwater pumping adjacent to Lake Tegel (~ 100 m inland; Figure 4.1): the majority of infiltrating water travels through the clogged permeable sands at the lake margins (Massmann et al. 2007). In fact, the lake margins are seasonally perched > 2 m below the sediment-water interface during the summer's low flows and high drinking water demand (Ziegler 2001). Hence, the shoreline setting is more relevant for solute behavior in infiltrating water.

Advection into the groundwater table, while not impacting the calculations of the *in situ* rate coefficients, certainly affects the chemistry of the sediments. The constant reaction of Fe and Mn oxides in the absence of significant input to the sediments leads to their exhaustion, especially in the case of less abundant Mn oxides (von Gunten and Zobrist 1993). In an experimental manipulation, the isolation of ocean basin sediments from particulate input resulted in the exhaustion of Mn oxides in ~ 100 d (Balzer 1982).

The relative lack of "reducible oxides" at and just above (10–16 cm depth) the peaks in dissolved Fe and reduction rate (12 cm) reflects reductive dissolution over a long time scale without comparable Fe and Mn oxide input. Subsequent transport through sediments and aquifer material prevents diffusion of reduced Fe and Mn to oxic regions, where it might be reoxidized. Reduced Mn and Fe thus travel along the bank infiltration flow path, as is typical in eutrophic bank filtration systems (von Gunten et al. 1994).

Acknowledgements

Sarah Griffis, supported by a Caltech Summer Undergraduate Research Fellowship, performed sequential extractions of sediments. Rich Wildman measured sediment particle size and assisted in the assessment of advection at Lake Tegel. We thank G. Massmann and T. Taute for useful site discussions and coordination with the Berlin Waterworks (Berliner Wasserbetriebe). We also thank J. Morgan and J. Adkins for helpful discussions about HMO-doped gel probe deployment and modeling, S. Hug and L. Roberts for assistance with the foil gel probe pouches, R. Saladin, M. Bonalumi, M. Kunz, and A. Müller for assistance with particle size analysis, and M. Huettel for helpful discussions regarding groundwater flow. We gratefully acknowledge funding from Eawag and NSF EAR-0525387, as well as support from an NSF Graduate Research Fellowship.

Chapter 5

Manganese Oxidation Induced by Water Table Fluctuations in a Sand Column

Abstract

On-off cycles of production wells, especially in bank filtration settings, cause oscillations in the local water table, which can deliver significant amounts of dissolved oxygen (DO) to the shallow groundwater. The potential for DO introduced in this manner to oxidize manganese (Mn), mediated by the obligate aerobe *Pseudomonas putida* GB-1, was tested in a column of quartz sand fed with anoxic influent solution and subject to 1.3 m water table changes every 30–50 h. After a period of filter ripening, 100 μM Mn was rapidly removed during periods of low water table and high dissolved oxygen concentrations. The accumulation of Mn in the column was confirmed by XRF analysis of the sand at the conclusion of the study, and both measured net oxidation rates and XAS analysis suggest microbial oxidation as the dominant process. The addition of Zn, which inhibited GB-1 Mn oxidation but not its growth, interrupted the Mn removal process, but Mn oxidation recovered within one water table fluctuation. Thus transient DO conditions could support Mn oxidation, and this process could be more relevant in shallow groundwater than previously thought.

Introduction

Groundwater extracted for drinking water often has manganese (Mn) and iron (Fe) concentrations above the WHO guidelines (Massmann et al. 2007, de Vet et al. 2010). Post-extraction treatment in aerated sand filters is effective in decreasing Mn and Fe concentrations (Mouchet 1992), but it is possible that well operation could promote *in situ* Mn and Fe removal. On-off cycles of production wells in bank filtration sites, for example, cause oscillations in the local water table (Massmann and Sültenfuß 2008). These fluctuations entrap air and deliver O_2 to the shallow groundwater (Beyerle et al. 1999, Williams and Oostrom 2000, Kohfahl et al. 2009).

Subsurface Fe removal exploits this process in (partly) controlled systems: O_2-saturated groundwater is injected into the subsurface to oxidize Fe. Resumption of groundwater extraction from the well leads to Fe(II) sorption to Fe(III) oxides, and upon breakthrough of Fe, another pulse of O_2-saturated groundwater is injected. Succeeding cycles lead to an expansion of the zone of Fe removal and increased efficiency in the process, with no significant clogging (Hallberg and Martinell 1976, Appelo et al. 1999, Mettler et al. 2001). It has been observed at some sites that subsurface Fe removal wells require less frequent rehabilitation than typical extraction-only groundwater wells (van Beek 1985, van Halem et al. 2011).

In comparison with Fe, the kinetics of Mn oxidation by O_2 are much slower and require microbial mediation at circumneutral pH (Morgan 2000, Tebo et al. 2004). The presence of dissolved Fe(II) also precludes significant Mn oxide accumulation, as Fe(II) rapidly reduces Mn oxides (Postma and Appelo 2000). Mn removal in subsurface Fe removal sites is limited (Mettler et al. 2001, van Halem et al. 2011), and often Mn

oxidation is omitted entirely from groundwater geochemical modeling (Thomas et al. 1994, Kübeck et al. 2009).

Nevertheless, the transient oxygen dynamics in well fields, especially bank filtration sites, suggest that the potential for *in situ* Mn oxidation exists, especially with low-Fe groundwater. This study tested whether water table fluctuations, similar in amplitude and frequency to those in a bank filtration site in Berlin, Germany (Massmann and Sültenfuß 2008), could supply enough dissolved oxygen (DO) to oxidize Mn. *Pseudomonas putida* GB-1, an obligate aerobe and well-studied Mn oxidizing bacterium, was selected to colonize a column of quartz sand with anoxic influent, subject to > 1 m water table fluctuations.

Experimental Section

Reagents

All chemicals used were reagent grade and used without further purification. All water used was 18 MΩ-cm deionized water (Barnstead, Nanopure). Solutions were stored in plastic containers that had been acid-washed in 5% hydrochloric acid. All nitric acid solutions were made with trace-metal-grade HNO_3 (Merck Suprapur, 65%).

Bacterial strain, media, and growth conditions

Pseudomonas putida strain GB-1 (generously provided by C. M. Hansel, Harvard University) was grown in Luria Broth (LB) at room temperature (23.2°C) from LB agar plates. In early stationary phase, cells were harvested by centrifugation (20 minutes at

4,000g) and resuspended in MSTG growth medium (Parikh and Chorover 2005) at pH 7.5: 2 mM $(NH_4)_2SO_4$, 0.25 mM $MgSO_4$, 0.4 mM $CaCl_2$, 0.15 mM KH_2PO_4, 0.25 mM Na_2HPO_4, 10 mM HEPES, 0.01mM $FeCl_3$, 0.01 mM EDTA, 1 mM glucose, and 1 mlof trace metal solution (10 mg l^{-1} $CuSO_4 \cdot 5H_2O$, 44 mg l^{-1} $ZnSO_4 \cdot 7H_2O$, 20 mg l^{-1} $CoCl_2 \cdot 6H_2O$, and 13 mg l^{-1} $Na_2MoO_4 \cdot 2H_2O$). For Mn oxidation experiments, 0.1 mM $MnCl_2$ was added to MSTG media. For the column study, 5-l batches of MSTG were filter-sterilized (0.45 μm nitrocellulose, Whatman) and 1 mg l^{-1} NaBr was added to alternate batches, which had no effect on cell growth or Mn oxidation capacity. Growth of all bacteria was carried out with autoclaved or ethanol-rinsed materials under pure culture conditions.

Reduction assays

To determine whether MSTG media and *P. putida* GB-1 were able to reduce Mn oxides, 3 batch experiments with hydrous Mn oxide-doped gels (Farnsworth and Hering 2010) were conducted, with 3 replicates each. Because the microbial cells are physically separated from the Mn oxide inside the gels, the assay could separately account for Mn reduction inside the gel and Mn re-oxidation in solution, outside the gel. 25 ml MSTG medium was added to sterile 50 ml centrifuge tubes. Two of the batches were inoculated with 100 ml GB-1 from a dense (OD_{600} ~ 1.0) LB culture. At t=0, 3 hydrous Mn oxide-doped gels each were added to the non-inoculated batch ("blank") and one of the inoculated batches ("exponential"). All three batches were added to a rotary shaker at 180 rpm at room temperature. After the onset of stationary phase, at t=15 h, 3 hydrous Mn oxide-doped gels were added to the second inoculated batch ("stationary"). At t=64 h, the gels were harvested and the solutions sampled. In both the gels and the solutions,

the remaining Mn was extracted first with 0.05 M $Cu(NO_3)_2$ in 0.05 M $Ca(NO_3)_2$, then with 0.5% hydroxylamine-HCl to give an approximate measure of Mn(II) and total Mn (Warden and Reisenauer 1991). Extracted solutions were filtered (0.2 μm nitrocellulose, Whatman), diluted, and analyzed with ICP-MS (Agilent 7500cx). Solutions were also monitored for OD_{600} at 15 and 64 h. Gel Mn data were analyzed using the MATLAB code provided in the literature (Farnsworth et al. 2010) to estimate the pseudo-first-order rate constants for Mn oxide reduction.

Oxidation assays

At the end of the column experiment, a series of batch experiments were used to compare the oxidizing activity of the column effluent, the column influent, and the GB-1 culture on agar plates at 4°C. 25 ml MSTG medium was added to sterile 50 ml centrifuge tubes. Freshly prepared filter-sterilized medium was added to 4 tubes and degassed column influent solution was added to a fifth tube. 15 μM $ZnCl_2$ and 100 μl column effluent were added to one of the fresh MSTG batches. 100 μl of the column effluent were added to a second fresh MSTG batch, and a third batch was inoculated directly from the GB-1 culture on a refrigerated agar plate. The fourth batch was not inoculated. After 34 h shaken at 180 rpm at room temperature, samples were collected for OD_{600}. Samples of Mn(II) and total Mn (extracted as in reduction assays) were analyzed with ICP-MS.

Column design and flow conditions

Plastic flanges were glued to the ends of an 8-cm-inner-diameter, 1.5-m-length clear PVC pipe (wall thickness: 5 mm). Removable plastic plates were affixed to the flanges with screws, and sealed with a rubber O-ring between the plates and flanges. The influent and

effluent ports were through the plastic plates at top and bottom. In addition, the column was fitted with three side ports (25, 50, and 75 cm from the column base) and a ventilation valve 7.5 cm from the column top. PVC tubing (wall thickness: 2 mm) connected the influent port to a 10-l reservoir and the effluent port to a 3-way splitter open to the atmosphere. In downflow mode, water flowed by gravity into the column, and the height of the splitter controlled the height of the water table inside the column (Figure C.1).

Ten kg uniformly sized quartz sand (Fontaineblau, BDH Prolabo, 0.24 mm average diameter) were slurry-packed in the column and held in place by a plastic mesh (pore size 0.088 mm) lining the bottom plate. The sand filled 122 cm of the column with a porosity of 0.39. The filled column was then flushed in upflow mode with 3.5 l of 5% HCl, followed by > 50 l of 1 mM NaBr solution bubbled with N_2 (99.999%, < 2 ppm O_2) to flush the acid and to remove the oxygen in the column; the side ports and ventilation valve were closed. Once the effluent dissolved oxygen (DO) was < 10%, the column was switched from upflow to downflow, and the influent solution was switched to N_2-sparged MSTG without Mn. At this time, a 0.45 μm nitrocellulose filter membrane (Protran, Whatman) was added between the top plate and the O-ring. The sand was inoculated with 100 ml *P.putida* GB-1 culture (3.2×10^{11} cells l^{-1}) injected in the three ports and added directly through the top of the column. The system was allowed to equilibrate with no flow for 3 h, after which flow of N_2-sparged MSTG with Mn commenced (t = 0).

Flow through the column was maintained at an average of 3.2±1.2 l d^{-1}, or approximately one pore volume per day at the high water level. The visually observed water level inside the column was lowered from approximately 135 cm to 32 cm after

30–50 h by decreasing the splitter height, then raised again after 30–50 h by restoring the splitter height (Figure C.1). The ventilation valve was open to allow air entry in the drained and refilled pore volume. Water table fluctuations with flow continued for 615 h; short flow interruptions (< 2 h) were required to degas fresh MSTG in the influent reservoir. Alternate batches of MSTG included 1 mg l^{-1} NaBr as a tracer to provide a qualitative assessment of the flow through the column over time. After 451 h (4 water table fluctuations), 15 μM $ZnCl_2$ was added to all subsequent influent solution.

The operation of the column was designed to minimize *P. putida* GB-1 taxis into the influent reservoir, as MSTG passed through a 0.45 μm filter and entered the column dropwise, mostly from the middle of the slightly sagging filter. Some MSTG, however, flowed intermittently along the column walls, and over 4 d, the bacteria were able to swim into the filter, most likely along these flow paths; Mn oxide and an opaque precipitate were observed along flow paths after 1 d of flow. Influent filters were therefore changed every 2–5 d when the clogged filters resulted in flow rates < 2.2 l d^{-1}. The absence of DO in the influent solution inhibited significant microbial growth (i.e., no visually observable turbidity), but introduction of air to influent solution from the end of the experiment did yield cell growth (Table C.1).

Sampling and analyses

Samples were taken directly from the base of the column and from the collected effluent. Samples from the column base were analyzed for DO (polarographic DO probe, Thermo Electric) and pH (Ross Sure-Flow, Thermo Electric), and the volume of the collected effluent was volumetrically estimated to calculate the average flow rate. Filtered (0.2 μm cellulose acetate, VWR) and unfiltered subsamples of all effluent samples were diluted

100× with 1% HNO_3 for ICP-MS (Agilent 7500cx). The DO probe was calibrated before each sample; the pH electrode was calibrated daily.

At the end of the column experiment, the column was drained and frozen for 3 days. It was then thawed and the sand removed with a plastic core tube. Vertical sections of the sand (from the top of the column: 2×3.5 cm, 2.5 cm, and 9×12.5 cm in length) and one sample of unused sand were freeze-dried and milled for 90 s at 30 Hz with a ZrO_2 milling set (< 50 μm grain size, Retsch MM400), then pressed into 32 mm pellets for XRF analysis (Spectro XEPOS). A subsample (180 mg) from the top section was thoroughly mixed with 20 mg of wax and pressed into a pellet (diameter: 1.3 cm) for analysis by Mn K-edge X-ray absorption near edge structure (XANES) and extended X-ray absorption fine structure (EXAFS) spectroscopy. Spectra were measured at the XAS beamline at the Angströmquelle Karlsruhe (ANKA, Karlsruhe, Germany). The Si(111) monochromator was calibrated by setting the first inflection point of the absorption edge of a Mn metal foil to 6539 eV. The sand pellet was measured at room temperature in fluorescence mode using a 5-element Ge solid state detector. Spectral data processing and linear combination fitting (LCF) were performed using the software code Athena (Ravel and Newville, 2005). The XANES spectrum was evaluated from 6530 to 6640 eV; the EXAFS spectrum from 2 to 10 $Å^{-1}$ (k-range relative to E_0 of 6550 eV). Reference spectra for LCF included aqueous Mn^{2+} (100 mM $Mn(NO_3)_2$; measured at SUL-X beamline at ANKA), δ-MnO_2 and hexagonal birnessite (phyllomanganate reference spectra from literature (Webb et al. 2005), kindly provided by Sam Webb, SSRL).

Data analysis

Hydraulic conductivity during the experiment was calculated with the Darcy equation:

$$K = v_D \frac{L}{\Delta H} \tag{5-1}$$

where K is the hydraulic conductivity, v_D is the Darcy velocity equal to the volumetric flow rate divided by the cross-sectional area, L is the column length, and ΔH is the head difference between the column water level and the effluent splitter. The dispersion coefficient of the column was estimated from Br breakthrough with pulsed inlet concentration (Figure C.2). Smooth breakthrough curves at constant water levels (i.e., 0–48 h, 190–234 h, 239–270 h, 326–358 h, and 560–592 h) were modeled in CXTFIT (Toride et al. 1995) to solve for the dispersion coefficient, D. Pseudo-first-order Mn removal rates were estimated from the 1-D advective-dispersive transport equation:

$$\frac{\partial C}{\partial t} = D\frac{\partial^2 C}{\partial x^2} - \frac{v_D}{\varphi}\frac{\partial C}{\partial x} - kC \tag{5-2}$$

where C is the dissolved Mn(II) concentration, D is the dispersion coefficient, φ is the porosity, and k is a pseudo-first-order removal rate. Solving for local minima in C(t), with a Peclet number >>1 (advection dominates dispersion), this equation simplifies to:

$$\frac{\partial C}{\partial t} = -\frac{v_D}{\varphi}\frac{\partial C}{\partial x} - kC = 0 \ . \tag{5-3}$$

Integration over the column length yields the following expression for k:

$$k = -\frac{v_D}{\varphi \cdot L}\ln\frac{C}{C_0} \tag{5-4}$$

where C/C_0 is the value at the local minimum. Damköhler numbers, which assess the ratio of a reactive flux to advective flux, were calculated with this expression (Battersby et al. 2006):

$$Da = \frac{k \cdot C \cdot V}{Q \cdot C} \tag{5-5}$$

where k is the pseudo-first-order rate coefficient [h^{-1}], V is the column volume [l], and Q is the volumetric flow rate [l h^{-1}]; the Mn concentration, C, cancels out from the top and bottom of equation (5-5). For Da > 3, a reaction can be assumed to reach completion.

Results and Discussion

Water table fluctuations and dissolved oxygen

Over 615 h, the water table inside the column was oscillated 6 times from a high water level to a water level approximately 1.3 m lower and back to the high water level (Figure 5.1a); for clarity of description, one "fluctuation" or "oscillation" refers to a complete high-low-high water table cycle. The level of wetted sand was visually estimated to be ~ 32 cm above the column base, but the actual water table was calculated to be < 5 cm based on the hydraulic conductivity of the column (calculated at the high water level). For sand with a 0.22 mm grain diameter and a porosity of 0.39, a 30 cm capillary fringe height is reasonable (Lohman 1972). The hydraulic conductivity varied between 0.005 and 0.017 cm s^{-1} with no significant trend during column operation.

Air entered the unsaturated pore spaces when the water table was low, and was potentially entrapped when the water table was raised. The anoxic column influent acquired DO as the solution percolated downward through the unsaturated sand (maximum effluent DO of 3.6 mg l^{-1} = 42% saturation at 23.2°C), but did not acquire significant amounts of DO (< 1 mg l^{-1}) when the water table was high. Effluent DO levels are "net" DO concentrations, which reflect oxygen mass transfer from the gaseous phase to the dissolved phase as well as DO consumption by microbial respiration; the

actual dissolved oxygen delivered to the aqueous phase is unknown. Some early problems with leaks through the side ports, as seen in the sharp drop in water level around 100 h, did not significantly affect DO dynamics.

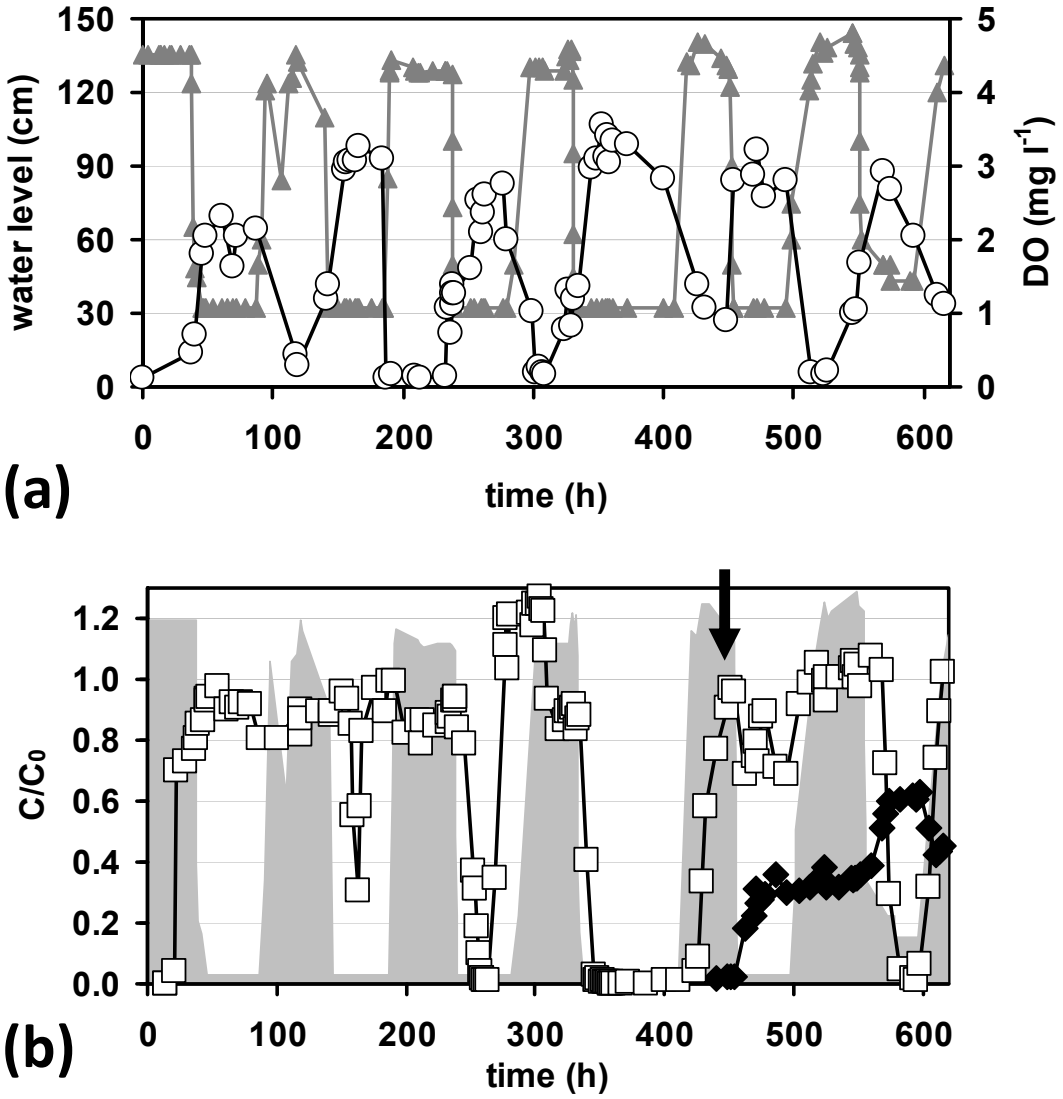

Figure 5.1. (a) Changes in the visible water level in the column (▲) and the effluent dissolved oxygen (○) over time. (b) Filtered relative effluent concentrations of Mn (□, C_0 = 100 μM) and Zn (◆, C_0 = 15 μM). The arrow denotes the addition of 15 μM Zn to the influent. For reference, the water level in the column is shown in the shaded profile (note the vertical scale is different than (a)).The residence time of the column was approximately 16.3 h.

Manganese removal and filter ripening

After Mn uptake in the column in the first 1–2 pore volumes of influent (t < 30 h), Mn removal from the column influent coincides with lower water levels, beginning 42 h after the first water table decrease (Figure 5.1b). The onset of Mn removal occurs 16, 8, and 4 h after the subsequent water level decreases (Table 5.1). The duration of the Mn removal also increases with 3 subsequent water level fluctuations, from approximately 14 h to 76 h in the fourth oscillation. Furthermore, the Mn removal increased to > 99% by the third oscillation. Estimated pseudo-first-order rate constants also increase with the first 4 oscillations (see further rate discussion below). These parameters are all indicative of "filter ripening" processes, which are typical in water and wastewater treatment sand filters (Frischherz et al. 1985, Mouchet 1992). Two regions of Mn washout ($C/C_0 > 1$) at 280 h and 513 h are likely a release of adsorbed Mn(II) in the column after a 10% decrease in influent Mn concentration due to inter-batch heterogeneity of MSTG medium.

Table 5.1. Mn removal parameters for each water table oscillation

oscillation	lag phase (h)	duration of removal (h)	minimum C/C_0	pore velocity cm h^{-1})	k (h^{-1})	Da[a]
1	42	14	0.804	7.2	0.01	0.22
2	16	10	0.309	6.1	0.06	1.2
3	8	24	0.009	6.2	0.24	4.7
4	4	76	0.002	7.3	0.37	6.2
5[b]	28	17	0.688	7.5	0.02	0.41
6	19	29	0.011	6.5	0.24	4.5

[a] Damköhler number, the ratio of reactive flux to advective flux
[b] 15 μM $ZnCl_2$ was added to the influent at the beginning of this oscillation.

As low water levels enhanced oxygen delivery to the aqueous phase, Mn removal at low water levels is consistent with Mn oxidation. Elevated DO was present in the effluent during the periods of greatest Mn removal. This is expected, since the column was

colonized with *P. putida* GB-1, an obligate aerobe whose ability to oxidize Mn is oxygen-dependent (Okazaki et al. 1997). In batch studies, *P. putida* GB-1 commences Mn oxidation at the end of exponential phase, approximately 12 h after inoculation in MTSG at 30°C (Parikh and Chorover 2005). Orange-brown precipitates were visible on the sand at the top of the column after 44 h, and with subsequent water table fluctuations, they increased in spatial extent. XAS with linear combination fitting analysis further confirmed that the Mn in the topmost part of the column at the end of the experiment was Mn(IV) oxide (spectral combination of hexagonal birnessite and δ-MnO_2) with ca. 20% adsorbed Mn(II) (Figure C.3, Table C.2). XAS studies suggest *P. putida* MnB1, which is closely related to GB-1, and *Bacillus* sp. SG-1 produce similar Mn oxides (Villalobos et al. 2003, Webb et al. 2005). Therefore, filter ripening processes for Mn removal may be related to the development of an active zone of Mn oxidation.

Microbial biofilm growth and physiological adaptation to the column conditions likely contribute to the filter ripening, or enhanced Mn removal over time. Common in groundwater (DePalma 1993) and closely related to a strain isolated from Mn-oxide encrustations on water pipes (MnB1) (Caspi et al. 1998), *P. putida* GB-1 forms biofilms attached to negatively charged surfaces (like silicates). Mn oxidation subsequent to attachment does not interfere with adhesion (Parikh and Chorover 2005), although it does result in a Mn oxide coating of the cell walls; complete coating of actively oxidizing microbial surfaces may account for the sharp increases in effluent Mn during filter ripening. Based on the appearance of planktonic cells (and in some cases, biofilm and Mn oxides) in the column effluent, the initial inoculation of *P. putida* GB-1 quickly (< 60 h) spread through the sand column. The absence of biofilm and Mn oxides observed in

the collected effluent after three water table fluctuations suggests that the biofilm in the column became less susceptible to washout over time. *P. putida* mt-2, a weak Mn oxidizer related to GB-1 (Francis and Tebo 2001), survived 24 h periods of anoxia in batch experiments by up- and down-regulating gene expression based upon DO availability (Martinez-Lavanchy et al. 2010), further suggesting microbial adjustment to the column conditions was a critical component of filter ripening.

The addition of 15 μM Zn at the beginning of the fifth water table oscillation (451 h) interfered with the Mn removal process (only 31% removal). Although already present in MSTG at a low concentration (150 nM), 15 μM Zn in the medium inhibited microbial Mn oxidation; cell growth was slightly enhanced (Table C.1). The lag phase for removal increased from 4 h to 28 h, and the duration of removal decreased from 76 h to 17 h (Table 5.1). Nevertheless, 99% Mn removal was restored within one water table oscillation, with a lag phase of 19 h and a 29 h duration of removal. The estimated pseudo-first-order rate constant similarly recovered to that of oscillation 3 (0.24 h^{-1}), all despite the continued presence of Zn.

The Mn and Zn content in the column solids at the end of the experiment (Figure 5.2) lead to one possible mechanism of microbial adjustment to the presence of Zn: the physical separation of Zn removal and Mn removal zones. The Mn concentration had a steep gradient from 210 mg kg^{-1} at the top of the column to 9 mg kg^{-1} in the 63–75 cm section, for an accumulation zone of approximately 60 cm. Mn was above the 6 mg kg^{-1} sand background throughout the profile, and the total Mn accumulation (XRF data, 2.42 mmol) was in excellent agreement with the total Mn removal from solution ($C/C_0 \times Q$, 2.46 mmol). Zn also had a steep gradient from 8 mg kg^{-1} at the top of the column to < 2

mg kg^{-1} in the 100–113 cm section, for an accumulation zone of approximately 22 cm. Below the accumulation zone, Zn was ≤ 1.5 mg kg^{-1}, the sand background. Zn accumulation (48 μmol) was in acceptable agreement with the total Zn removal from solution (93 μmol), considering that the Zn data approached the XRF practical quantitation limit (~ 1 mg kg^{-1}) and that the initial flush of acid through the column may have resulted in lower initial Zn in the column than measured in the unused (background) sand. A steep gradient in solid-phase P, perhaps indicative of biofilm, was also measured (Figure C.4), whereas Br was constant with depth (not shown, 0.3 mg kg^{-1}). Thus, it is possible that Zn was adsorbed to older Mn oxides or biofilm material in the first cm of sand, then new Mn was oxidized below this zone. Micro-scale zonation is also possible. The lack of Zn breakthrough (maximum $C/C_0 = 0.63$, Figure 5.1b) suggests the combined sorption capacity of the sand, Mn oxide, and biofilm was not reached.

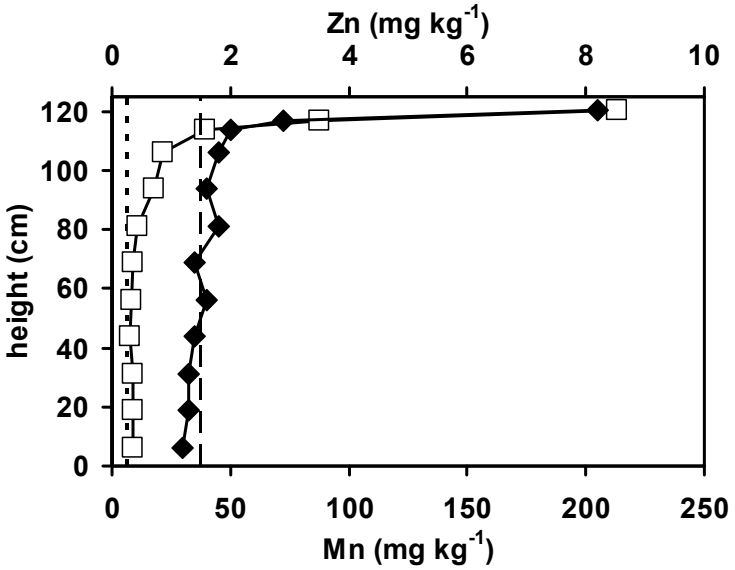

Figure 5.2. XRF profile of Mn (□) and Zn (◆) along the column at the end of the experiment. Dashed lines indicate the background Mn (short dashes) and Zn (long dashes) of unused sand. The plotted height is the average of the vertical section.

Rates of Mn removal

Mn removal rates were estimated with 1-D advective-dispersive transport and a pseudo-first-order sink term. The dispersion coefficient in the column was between 1 and 7 cm^2 h^{-1}, which corresponded to Peclet numbers between 120 and 700. For Pe >>1, the dispersion term in the transport equation could be omitted. For the minima in C vs. t $\left(\frac{\partial C}{\partial t} = 0\right)$, pseudo-first-order Mn removal rates then depended only on $C/C_{0,\,min}$, the length of the column, and the pore velocity (Table 5.1). These rates serve merely as a lower bound for the rate constant responsible for the decrease in C/C_0, since only for oscillation 4 was steady state clearly reached (Figure 5.1b). Furthermore, the minimum measurable value of C/C_0 was 0.001, based on the practical quantitation limit of the ICP-MS (0.9 nM) and 100-fold sample dilution. The Damköhler numbers for these rates ranged from 0.2 to 6.2, which suggests that for low rates in oscillations 1, 2, and 5, the advective flux prevented the removal reaction from reaching completion. Otherwise, the rates in the column were not limited by flow conditions.

Manganese removal in the column is a net effect of multiple processes including abiotic reduction and oxidation by the microbial medium, microbial oxidation and reduction, and oxide-catalyzed oxidation. Photoreduction of Mn is assumed to be insignificant in the sand column (Xyla et al. 1992). Mn adsorption to oxide surfaces has a reported (Davies and Morgan 1989) half-life of 5 min, which is insignificant on the multi-hour time scales of Mn removal; sorption to biofilm components is assumed to be similarly rapid. Mn-oxide-doped gels were used to assess the ability of the microbial medium and *P. putida* GB-1 to reduce Mn. Pseudo-first-order rate constants were 0.003

h^{-1} and 0.005 h^{-1} for the medium alone and the medium with cells, respectively (Table C.3). These rate constants are in the range of O_2- and nitrate-reducing sediments (< 8 cm depth) in a German lake, measured with the same gel technique (Farnsworth et al. 2010). Oxidation by the microbial medium was insignificant (Figure C.5).

Below pH 9, abiotic oxidation rates are generally slow compared to microbial oxidation rates (Morgan 2005). The effluent pH varied between 6.35 and 7.55, despite a constant influent pH of 7.5 (Figure C.6), which further suggests that abiotic oxidation rates were irrelevant. Estimates of homogeneous (Morgan 2005) and surface-catalyzed (by both quartz sand (Davies and Morgan 1989) and Mn oxide (Morgan 2000)) Mn oxidation at pH 7 with full oxygen saturation indicate that abiotic oxidation is a minor contribution to the observed net oxidation rates (Table 5.2). Despite a large quantity of sand available to oxidize Mn, its low surface area (0.01 m^2 g^{-1} estimated for spherical grains) and low adsorption of Mn(II) at circumneutral pH result in a rate 3 orders of magnitude lower than the lowest observed rate. Further details on the rate calculations are available in Appendix C.

Thus the net observed oxidation rates (1–37 μM h^{-1}) are assumed to derive almost entirely from microbial oxidation. Although not directly confirmed at the end of the experiment, *P. putida* GB-1 is assumed to be the only microorganism in the column (Table C.1). In shaken containers with dense (ca. 10^{12} cells l^{-1}) cultures, *P. putida* GB-1 has been shown (Okazaki et al. 1997) to oxidize Mn as fast as 240 μM h^{-1}. *Leptothrix discophora* SS1, another common Mn-oxidizing aerobe, oxidized Mn at rates up to 390 μM h^{-1} under the same batch conditions (Boogerd and de Vrind 1987). That these rates were measured in undefined Lept medium, which contains 0.5 g l^{-1} each of yeast extract

and Casamino acids, accounts for some enhancement relative to the observed rates in defined minimal MSTG medium.

Table 5.2. Potential rates of Mn oxidation and reduction in the column

oxidation	homogeneous (Morgan 2005)	2×10^{-5} μM h^{-1}
	SiO_2-catalyzed (Davies and Morgan 1989)	2×10^{-3} μM h^{-1} [a]
	Mn oxide-catalyzed (Morgan 2000)	0.03 μM h^{-1} [b]
	P. putida GB-1 (Okazaki et al. 1997)	240 μM h^{-1} [c]
	Leptothrix discophora SS1 (Boogerd and de Vrind 1987)	390 μM h^{-1} [c]
reduction	MSTG	0.3 μM h^{-1}
	MSTG + *P. putida* GB-1	0.5 μM h^{-1}
net observed oxidation rate	oscillation 1 (minimum)	1 μM h^{-1}
	oscillation 4 (maximum)	37 μM h^{-1}

[a] Rate assumes oxidation occurs throughout the column with 100% DO saturation.
[b] Rate uses the average final solid phase Mn (20 mg kg^{-1}) throughout the column with 100% DO saturation.
[c] Rate measured for ca. 10^{12} cells l^{-1} in Lept medium (Boogerd and de Vrind 1987) with 100% DO saturation

Two additional factors that contribute to the slower measured rates are the pH and dissolved oxygen. General bacterial cell physiology may lead to the accumulation under anaerobic conditions of metabolites, which can then deliver protons upon reintroduction of oxygen (Balcke et al. 2004). The general inverse trend of pH and DO (Figures 5.1a and C6) suggests this may be the case. For *L. discophora* SS1, the maximum oxidation rate occurs at pH 7.5, with a steep decline to 30% of the maximum rate (Zhang et al. 2002) or no oxidation at all (Boogerd and de Vrind 1987) at pH 6.5. On the other hand, pH decreases were observed during both growth of *L. discophora* and Mn oxidation (the latter is predicted from stoichiometry as well) (Boogerd and de Vrind 1987), so it is difficult to assess if the observed pH dynamics are merely a by-product of microbial

growth and oxidation in the top cm of the column or if they actively limited a large portion of the microbial community.

Experiments with varying delivery rates of DO to GB-1 batch cultures revealed a strong dependence of Mn oxidation rate on the measured DO in late logarithmic phase (Okazaki et al. 1997). Although its growth was unaffected by DO concentrations between 10–25% saturation (20°C), Mn oxidation required DO > 14% in late logarithmic phase. The DO concentrations in that study reflect a balance between the delivery rates (enhanced by variable shaking speed) and microbial consumption, not an absolute cutoff in oxygen concentration for Mn oxidation; even under rigorous shaking, the DO concentration in early- to mid-logarithmic phase was nearly zero (Okazaki et al. 1997). Generally, in the presence of oxygen-consuming processes, oxygen mass transfer across the air-water interface is enhanced (Haberer et al. 2011); this is expected in the column as well. Interestingly, the maximum oxidation rate in early stationary phase corresponded with a DO of approximately 27% saturation (2.5 mg l^{-1}) (Okazaki et al. 1997), which is similar to the highest measured DO in the column effluent (3.6 mg l^{-1}). Literature studies of *P. putida* species that aerobically biodegrade organics similarly show decreasing degradation rates proportional to DO exhaustion, which rapidly recover upon reintroduction of oxygen (Balcke et al. 2004, Bauer et al. 2009, Martinez-Lavanchy et al. 2010). Thus, the fluctuation of DO levels in the column between < 1 mg l^{-1} and 3.6 mg l^{-1} (maximum) inhibited the microbial Mn oxidation rate, relative to those measured in fully oxygenated batches.

Implications for groundwater systems

The downflow setup, necessary to prevent *P. putida* taxis into the influent solution, limited the amount of air entrapment possible. This arrangement is more similar to rain percolation than to water table fluctuations in the field, for which rising water levels are expected to derive from lateral or upward water flux. Although the Peclet number and the frequency and amplitude of the water table fluctuations (Massmann and Sültenfuß 2008) were chosen to be representative of bank filtration sites in Berlin, Germany, the microbial medium and microbial community are not representative of field conditions. High amounts of phosphate (0.4 mM) and organic carbon (180 mg l^{-1} glucose) are unlikely in uncontaminated shallow aquifers; even numerical dominance of *P. putida* species in soils generally means < 14% of culturable microbes (DePalma 1993). The purpose of this study, however, was to test whether the DO supplied by water table fluctuations is sufficient for Mn oxidation. Complete removal of 100 μM Mn(II) was indeed possible with the supplied DO; this Mn concentration is ten times higher than groundwater Mn concentrations considered to be problematic (or at least, which require treatment post-extraction) in Berlin (Massmann et al. 2008b) and Fredericton, Canada (Thomas et al. 1994). In general, Mn oxidation and transient DO concentrations are largely ignored in groundwater geochemical modeling (Thomas et al. 1994, Kübeck et al. 2009), but this study suggests that Mn oxidation in shallow groundwater could be more relevant than previously thought.

Key aspects that could affect the presence of a Mn oxidation zone in shallow groundwater include the source of the Mn(II), the depth of DO penetration, the depth of microbial Mn-oxidizing activity, and the amount of time for the microbial community to

adjust to the available Mn. Vertical zonation of bank filtrate has been previously observed (Massmann et al. 2008b), and if the Mn(II) is present below the depth of DO penetration and/or microbial Mn-oxidizing activity, very little *in situ* Mn oxidation potential exists. Microbial communities in sand filters for Mn removal require a notoriously long time (≥ 8 weeks) for startup (Frischherz et al. 1985, Mouchet 1992), and Fe^{2+} and ammonium interfere with Mn-oxidation (Frischherz et al. 1985, Katsoyiannis and Zouboulis 2004, de Vet et al. 2010). Even under ideal conditions, water treatment processes may still provide greater efficiency and faster rates than *in situ* Mn oxidation; removal rates in this study were 100× slower than those for aerated groundwater treatment columns with beads coated in Mn oxides and a mixed *Gallionella* and *Leptothrix* biofilm community (1044 μM h^{-1}) (Katsoyiannis and Zouboulis 2004). Furthermore, massive microbial growth and Mn oxide formation in the aquifer could lead to clogging, although no significant change in hydraulic conductivity was observed in this study. Nevertheless, engineering studies with longer time horizons and larger-amplitude and less frequent water table oscillations, which would deliver more oxygen to the shallow groundwater, could perhaps optimize the *in situ* oxidation process to provide intransient Mn removal.

Acknowledgements

We acknowledge financial support from Eawag, an NSF Graduate Research Fellowship, and NSF EAR-3 0525387. Colleen Hansel and Deric Learman (Harvard University, Boston, USA) generously provided *P. putida* GB-1 and assisted in its cultivation. Andreas Voegelin performed all XAS analysis. We acknowledge the Angströmquelle

Karlsruhe (ANKA, Karlsruhe, Germany) for the provision of beamtime at the XAS and SUL-X beamlines and thank Stefan Mangold, Jörg Göttlicher, and Ralph Steininger for their assistance during data collection. Sam Webb (Stanford Synchrotron Radiation Laboratory, Menlo Park, USA) is acknowledged for kindly providing reference XAS spectra for different Mn-oxides.

Chapter 6

Mn and Fe dynamics in the shallow groundwater adjacent to Lake Tegel, Berlin, Germany

Abstract

Water table oscillations due to on-off pump cycles in well fields have the potential to introduce dissolved oxygen into the shallow groundwater. As presented in Chapter 5, this amount of dissolved oxygen is sufficient to oxidize manganese (Mn), and presumably iron (Fe), in laboratory-scale experiments. In this study, we looked for evidence of Mn and Fe accumulation in shallow aquifer sediments adjacent to a bank filtration production well. However, XRF analysis of sediments showed no significant accumulation of Mn or Fe as a function of depth. The Mn sorption capacity of the deep aquifer sediments was relatively low as determined in sorption experiments with Mn-spiked artificial groundwater. Sorbed Mn concentrations under ambient conditions were estimated, on the basis of sorption experiments, to be between 7 and 16% of the total Mn concentration determined by XRF. Although XAS analysis of sediments revealed a slight increase in the relative proportions of Mn(II) and Fe(II) with depth, both elements' solid-phase speciation was dominated by clay- and primary-mineral-associated fractions, suggestive of the sediment background. The lack of evidence for *in situ* oxidation at this borehole suggests a chemical or hydrological inhibition of the oxidation process.

Introduction

In bank filtration, groundwater is extracted from a well near a river or lake. This induces infiltration from the surface water body, thereby improving the quality of water recovered and making it more consistent. Manganese (Mn) and iron (Fe) can be released into bank filtrate along its flow path to the production well to an extent that necessitates drinking water treatment after extraction (de Vet et al. 2010). In Berlin's bank filtration well fields, this involves aerated sand filtration (Massmann et al. 2007). Berlin's bank filtration well fields are also subject to well clogging, which is remediated by occasional injection of H_2O_2 pulses to remove Fe- and/or Mn-oxidizing biofilms from the well screen. Anecdotal evidence from observation boreholes suggests that Mn oxidation can also occur in the aquifer sediments adjacent to production wells. The conditions under which this occurs are unknown (C. Menz, personal communication).

Bank filtration sites with $\geq$ 1 m water table fluctuations at least every 2 days entrap sufficient air to oxidize Mn in the presence of a mature Mn-oxidizing community (Chapter 5). Bank filtrate in Switzerland was estimated to contain an excess of ~ 10% air due to entrapment of bubbles during flow with an oscillating water table (Beyerle et al. 1999). Excess air estimates in Berlin suggest that similar amounts of air entrapment occur at Lakes Tegel and Wann bank filtration sites, although significantly more air entrapment occurs at an artificial recharge basin adjacent to Lake Tegel (Massmann and Sültenfuß 2008). Modeling shows that air entrapment from water table fluctuations likely dominates dissolved oxygen delivery in bank filtrate (Kohfahl et al. 2009). Air entrapment in Berlin bank filtration sites thus affects dissolved oxygen delivery to the

shallow subsurface, and could be responsible for the development of Mn oxide layers adjacent to production wells.

To search for evidence of *in situ* Mn oxidation, aquifer sediment samples were collected from an observation well borehole adjacent to a bank filtration production well at Lake Tegel, Berlin, Germany. The production well is between the lake shore and an artificial recharge pond, and its high water level fluctuates between 5 and 12 m below the ground surface. Depth-averaged sediment samples were taken in 1 m increments from 5 to 25 m below the ground surface to look for gradients in Mn and Fe concentrations and speciation that would reflect a gradient in the dissolved oxygen delivered to the shallow groundwater.

Experimental Section

Sample collection

Samples were collected from a well borehole 3 m inland of production well 18 of the Hohenzollernkanal well gallery, south of Lake Tegel, Berlin, Germany (Figure 6.1). Production well 18 is 40 m deep, screened between 20 and 37 m. The aquifer sediments at those depths are Pleistocene, porous, glaciofluvial and fluvial mainly fine- to medium-sized sands of the Saale and Weichsel glaciation. Below 40 m, a continuous organic-rich clay aquitard of the Holstein interglacial period limits the infiltration of the ambient deep groundwater (Massmann et al. 2007). As of March 2010, production well 18 had been in operation only 2 years, replacing an older well that was removed from service.

The sample borehole was drilled with a gauge driller, using ambient groundwater as drilling fluid and yielding 1 m depth-averaged samples. The samples were necessarily disturbed, and further, the drilling equipment had a rusty exterior. Upon removal from the borehole, sediments (5–25 m) were collected in sealed acid-washed plastic bags and stored on ice until they were frozen in the lab.

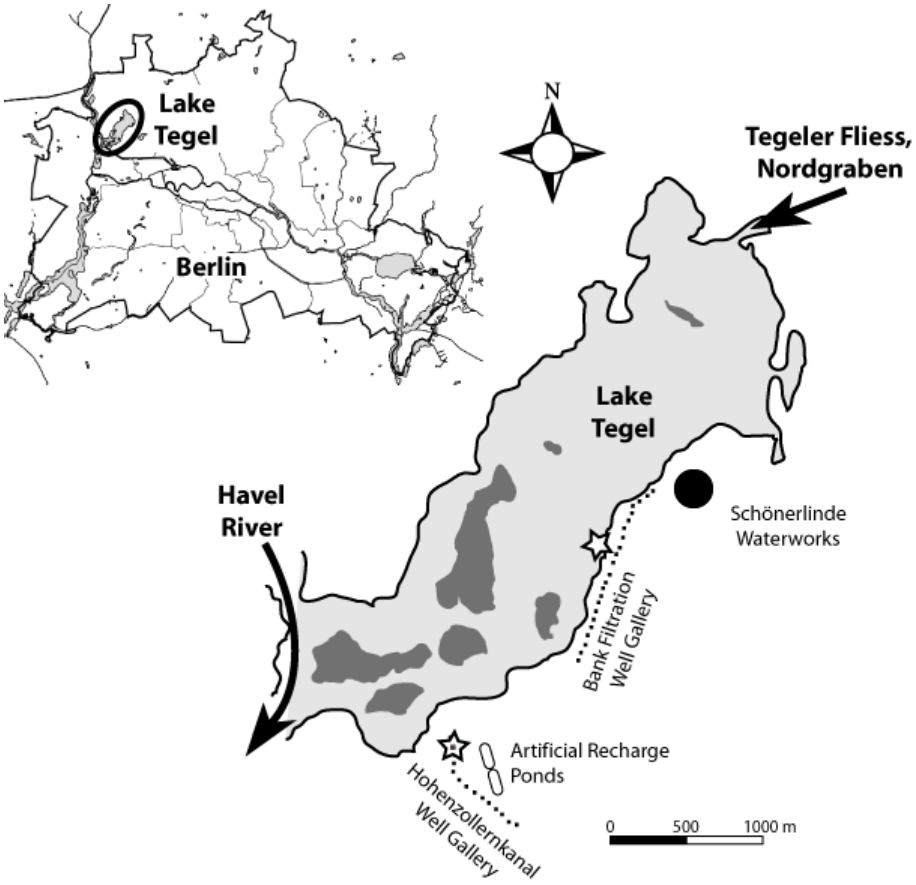

Figure 6.1. Map of sampling locations and bank filtration well galleries at Lake Tegel. Production well 18 is highlighted with a star in the Hohenzollernkanal Well Gallery. For reference, the shoreline sampling location in Chapter 4 is starred as well.

Sample analysis and characterization

Samples were freeze-dried before analysis. For XRF and XAS, samples were sieved (#25, < 707 μm) and milled for 30 s at 30 Hz with a ZrO_2 milling set (< 50 μm, Retsch MM400). XRF samples were diluted with wax and pressed into 32 mm pellets for analysis (Spectro XEPOS). Four samples (5–6 m, 8–9 m, 11–12 m, and 23–25 m) were loaded in plastic cells between Kapton tape for XAS analysis. Mn K-edge X-ray absorption near edge structure (XANES) and Fe K-edge XANES and extended X-ray absorption fine structure (EXAFS) spectra were measured at room temperature at the XAS beamline at the Angströmquelle Karlsruhe (ANKA, Karlsruhe, Germany). The Si(111) monochromator was calibrated by setting the first inflection point of the absorption edge of Mn and Fe metal foils to 6539 eV and 7112 eV, respectively. The Mn spectra were collected in fluorescence mode using a 5-element Ge solid state detector; the Fe spectra were measured in transmission mode. Spectral data processing and linear combination fitting (LCF) were performed using the software code Athena (Ravel and Newville 2005). Reference spectra for Mn included triclinic Na-birnessite, Mn(II)-reacted ferrihydrite, aqueous Mn^{2+} (100 mM $Mn(NO_3)_2$), chlorite (CCa-2, Source Clay Repository), and rhodochrosite. Reference spectra for Fe included 2-line ferrihydrite, lepidocrocite, Source Clay Repository clays illite (IMt-1) and chlorite (CCa-2), and aqueous Fe^{2+}.

Mn sorption experiments were conducted with the 23–25 m depth-averaged sample in artificial groundwater (AGW) at pH 8. Artificial groundwater was designed based on the adjacent artificial recharge water composition at Lake Tegel (Massmann et al. 2006) (Table 6.1). $MnCl_2$ concentrations (0–100 μM) were spiked in 20 ml AGW

with 0.5 g sediment, with three replicates. After 24 h on an end-over-end shaker, supernatant samples were diluted with 1% HNO_3 for ICP-MS analysis (Agilent 7500cx). pH values at the end of the experiment were not significantly different from 8.0 (range 8.01–8.03).

Table 6.1. Composition of artificial groundwater for sorption experiments. Based on artificial recharge water composition at Lake Tegel (Massmann et al. 2006)

component	concentration (mM)
$CaCO_3$	2.1
NaCl	1.5
$MgCl_2$	0.4
$KHSO_4$	0.24
$NaNO_3$	0.15
HEPES	10
pH	8.0

Results and Discussion

Sediment composition and sorption capacity

Sediments were mainly sandy in appearance, with some bits of rock, shells, and black particulate organic matter interspersed. Sediments were visibly coarser with depth. A vertical gradient in sediment color was evident during drilling: light-colored sand down to 5 m below the ground surface, brown at 5–6 m depth, and fading of the brown to grey within 22 m. This corresponds with the local groundwater levels, which fluctuate between 5 and 12 m below the ground surface (Massmann and Sültenfuß 2008); the water table was approximately 6 m below the ground surface at the time of drilling. XRF data show declining values of Mn and Fe with depth, although the concentrations of both elements are relatively low (< 3.3% Fe, < 80 ppm Mn) and show heterogeneity between

subsequent depths (Figure 6.2a). Plotted against each other, Mn and Fe appear to be linearly correlated (Figure 6.2b), although samples from the shallowest 4 depths (5–9 m below the ground surface) show some evidence of Fe accumulation relative to Mn. Other XRF-measured elements showed no significant trends with depth, sometimes with high heterogeneity for subsequent depths (not shown).

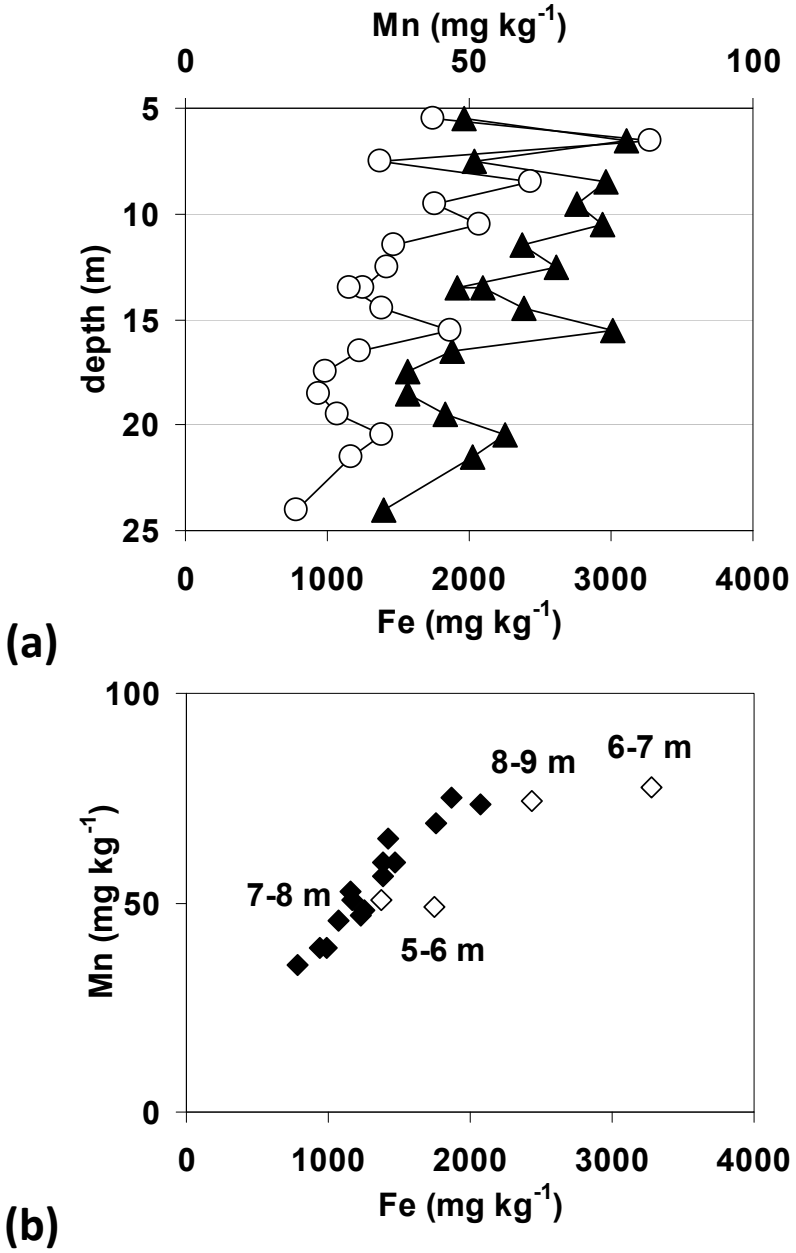

Figure 6.2. XRF concentrations of Mn (▲) and Fe (○) as a function of depth in the aquifer (a). Replicate samples at 13.5 m show the approximate variability of XRF data relative to inter-depth heterogeneity. For XRF Mn concentrations plotted against Fe concentrations (b), the top 4 m of sediments are labeled and plotted unfilled.

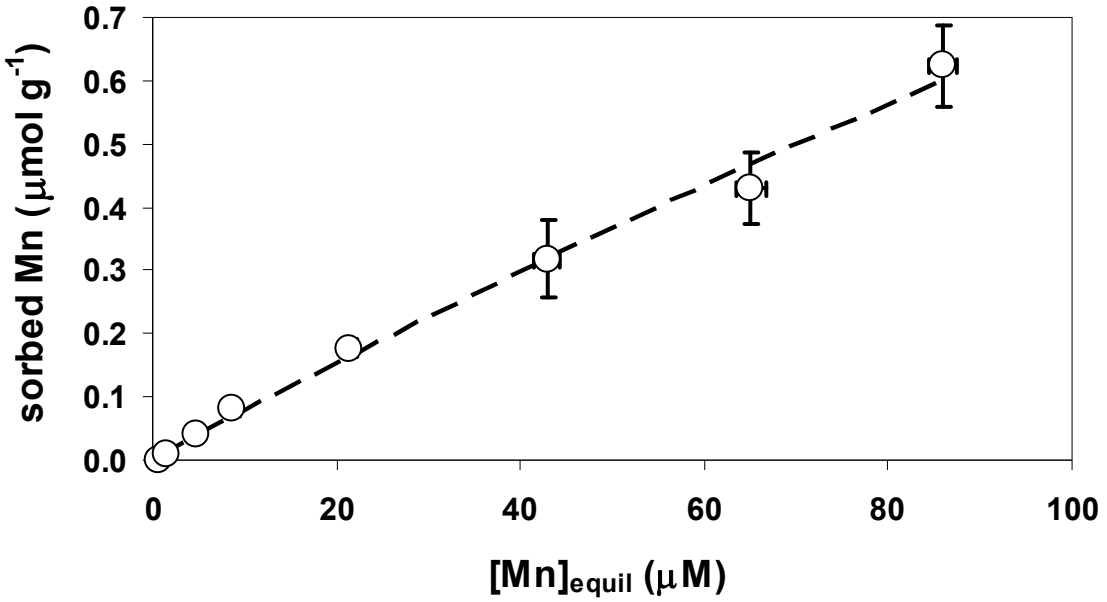

Figure 6.3. Mn sorption isotherm on aquifer sediments 23–25 m depth at pH 8. Dashed line shows the Freundlich isotherm (q_{max} = 4.6 μmol g^{-1}, K = 0.0017).

The sorption isotherm for Mn on the 23–25 m sediment showed nearly linear sorption up to 100 μM Mn in solution, with a maximum loading of 0.62 μmol Mn g^{-1} (Figure 6.3). At the average dissolved Mn concentrations in the groundwater (9 mM, Table 6.2), 0.1 μmol Mn are predicted to be adsorbed per g of aquifer sediments, or approximately 5.5 mg kg^{-1}. In comparison to XRF Mn concentrations of 35–78 mg kg^{-1}, the sorption capacity of the sediments is quite low (< 20% total Mn).

Table 6.2. Average groundwater composition in production well 18

parameter	average value
pH	7.3
redox potential	130 mV
electrical conductivity	750 µS cm^{-1}
DOC	5.1 mg l^{-1}
Fe^{2+}	7.2 µM
Mn^{2+}	9.1 µM
NO_3^-	18 µM
NO_2^-	3.5 µM
NH_4^+	13 µM
SO_4^{-2}	1.3 mM
total PO_4	1.6 µM
Cl^-	1.5 mM

Fe and Mn speciation

Speciation of Fe and Mn at four depths was determined with XAS. The depths included the highest groundwater level (5–6 m), the lowest groundwater level (11–12 m), an intermediate level (8–9 m), and a deep, presumably anoxic, level (23–25 m). If the water table fluctuations from pump operations indeed entrapped a gradient of dissolved oxygen in the shallow groundwater, the solid phase Fe and Mn speciation could reflect the change in sediment redox status as a function of depth.

Some significant limitations hindered this analysis. Mn concentrations were at the very low end for XAS measurements, which resulted in spectra inappropriate for EXAFS analysis. Mn XANES spectra were not very smooth, which interferes with LCF. The samples' redox status was unavoidably disturbed during the drilling process. Ambient groundwater was pumped into the borehole without concern for redox status, although the air temperatures were just above freezing (1–3°C) and samples were rapidly

stored on ice in plastic bags. Although this would likely preserve reduced Mn, which is slow to oxidize (Morgan 2000), in samples, more rapid oxidation of Fe is possible. Furthermore, rust particles from the well borer likely entered the samples to some degree.

Nonetheless, Mn XANES show that almost all Mn was present in the reduced form (oxidation states II and III; Figure 6.4). There is a slight increase in the proportion of Mn(II) with depth, but none of the available reference spectra, including rhodochrosite ($MnCO_3$), provide a very good fit of this spectrum. This suggests the presence of some alternate Mn(II)-bearing phase (i.e., not Mn(II)-bearing ferrihydrite, aqueous Mn(II), chlorite, or rhodochrosite) in the aquifer.

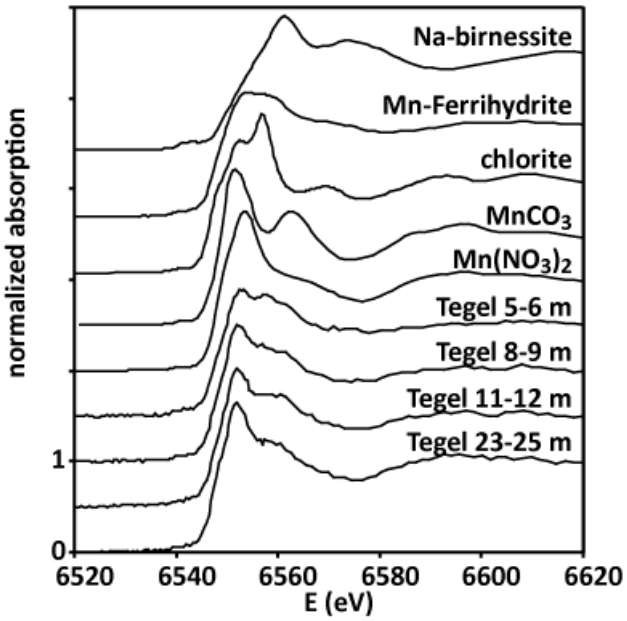

Figure 6.4. Mn K-edge XANES spectra of Lake Tegel aquifer samples from different depths compared to reference spectra of triclinic Na-birnessite, Mn^{2+}-reacted ferrihydrite (sorbed Mn likely partly oxidized to Mn(III)), aqueous Mn^{2+} (100 mM $Mn(NO_3)_2$), chlorite CCa-2 (Source Clay Repository), and rhodochrosite

Fe spectra show a slightly increasing proportion of Fe(II) with depth (Figure 6.5). Comparison to reference spectra suggests dominance of Fe(III) (hydr)oxides, like ferrihydrite and lepidocrocite (possibly from the well borer or air exposure), and Fe(II) and Fe(III) in phyllosilicates, like illite and chlorite. The presence of Fe(II) and Fe(III) in primary Fe-bearing minerals cannot be excluded.

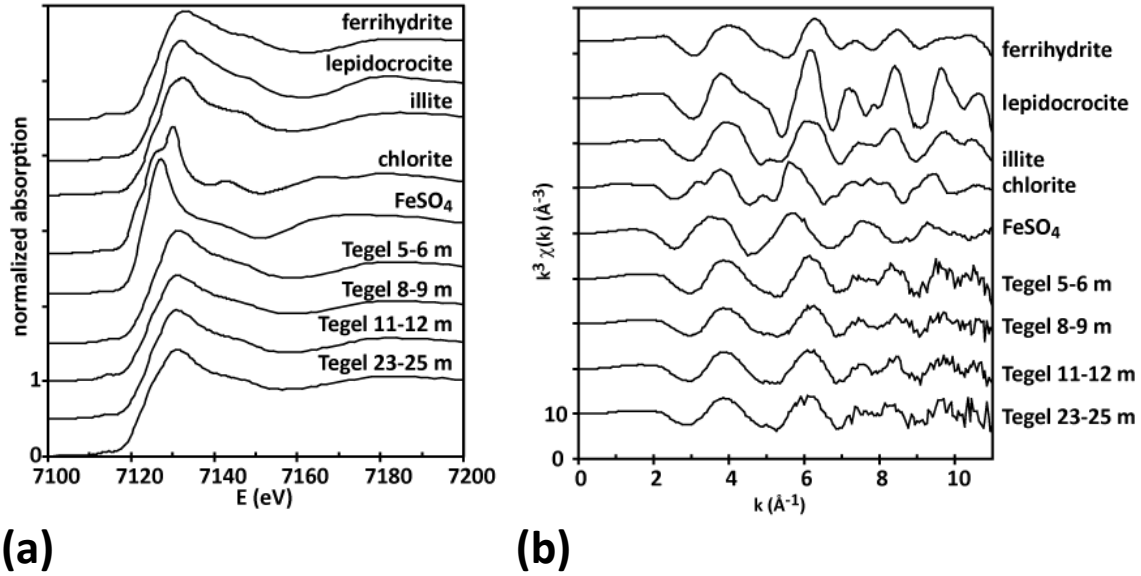

Figure 6.5. Fe K-edge XANES (a) and EXAFS (b) spectra of Lake Tegel aquifer samples from different depths compared to reference spectra of 2-line ferrihydrite, lepidocrocite, Source Clay Repository clays illite IMt-1 and chlorite CCa-2, and aqueous Fe^{2+}

The XAS data suggest much of the Fe and Mn is associated with clays, with low concentrations not indicative of significant accumulation. This suggests that these aquifer samples adjacent to Lake Tegel reflect the sediment background, rather than a significant change in solid-bound Fe and/or Mn. Both Fe and Mn bound in clays have complex redox chemistry that would have required a larger suite of standards at different

redox conditions as well as better preservation of the sediment's ambient redox status, in order to analyze the speciation more precisely.

Lack of accumulation of Mn and Fe

Overall, the XRF and XAS data suggest no significant Mn or Fe accumulation in these aquifer sediments, despite favorable conditions for oxide formation upon the introduction of dissolved oxygen. Synchrotron data suggests that Fe and Mn are bound to clays, although whether that reflects sorption to a depth-dependent clay fraction or transport of Mn and Fe bound to clay colloids is unknown. Lack of significant accumulation of Fe, which rapidly oxidizes in the presence of oxygen (Wehrli and Stumm 1989), suggests that Fe and oxygen do not normally co-occur in the shallow groundwater. A nearby lake bank filtration site with similar hydrogeology has vertical redox zonation in the shallow groundwater, such that Mn^{2+}- and Fe^{2+}-containing groundwater are 12–15 m below the groundwater surface (Massmann et al. 2008b). If the groundwater is similarly zonated at the Lake Tegel site, the lack of accumulation could indicate that oxygen does not reach the depths of Mn^{2+}- and Fe^{2+}-containing groundwater.

Mn oxidation in particular depends on microbes at circumneutral pH (Morgan 2000), and is sensitive to the presence of ions in the groundwater that either inhibit or reverse oxidation. Fe(II), for example, reduces Mn oxides with a Fe(II, III) oxide by-product (Postma and Appelo 2000, Villinski et al. 2001). If all of the Mn in the local groundwater (9 μM, Table 6.2) were oxidized in the sediments, the local Fe concentration (7 μM, presumably Fe(II)) could reduce up to 3.5 μM, or 39% of the Mn. Ammonium (13 μM) inhibits Mn oxidation and must be fully removed before Mn oxidation can commence in sand filters (Frischherz et al. 1985, de Vet et al. 2010), although 4 mM

NH_4^+ in the MSTG minimal medium did not inhibit Mn oxidation in Chapter 5. Local groundwater concentrations from the production well reflect both temporal integration of contact with aquifer solids and spatial averaging over the groundwater volume accessed by well pumping, so it is difficult to hypothesize about the actual Mn, Fe(II), or ammonium concentrations at relevant depths in the aquifer. Although not assessed in this study, the prevalence of Mn oxidizing capacity is assumed to be ubiquitous (Francis and Tebo 2001) in this aquifer. The amount of time needed for the development of an active Mn-oxidizing microbial consortium is unknown. In sand filters this is normally 8–20 weeks (Frischherz et al. 1985, Mouchet 1992); production well 18 had been in operation for 2 years as of the sampling date.

The presence of Mn accumulations in shallow sediments in some locations around Berlin (C. Menz, personal communication) suggests that the conditions for Mn and Fe oxidation exist in some areas of the aquifer. The groundwater extracted from production well 18 comes from three sources: bank filtrate from Lake Tegel (~ 210 m away), recharged water from an artificial recharge pond (~ 170 m away), and the ambient groundwater. The hydrological balance between these sources strongly influences the entrapped air content in the groundwater (Massmann and Sültenfuß 2008) and the depth and concentration of dissolved Mn and Fe (Massmann et al. 2008b). Artificial recharge basins, for example, entrap large amounts of air, but the dissolved oxygen is consumed in the shallow sediments of the basins. Adjacent to wells, less air is entrapped from on-off cycles than from recharge basins, but more dissolved oxygen is transported deeper in the aquifer (Greskowiak et al. 2005, Massmann and Sültenfuß 2008). Future study of *in situ* Mn oxidation in this area should focus on more ideal hydrologic setting and groundwater

composition: frequent water table fluctuation of high amplitude, low concentrations of Fe^{2+} and ammonium, and a shallow depth to the Mn-containing groundwater.

Acknowledgements

Christian Menz organized the well drilling in Berlin and provided the average groundwater composition at the production well. Andreas Voegelin performed all XAS measurements and data analysis. The Angströmquelle Karlsruhe (ANKA, Karlsruhe, Germany) provided beamtime at the XAS beamline, and Stefan Mangold assisted during XAS data collection.

Chapter 7

Conclusions

Summary

In this study, we investigated the behavior of Mn and Fe under two types of changing redox conditions: as oxic surface water entered shallow sediments and was reduced, and as reduced groundwater became exposed to oxygen and was oxidized. The oxic-to-reduced transition was probed with a newly developed method to measure *in situ* reduction rates as a function of depth, with sub-cm resolution. The reduced-to-oxidized transition was investigated in a laboratory-scale column experiment, whose frequency and amplitude of water table oscillations were designed to simulate field conditions. For both types of redox transitions, laboratory study was complemented with a field investigation in the shoreline bank sediments and the aquifer sediments, respectively, at Lake Tegel, Berlin, Germany.

In situ rates of reductive dissolution

The Mn oxide-doped gels developed in Chapter 3 can assess *in situ* reduction rates in a variety of saturated settings. With the AQUASIM (Chapter 3) and MATLAB (Chapter 4) models, the mass loss of Mn from a gel over time can be easily converted to a pseudo-

first-order rate coefficient for the reaction taking place at the Mn oxide surfaces inside the gel. Without accounting for diffusion in the model, the rate of Mn reduction would be underestimated by as much as 1–3 orders of magnitude.

Even with such accounting, the gels physically separate the electron acceptor (Mn oxide) from Mn-reducing microbes. Gel pore size is estimated to be between 2 nm and 1 μm (Chrambach and Rodbard 1971, Rüchel and Brager 1975, Patras et al. 2000); the dimensions of *Shewanella oneidensis* MR-1 are approximately 0.6 μm × 3 μm (Abboud et al. 2005). Modeling suggests that gels capture 35% of the reduction capacity of *S. oneidensis* MR-1, which may be attributable to extracellular electron shuttles and nanowires, but not to direct enzymatic contact with the Mn oxide (Nielsen et al. 2010).

More recent literature has identified flavins as the primary electron shuttle produced by *Shewanella* species (Marsili et al. 2008, von Canstein et al. 2008), and the kinetics of Fe oxide reduction by enzymes in the *S. oneidensis* MR-1 cell wall, mediated by riboflavin, have been modeled (Ross et al. 2009). A preliminary attempt to adopt the literature parameters in the AQUASIM model presented in Chapter 3, however, was unsuccessful. The modified model featured the enzyme omcA and reduced flavins (600 nM) initially in the bulk solution. The flavins could diffuse into the gel, become oxidized as they reduced Mn oxide, and diffuse out of the gel to be re-reduced by the enzyme omcA. Sensitivity analysis suggests that the diffusion gradient was too low for the rapid flavin recycling needed to reproduce the dissolved Mn concentrations observed in the bulk solution. This could be evidence for nanowires or some penetration of MR-1 in the gel, which would bypass the slow diffusive flux of low concentrations of an electron shuttle. Further research that takes advantage of the Mn-doped gels' physical constraints

on microbial physiology could lead to interesting results. For example, in Chapter 5, this technique was used to quantify rates of Mn *reduction* by a Mn-*oxidizing* microbe.

The main practical limitations of Mn-doped gel probe deployment include the sediment's physical characteristics and chemistry. The ladder-like sample holder is deployable by hand in sandy sediments without gravel, which can rip the membrane covering the gels and block insertion; low porosity clayey sediments can also resist the force of insertion. Low porosity sediments can furthermore increase the time for diffusive equilibration of the porewater with the gels (Harper et al. 1997).

The data collected in Chapter 4 suggest that measured Mn oxide reduction rates from Lake Tegel reflect some interaction with dissolved Fe, presumably Fe(II), in the sediment porewater. If Fe(II) is the reductant directly responsible for Mn reduction in these sediments, then the time to reach diffusive equilibrium with the gels is important to consider. The MATLAB model in Chapter 4 does not consider the diffusion of the reductant into the gel, nor does it represent the reaction kinetics as second-order (first-order in both [reductant] and [Mn oxide]), as literature proposes for Fe(II) (Villinski et al. 2003) and sulfide (Burdige and Nealson 1986). With an infinite source of Fe(II) in the sediments, modeling suggests that diffusive equilibrium with the gels (C_{gel} = 0.995 $C_{porewater}$) should occur within 4 h. Further refinement of the MATLAB model could incorporate the second-order kinetics for Mn reduction by Fe(II) or sulfide and the diffusion of the reductant into the gel. This refinement could perhaps resolve the discrepancy between the *in situ* Mn oxide reduction rates and the rates expected from extrapolation of laboratory experiments to field conditions.

It is worth remembering, though, that the Mn-oxide-doped gels are single-point estimates of reduction rates. Modeling of the two end points (before and after deployment) and diffusion through the gel can generate a lot of data, but many assumptions underlie these rates. Nevertheless, comparisons with *in situ* Mn reduction rates from a variety of field settings suggest that the rates in Chapter 4 are reasonable. A recent compendium of bacterial Mn oxide reduction rates found that the average surface area normalized rate with zero-order kinetics was 1.47×10^{-7} mol m^{-2} h^{-1} (Bandstra et al. 2011), which is comparable to the shallow *in situ* reduction rates measured in Lake Tegel sediments (9.4×10^{-7} mol m^{-2} h^{-1}).

Finally, gel-derived *in situ* Mn reduction rates represent the potential for sediment to reduce Mn oxides rather than actual Mn reduction rates. Mn oxide reduction can be mediated by microbes with versatile electron transport chains (Ruebush et al. 2006), as well as by reduced porewater species such as Fe(II) and sulfide (Burdige and Nealson 1986, Villinski et al. 2003). These mobile constituents can occur in porewater independent of the location of Mn oxides, and thus solid-phase analysis of adjacent sediments should accompany Mn-oxide-doped gels in order to interpret the trends of rate constants with depth. At the shoreline of Lake Tegel, where deposition of Fe and Mn oxides is low, the highest Mn oxide reduction rates corresponded with depths most depleted in the operationally defined "reducible oxides" fraction. Increasing proportions of operationally defined "carbonate bound" and "organic and sulfide bound" Fe and Mn below this depth suggested that the highest measured rates did occur at the interface between more oxic sediments < 10 cm depth and more reduced, possibly sulfidic, sediments > 15 cm depth.

Oxidizing conditions induced by water table oscillations

In a quartz sand column with anoxic influent solution, downward percolation through unsaturated sand led to oxygen mass transfer to the dissolved phase, but no significant dissolved oxygen was acquired when the water table was high. Effluent dissolved oxygen levels, which reflect the "net" of oxygen transfer to the dissolved phase as well as consumption by microbial respiration, varied between a maximum concentration of 3.6 mg l^{-1} and minimum concentrations of < 1 mg l^{-1}. The actual dissolved oxygen delivered to the aqueous phase is unknown; the presence of oxygen-consuming processes (i.e., cellular respiration and Mn oxidation) enhances oxygen mass transfer across the air-water interface (Haberer et al. 2011).

Rates of Mn oxidation in the inoculated column increased with time and subsequent water table fluctuations, but were ultimately slower than those of pure cultures of *Pseudomonas putida* GB-1. The oxygen delivery likely played a role in this slower oxidation rate, because even under vigorous shaking, the dissolved oxygen (DO) concentration in early- to mid-logarithmic phase GB-1 cultures was nearly zero (Okazaki et al. 1997). That is, even with extremely high rates of delivery, cellular respiration was able to outpace oxygen mass transfer to the dissolved phase. Other *Pseudomonas putida* species are able to regulate gene expression based on DO concentrations (Martinez-Lavanchy et al. 2010), and their rates of aerobic biodegradation depend on DO levels (Bauer et al. 2009, Martinez-Lavanchy et al. 2010).

Oxidation is thus theoretically possible in shallow groundwater with water table fluctuations. The level of air entrapment, the groundwater flow rate, and the ambient microbial community all regulate the potential Mn oxidation rate in a sedimentary

environment. Even so, maximum rates observed in the column were orders of magnitude lower than those observed in aerated groundwater treatment columns with beads coated in Mn oxides and a mixed *Gallionella* and *Leptothrix* biofilm community (Katsoyiannis and Zouboulis 2004). In an operational well field, post-extraction treatment specific to Mn and Fe removal may still be more efficient than any *in situ* oxidation process.

Field conditions necessary for *in situ* Mn and Fe oxidation

Despite the potential for water table fluctuations to induce oxidizing conditions in shallow groundwater (Chapter 5), no significant Mn or Fe accumulation was observed in aquifer sediments adjacent to a production well at Lake Tegel (Chapter 6). Solid-phase Mn and Fe, as determined by XRF, declined slightly with depth, but were generally low (< 3.3% Fe, < 80 ppm Mn). Less than 20% of the Mn accumulation was attributable to sorption, based on sorption experiments with Mn-spiked artificial groundwater. XAS-determined solid-phase speciation of Mn and Fe did show increasing amounts of phyllosilicate-bound Mn(II) and Fe(II) with depth, but evidence for a transition from metal oxides to reduced species with depth was modest at best.

Assuming that Mn oxidizing microbes were present in this sediment, which was subject to up to 7 m of annual water table change, why did no significant Mn or Fe oxidation occur in the solid phase? Ammonium, which inhibits microbial Mn oxidation in sand filters, and dissolved Fe, presumably Fe(II) which can reduce Mn oxides, were both present in the groundwater extracted from the production well 3 m from these sediments. Furthermore, other microbial respiration may dominate oxygen consumption in the capillary fringe and shallow groundwater. But the lack of significant Fe

accumulation suggests that Fe(II) and dissolved oxygen do not co-occur in this groundwater, as abiotic Fe(II) oxidation by oxygen is rapid at circumneutral pH (Wehrli and Stumm 1989). Previous characterization of the redox conditions in Berlin's lake bank filtration sites found vertical redox zonation of the infiltrating groundwater (Massmann et al. 2008b). If reduced Fe and Mn travel at greater depths than dissolved oxygen is able to penetrate, no significant oxidation would be expected.

Physical flow thus affects both the introduction of dissolved oxygen and the location of the "plume" of reduced Fe and Mn. The presence of Fe and Mn oxide accumulations at other boreholes in Berlin suggests that spatial heterogeneity may make flow conditions near other production wells more ideal for *in situ* oxidation. Optimization of *in situ* oxidation, as a "natural" pre-treatment process for bank filtrate, should focus on maximum air entrapment (e.g., large, frequent water table changes), shallow depth to the reduced Fe and Mn, and relatively low concentrations of ammonium. There is a risk that Mn oxides formed in the capillary fringe at low water levels could be reduced by Fe(II) upon re-saturation with reduced groundwater, but even this step would remove Fe(II) *in situ* and thereby decrease the treatment burden of the extracted bank filtrate.

Future research in inorganic geochemistry relevant to bank filtration

As bank filtration use is expanded, many aspects of biogeochemistry remain open to further research. Organic micropollutant degradation, microbial pathogen removal, and viral inactivation remain active areas of research, especially as related to optimization of the bank filtration process (Tufenkji et al. 2002, Greskowiak et al. 2006, Massmann et al.

2006, Castro and Tufenkji 2008, Massmann et al. 2008a, Gupta et al. 2009, Toze et al. 2010). Fundamental to these aspects, as well as to inorganic geochemistry, is the transient redox status of the bank filtrate. Changing the water table elevation during pumping delivers oxygen to the subsurface (Kohfahl et al. 2009), with the potential to deliver amounts in excess of air saturation, via entrapped bubbles in the aquifer sediments. Quantification of the excess air delivered and its vertical extent in the aquifer remains site-specific (Cey et al. 2008, Klump et al. 2008, Massmann and Sültenfuß 2008); better predictions of excess air for given a water table fluctuation and frequency in terms of aquifer porosity and flow rates could enhance site managers' ability to optimize *in situ* redox conditions for target contaminant removal.

The location of reaeration along the flow path also impacts the sequestration of Mn and other trace elements released in the reducing zone. In the absence of newly generated sorbents or transition to precipitation, elements sequestered via sorption will eventually breakthrough at the production well (Appelo et al. 1999, Oren et al. 2007, Spiteri et al. 2007). The oxygen levels and the travel time along the flow path required to produce significant oxide minerals merit further study. Oxidation that occurs too close to the production well, or during mixing with deeper water in the production well, leads to well screen clogging and decreased well yield (Hässelbarth and Lüdemann 1972, van Beek 1984, van Beek et al. 2009). As rehabilitation of production wells susceptible to clogging is expensive in the long term (Dillon et al. 2006), cost-effective and sustainable management is important. This ranges from proper site selection (to avoid settings and screened intervals with potential mixing of oxic infiltrate and anoxic groundwater (van

Beek 1984, van Beek et al. 2009)), to novel solutions for well rehabilitation, such as addition of bacteriophages to degrade Fe- and Mn-oxidizing biofilms (Gino et al. 2010).

Global climate change will certainly affect the performance of bank filtration systems. As has already been observed with seasonal differences in temperature (von Gunten et al. 1991, Bourg and Bertin 2002, Massmann et al. 2008b), warmer conditions stimulate microbial activity both directly via higher temperatures and indirectly via higher organic carbon loads in surface waters. This enhanced microbial activity would extend the reducing zone further into the aquifer, and in existing bank filtration systems, this essentially decreases the travel time of the bank filtrate through areas of potential sequestration of trace elements. Higher intensity precipitation and more frequent flooding are also expected under climate change. Bank filtration systems with a sufficient travel time have performed effectively under flood conditions in the past (Eckert and Irmscher 2006), but floods could affect the redox status of soils (Borch et al. 2010). Additionally, the infiltration flow paths for microbes and viruses may be short-circuited under flood conditions (Gupta et al. 2009). Accordingly, new systems would need to allow more distance between the surface water and the production well. Further considerations of bank filtration design in light of climate change, both in drought and flood conditions, have been recently reviewed (Sprenger et al. 2010).

The simplicity of bank filtration makes it a desirable pre-treatment step for drinking water in many locations. It could furthermore offer significant benefits in the developing world, where water treatment infrastructure is minimal (Lorenzen et al. 2010). Long-term bank filtration on the Rhine River in Düsseldorf has been largely effective despite periods of low-quality surface water and a chemical “shock” load in 1986

(Schubert 2002). Due to contamination of surface waters by untreated wastewater and agricultural runoff, the organic carbon load on bank filtration systems can be much higher in the developing world than in the developed world; column studies in Addis Ababa, Ethiopia, and Mathura, India, suggest that bank filtration alone is not sufficient to produce high quality drinking water (Abiye et al. 2009, Singh et al. 2010). Nevertheless, a more efficient technical water cycle, where wastewater treatment plant effluent is combined with surface water for bank filtration or other managed aquifer recharge, as has been implemented in Berlin, Germany (Massmann et al. 2007), Orange County, California (Clark et al. 2004), and Shafdan, Israel (Oren et al. 2007), could begin to improve surface water quality in urban centers in developing countries (Jimenez and Chavez 2004). Extended organic carbon oxidation at the Israeli site has mobilized Mn from the aquifer sediments, a clear example of the complex management issues in these types of systems. Further studies on the long-term feasibility of joint water and wastewater management could have major impacts on the quality of drinking water in the developing world.

The use of bank filtration in concert with advanced wastewater management requires sufficiently advanced geochemical models. Some sites (more frequently, those used for ASR and ASTR) have more complex water-rock interactions than described here, such as fluorite (CaF_2) precipitation (Lorenzen et al. 2010) or dissolution (Gaus et al. 2002), or As release from Fe sulfides (Price and Pichler 2006, Wallis et al. 2010). Aquifers can also undergo physical changes during pumping, such as clay dispersion (Konikow et al. 2001), that affect the withdrawal rate; interrelated physical and chemical changes must be balanced effectively and efficiently to maintain high-yield bank

filtration (Eusuff and Lansey 2004, Wiese and Nützmann 2009). Truly comprehensive models must incorporate these effects to optimize the desired treatment outcome and flow rate.

Wider implications

Bank filtration is far from the only setting in which water bodies undergo redox transitions. Natural infiltration in the hyporheic zone and in river- and lakebed sediments also induces a transition from oxic to reducing status. Permeable reactive barriers with Fe(0) intentionally create reducing conditions in oxic aquifers, usually for *in situ* remediation. In aquifer storage and recovery, oxic surface water is artificially introduced to reducing aquifers for storage. Oxidation of reduced groundwater is critical for aerobic biodegradation of organic contaminant plumes, and the impact of water table oscillations on the dissolved oxygen in those settings is an area of active research (Bauer et al. 2009). Surface waters, such as rivers, streams, and reservoirs, regularly undergo water level fluctuations. The interaction between those fluctuations and the adjacent groundwater could potentially create *in situ* reduction hotspots, due to infiltration of organic carbon from the surface water, as well as oxidation hotspots, due to the exposure of reduced solid-bound species to air-filled pores at low water levels. The behavior of Mn, Fe, and other trace metals in such dynamic redox conditions merits careful attention, especially when these water bodies are used for drinking water.

Appendix A

Supporting Information for

Chapter 3: A Hydrous Manganese Oxide Doped Gel Probe Sampler for Measuring *In Situ* Reductive Dissolution Rates: I. Laboratory Development

Contents: 6 tables and 8 figures

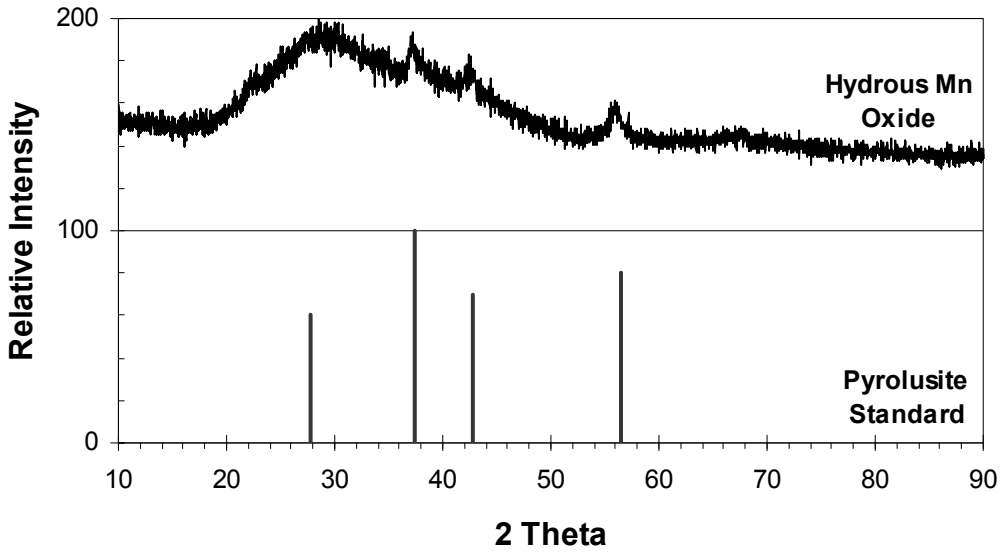

Figure A.1. X-ray diffractogram for synthesized HMO with the pyrolusite (β-MnO_2) standard, the best match for the small peaks. The broad, ill-defined peak is indicative of an amorphous solid.

Table A.1. Final mass balance in abiotic miniprobe reductive dissolution experiments

Reductant, pore size	(1) Total Lost from Gels	(2) Storage Soln. before Expt.[a]	(3) Reduced from Gels[b]	(4) Bulk Soln.	% Unaccounted[c]
Ascorbate 0.45 μm	7.39	3.68	3.71	3.55	2.2%
1.0 μm	7.50	3.68	3.81	3.70	1.5%

Listed data are μmoles of Mn.

[a] The percentage of Mn lost to the gel storage solution (50%) is relatively high in this example. Typically ≤ 20% of Mn leached into the storage solution.

[b] The amount of Mn reduced from the gels (3) is equal to the difference between the total Mn lost from the gels (1) and the Mn lost to the gel storage solution before the experiment (2).

[c] Perfect mass balance would lead to the amount of Mn reduced from the gels (3) equaling the amount of Mn measured in the bulk solution at the end of the experiment (4). The percentage is given as: $[(3) - (4)]\cdot(1)^{-1}$.

Table A.2. Basic components of MR-1 minimal medium[a]

Chemical	Concentration (mM or given)
Sodium Lactate	6
PIPES	3
Sodium Hydroxide	7.5
Ammonium Chloride	28.0
Potassium Chloride	1.34
Sodium Phosphate (monobasic)	4.35
Sodium Fumarate	30
Vitamins:	(nM)
d-biotin	81.9
folic acid	45.3
pyridoxine-HCl	486
riboflavin	133
thiamine-HCl·H_2O	141
nicotinic acid	406
d-pantothenic acid, hemicalcium salt	210
B12	0.74
p-aminobenzoic acid	365
thioctic acid	242
Amino Acids:	(mg l^{-1})
L-glutamic acid	2
L-arginine	2
DL-serine	2

[a] In addition, 10 ml of Wolfe's Mineral Solution (which comprises trace amounts of Mg, Mn, Na, Fe, Ca, Co, Zn, Cu, Al, B, and Mo salts) were added to this medium.

Although direct reduction of Mn oxide by the MR-1 medium was not tested, previous studies of the individual compounds suggest this would have a negligible effect on the measured rates. Fumarate, lactate, and ammonia do not appear to reduce Mn oxide when present in excess (Stone and Morgan 1984, Burdige and Nealson 1986). Only DL-lactic acid reduced MnO_2, at an average rate of 0.47 μmol m^{-2} h^{-1} at pH 5 (Wang and Stone 2006a), which corresponds to a range of 3.4–20×10^{-11} M s^{-1} for the conditions of our study; even at the maximum estimated rate, this would account for less than 5% of our measured HMO reduction rate.

Table A.3. Parameters input to or solved by AQUASIM model

Experiment		$[C_6H_7O_6^-]_{0,\ bulk}$ or $[Red]_{0,\ bulk}$ (mM)	$[HMO]_{0,\ gel}$ (mM)[a]	k ($M^{-1}\ s^{-1}$)	k″ (s^{-1})	A ($m^2\ l^{-1}$)	D_{Mn} ($cm^2 s^{-1}$)	$D_{A,\ bulk}$ or $D_{Red,\ bulk}$ ($cm^2 s^{-1}$)	$D_{A,\ gel}$ or $D_{Red,\ gel}$ ($cm^2 s^{-1}$)	V_{bulk} (ml)	χ^2
Abiotic	HMO gels	2.0	7.77	4.2	---	33.1	6.88e-6	3.0e-6	4.28e-7[b]	10	2.3
	MP 1.0 μm	2.0	6.68	4.2	---	28.5	6.88e-6	3.0e-6	1.03e-6[b]	25	2.0
Microbially-mediated	HMO	1.182	0.360[d]	3.5e-3	7.5e-6 [b]	1.53	---	---	---	55	2.6
	HMO gels	1.182[c]	10.2	3.5e-3[b]	---	25.0	6.88e-6	3.0e-6	4.28e-7	10	1.2
	MP 1.0 μm	1.182	6.59	3.5e-3[b]	---	28.1	6.88e-6	3.0e-6	1.03e-6	25	1.4

[a] This concentration is normalized to the volume of pore space in the gel, which is approximately 92.3% × 0.225 g × 1 ml g^{-1}, or 0.208 ml.

[b] Denotes a fitted parameter.

[c] Assumed to be 5 times Mn_T for this system.

[d] In this case, the HMO was added to the bulk solution, and no gel compartment was necessary. Consequently, no diffusion coefficients were needed for this simulation.

Table A.4. AQUASIM mass balance at steady state

Experiment		t_{ss} (h)	HMO_0 (μmol)	$Mn_{T,t}$ (μmol)	% Error[a]	Red_0[b] (μmol)	Red_{red}[c] (μmol)	$Red_{T,t}$ (μmol)	% Error[a]
Abiotic	HMO gels	6	1.794	1.792	0.07%	20	1.792	18.25	0.2%
	MP 1.0 μm	25.1	1.542	1.541	0.04%	50.03	1.541	48.6	0.2%
Microbially-mediated	HMO	150	19.8	19.8	0.01%	65.01	6.91[d]	58.25	0.2%
	HMO gels	360	2.364	2.362	0.06%	11.82	2.362	9.48	0.2%
	MP 1.0 μm	420	1.521	1.520	0.09%	29.55	1.520	28.01	0.08%

[a] % Error is the absolute value of either the difference between HMO_0 and $Mn_{T,t}$ divided by HMO_0, or the difference between Red_0 and the sum of Red_{red} and $Red_{T,t}$ divided by Red_0.

[b] Red denotes the reductant, either ascorbate (abiotic) or the generic reductant (microbially mediated).

[c] The amount of Red that is reduced is equal to the amount of Mn(II) produced.

[d] The amount of Red that is reduced is equal to 35% of the amount of Mn(II) produced.

Table A.5a. [Mn(II)] release over time:
HMO-doped gels and ascorbate (184 μM Mn_T)

Time (hrs)	0.5	1	2	3	4
$[Mn]_{diss}$ (μM)	38	64	116	132	145
Std Dev (μM)	7	1	16	27	8

Table A.5b. [Mn(II)] release over time:
Miniprobes, 0.45 μm membrane, and ascorbate (52 μM Mn_T)

Time (hrs)	0.6	1.7	3.25	4.75
$[Mn]_{diss}$ (μM)	4.0	12	20	25
Std Dev (μM)	1	1	2	2

Table A.5c. [Mn(II)] release over time:
Miniprobes, 1.0 μm membrane, and ascorbate (52 μM Mn_T)

Time (hrs)	0.6	1.7	3.25	4.75
$[Mn]_{diss}$ (μM)	5.7	14	21	25
Std Dev (μM)	1	1	2	2

Table A.5d. [Mn(II)] release over time:
HMO and *S. oneidensis* MR-1 (360 μM Mn_T)

Time (hrs)	0.25	0.5	0.75	1	1.5	2	3	4
$[Mn]_{diss}$ (μM)	0.5	8.1	4.8	3.7	24	34	39	60
Std Dev (μM)	4	13	11	10	4	35	21	39

Table A.5e. [Mn(II)] release over time:
HMO-doped gels and *S. oneidensis* MR-1 (295 μM Mn_T)

Time (hrs)	4.5	8	16	25	36
$[Mn]_{diss}$ (μM)	13	23	43	65	86
Std Dev (μM)	2	4	7	6	12

Table A.5f. [Mn(II)] release over time:
Miniprobes, 1.0 μm membrane, and *S. oneidensis* MR-1 (62 μM Mn_T)

Time (hrs)	7.9	14	20	26	38.8	63
$[Mn]_{diss}$ (μM)	-0.4	2.2	5.5	8.1	14	27
Std Dev (μM)	1	2	1	3	4	6

Table A.5g. [Mn(II)] release over time:
Miniprobes, 5.0 μm membrane, and *S. oneidensis* MR-1 (60 μM Mn_T)

Time (hrs)	7.9	14	20	26	38.8	63
$[Mn]_{diss}$ (μM)	0.6	4.1	7.4	10	17	29
Std Dev (μM)	1	1	2	3	4	7

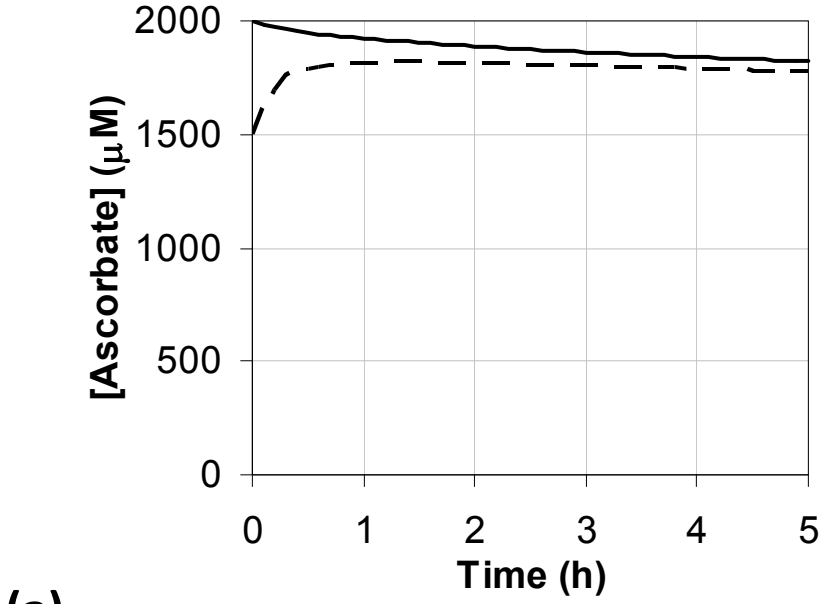

(a)

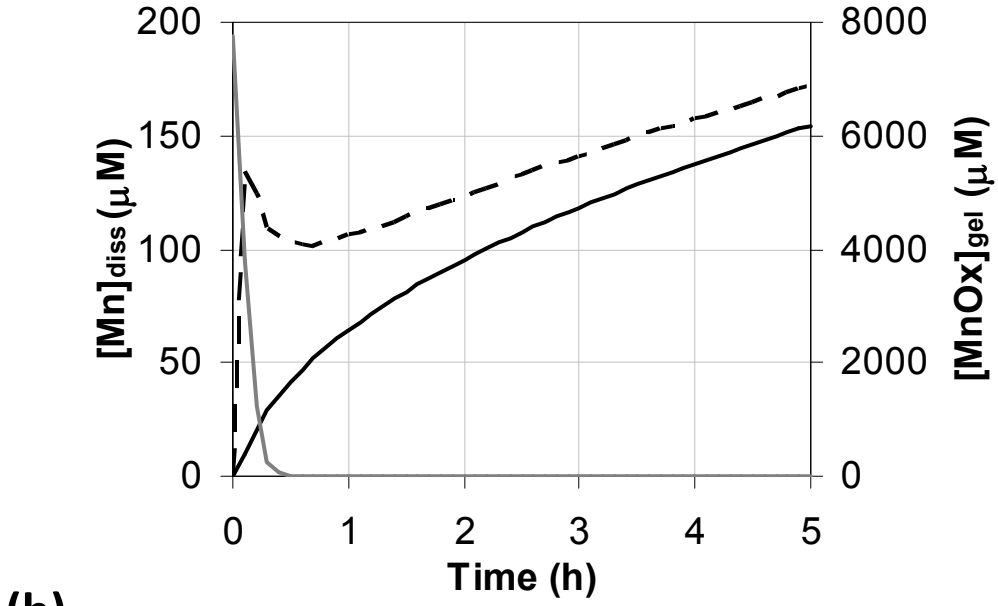

(b)

Figure A.2. AQUASIM model output for the reaction of ascorbate and HMO-doped gels in solution (modeled data is in Table A.5a). Shown are ascorbate (a) and dissolved Mn (b) in the gel (dashed line) and in the bulk (solid black line); the concentration of Mn oxide in the gel is represented with a solid gray line in (b).

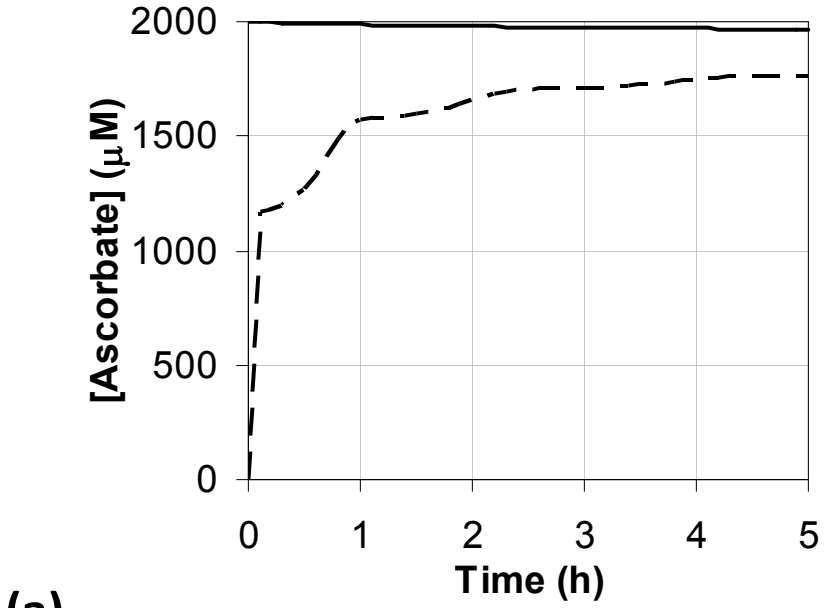

(a)

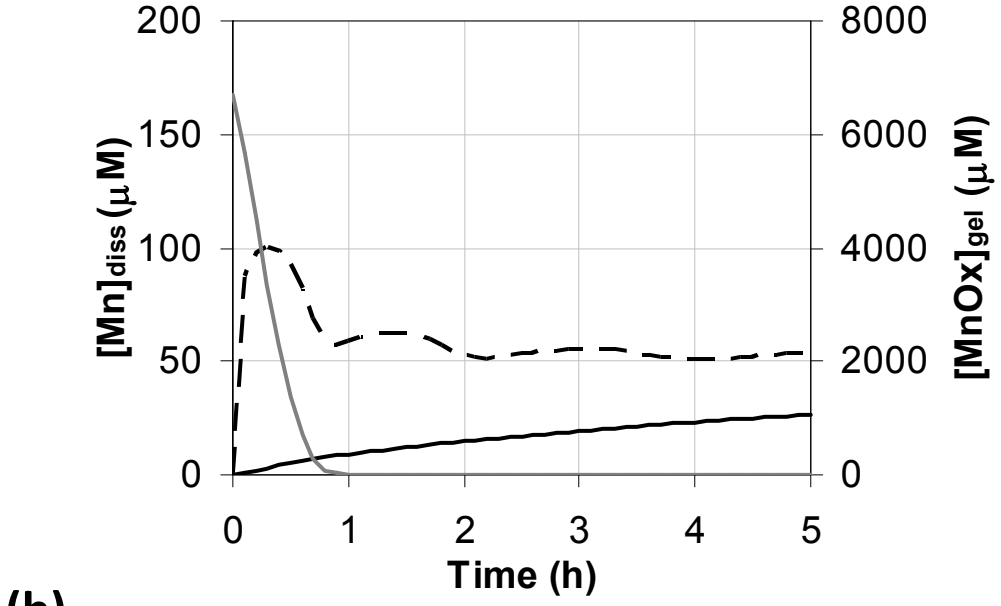

(b)

Figure A.3. AQUASIM model output for the reaction of ascorbate and HMO-doped gels in a miniprobe (1.0 μm membrane; modeled data is in Table A.5c). Shown are ascorbate (a) and dissolved Mn (b) in the gel (dashed line) and in the bulk (solid black line); the concentration of Mn oxide in the gel is represented with a solid gray line in (b).

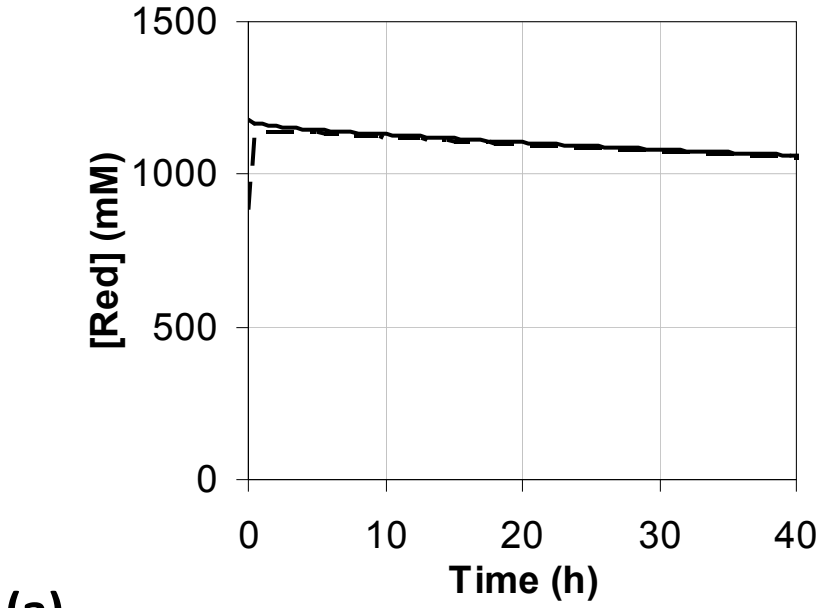

(a)

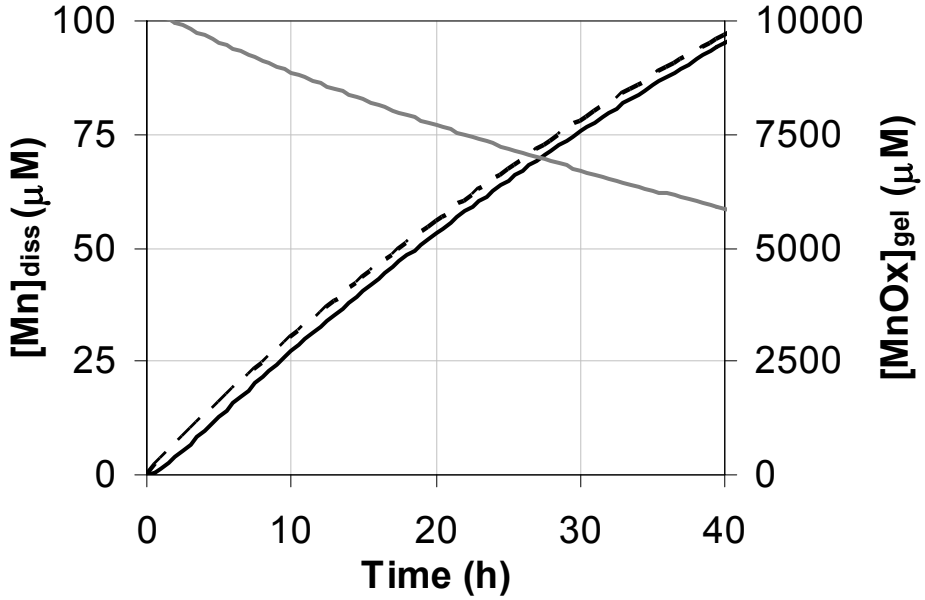

(b)

Figure A.4. AQUASIM model output for the reaction of *S. oneidensis* MR-1 and HMO-doped gels in solution (modeled data is in Table A.5e). Shown are the reductant "Red" (a) and dissolved Mn (b) in the gel (dashed line) and in the bulk (solid black line); the concentration of Mn oxide in the gel is represented with a solid gray line in (b).

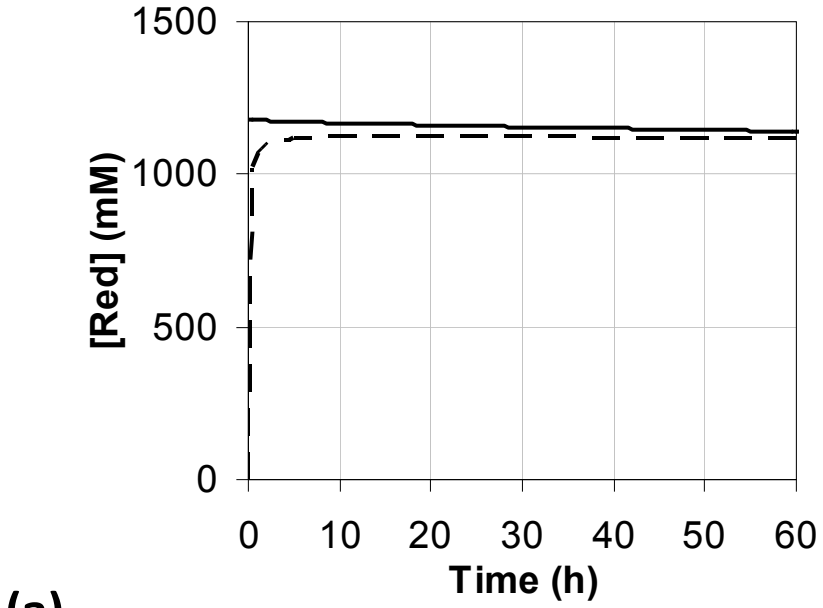

(a)

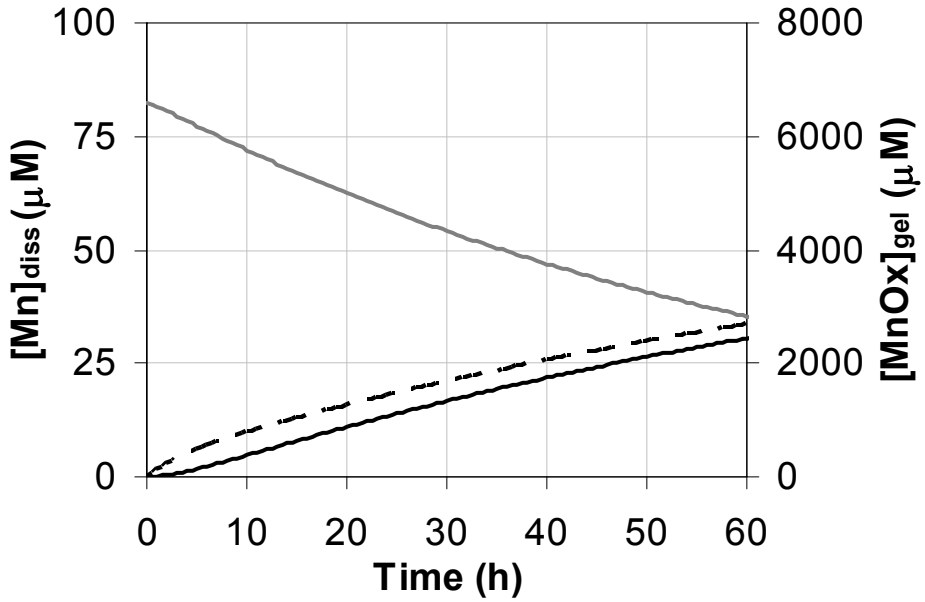

(b)

Figure A.5. AQUASIM model output for the reaction of *S. oneidensis* MR-1 and HMO-doped gels in a miniprobe (1.0 μm membrane; modeled data is in Table A.5f). Shown are the reductant "Red" (a) and dissolved Mn (b) in the gel (dashed line) and in the bulk (solid black line); the concentration of Mn oxide in the gel is represented with a solid gray line in (b).

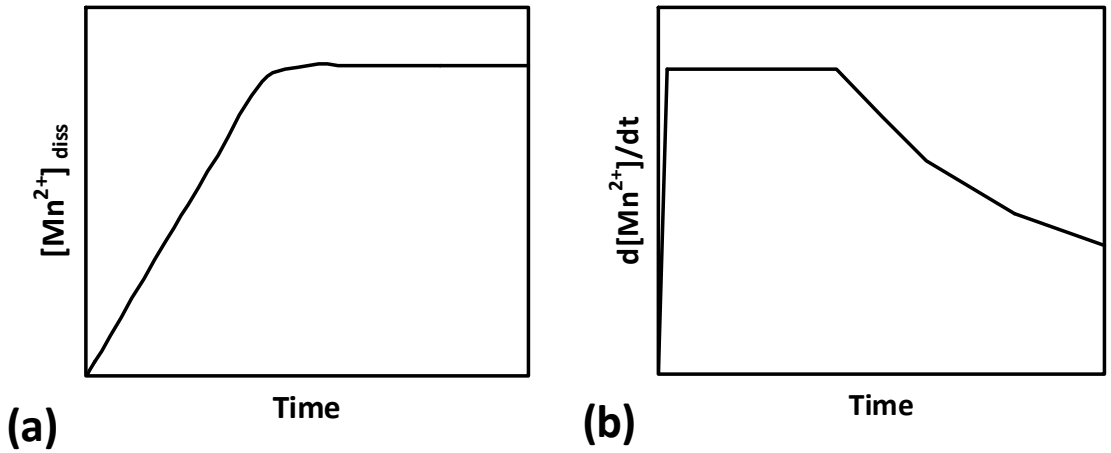

Figure A.6. Theoretical behavior of Mn reduction in an HMO-doped gel, in the absence of diffusion. Initially Mn^{2+} is produced at a constant rate (a), but when the HMO has been completely reduced, dissolved Mn^{2+} reaches a plateau. The reduction rate measured by the gel, which averages Mn loss over the cumulative time of deployment (b), would rapidly approach a plateau under steady-state conditions, but would decline after complete reduction of HMO; the gel method cannot determine when complete exhaustion has occurred during deployment.

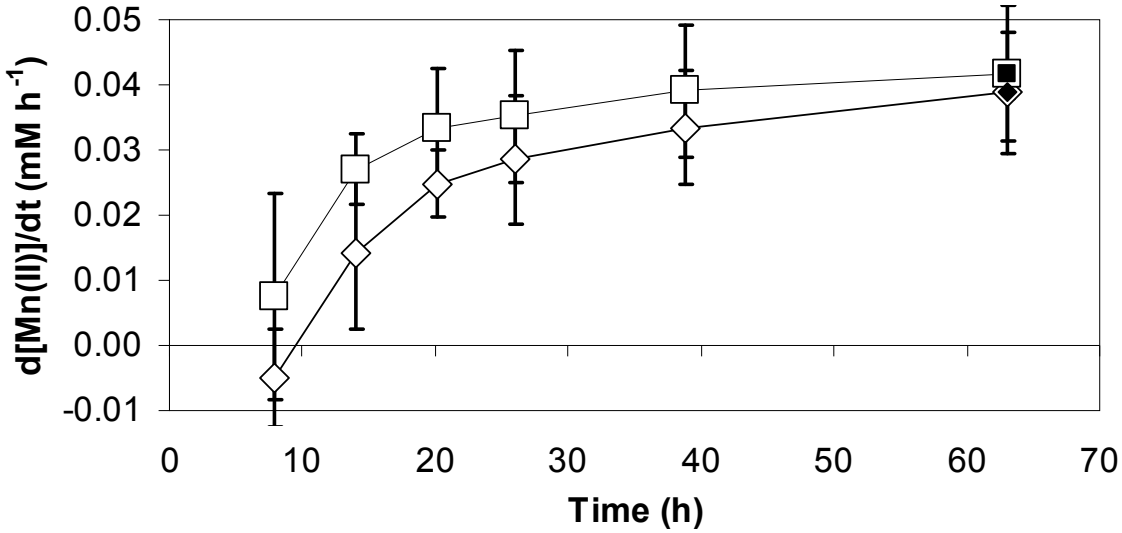

Figure A.7. Rate estimates as a function of time for the reaction of *S. oneidensis* MR-1 and HMO-doped gels in miniprobes.

The build-up of Mn(II) in the bulk solution over time was used to calculate the Mn loss from the gels as a function of time. For each time point, the cumulative Mn loss was divided by the time of reaction, and the resultant rates are plotted with unfilled symbols (squares for 1.0 μm membrane and diamonds for 5.0 μm membrane; raw data is in Table A.5f and g, respectively). The actual Mn recovered from the gels at the end of the experiment was used to calculate the points with filled symbols (standard deviations smaller than symbols). The two methods of rate calculation, from the solution phase and from the recovered gels, show remarkable agreement (this is possible because of the robust mass accounting in the experiment, as shown in Table A.1). This figure also shows that HMO-reduction rates with *S. oneidensis* MR-1 could be reasonably estimated by the gels after 39 h, even with an 8 h lag phase. Note that in contrast with Figure A.6b, diffusion has the affect of smoothing the approach of the plateau in d[Mn(II)]/dt vs. time. At the observed rate plateau, complete exhaustion of HMO would occur within 140 h.

Table A.6. Bias of clear gels co-located in the same miniprobe as HMO-doped gels (same conditions as experiment in Table A.5b, but Mn_T = 23.7 μM as 3 HMO-doped gels were replaced with clear gels). Concentrations were measured after 4 h.

[Mn] measured in solution (n=3 batches)	[Mn] measured in clear gels (n=3 batches×3 gels)
12.1±1.1 μM	194±105 μM

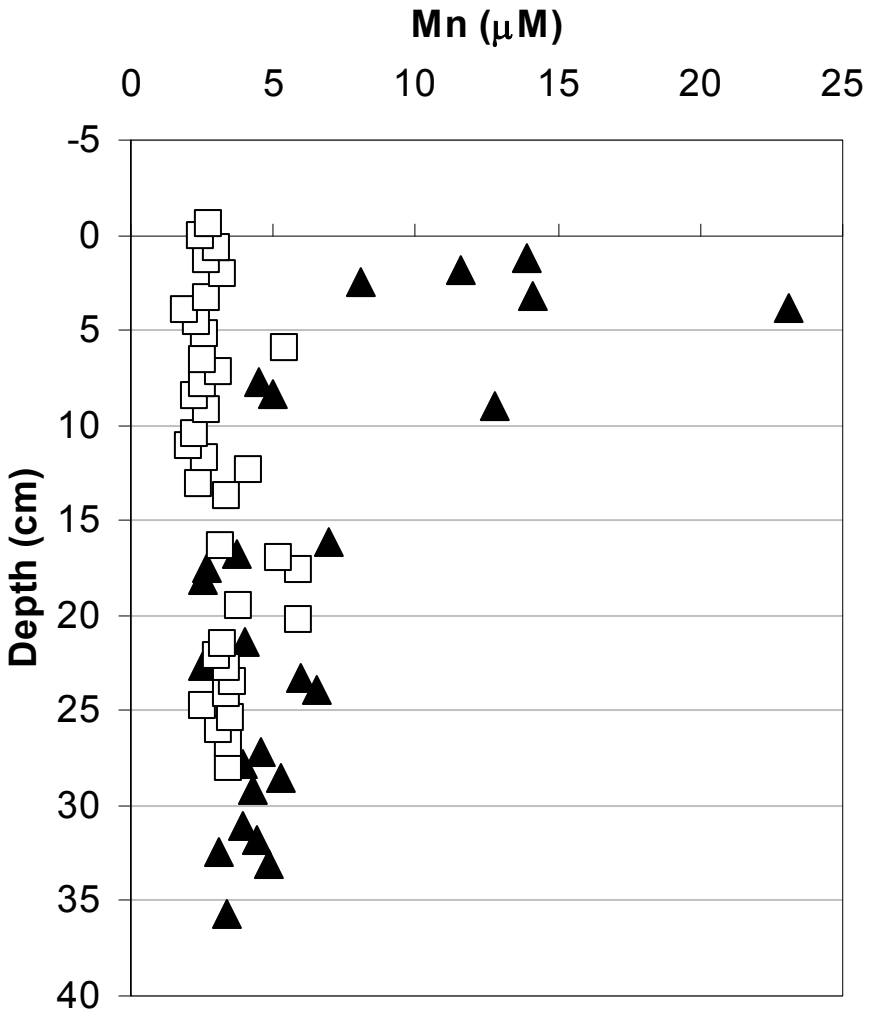

Figure A.8. Comparison of Mn concentrations measured in clear gels deployed in the same probe as HMO-doped gels (▲) and in a separate gel probe 85 cm away (□). The sediments were in a sabkha environment at Laguna Figueroa, Baja California, Mexico.

Appendix B

Supporting Information for

Chapter 4: A Hydrous Manganese Oxide Doped Gel Probe Sampler for Measuring *In Situ* Reductive Dissolution Rates: II. Field Deployment

Contents: 6 figures, 6 tables, and 1 MATLAB m-file code

Advection at the Lake Tegel Shoreline

The calm weather during deployment implies that exchange of surface water and sediment porewater due to wind-driven waves perpendicular to the shoreline was negligible. The main input flow to Lake Tegel from Nordgraben and Tegeler Fliess is 2.35 $m^3 s^{-1}$. For a lake cross-section approximately 1000 m wide and 8 m deep (Schauser and Chorus 2009), the average surface water velocity is ~ 25 m d^{-1} (parallel to the shoreline). However, this value was almost certainly much lower in our specific sampling location, which was protected by a barrier perpendicular to the shoreline that extended ~ 10 m into the lake. Thus, surface water flow is unlikely to affect our interpretation of sediment porewater chemistry.

Water levels in groundwater monitoring wells adjacent to the shoreline confirmed the presence of an unsaturated zone, with the depth to the water table 4.5 m below the lake water surface elevation. Infiltrating lake water should then be flowing vertically down through the area in which samples were collected, and thus this setting can be described with a generalized form of Darcy's Law appropriate for vertical flow:

$$\nu = K \cdot \left(\frac{\gamma(h_1 - h_2)}{\rho g L} + 1 \right) \qquad \text{(B-1)}$$

where ν is flow velocity (cm s^{-1}), γ is the specific weight of water, h_1 and h_2 are the water depths (m) at the two points, and L is the length (m) of the infiltration flow path (Bear 1972). The water depth at the sediment-water interface is 0.18 m (h_1), and the water depth at the groundwater table is 0 (h_2; pressure is assumed to be atmospheric). Using γ = 9.79 kN m^{-3}, ρ = 1000 kg m^{-3}, g = 9.8 m s^{-2}, L = 4.5 m, and the mean value for K, we estimate that the downward velocity of the infiltrating lake water was 0.055 cm s^{-1}.

In light of such downward advection, upward diffusion of dissolved species has little influence on these sediments. We can consider porewater Fe and Mn, as well as any *in situ* reductants, to reflect steady-state, rather than equilibrium, concentrations with stable redox boundaries, as seen in column studies (von Gunten and Zobrist 1993).

Table B.1. Lake Tegel sediment characterization

depth (cm)	porosity	particle size		hydraulic conductivity ($cm\ s^{-1}$)
		mean (µm)	mode (µm)	
0 - 5	0.43	303	302	5.6×10^{-2}
5 - 10	0.41	315	304	6.0×10^{-2}
10 - 15	0.50	266	321	6.4×10^{-2}
15 - 20	0.50	254	337	7.1×10^{-2}
20 - 27.5	0.55	333	382	6.7×10^{-2}

Because cores were collected so as to avoid compaction of sediment, porosity (ϕ) could be calculated as the volume of pore space in a core section (V_p) divided by the total volume of that core section (V_s). V_p was estimated as the dry mass of the sediment in a core section divided by an assumed density of 2.65 g cm^{-3} for sand (Bear 1972) and subtracted from V_s.

Particle size was measured with a Mastersizer 2000 (Malvern Instruments, Ltd., Worcestershire, U.K.) laser diffractometer following Sperazza et al. (2004) and Wildman (2009). Briefly, ~ 0.5 g of dry sediment was shaken in 5.5 g l^{-1} sodium hexametaphosphate for $\geq$ 4 h, and the sample-solution ratio was adjusted to give an obscuration of 20 ± 4%. Data were complied with the Mastersizer 2000 computer program (version 5.22, Malvern Instruments) using a particle absorbance index of 1.0 and a refractive index of 1.52. Five analytical replicates were averaged for each sample.

Table B.2. Porewater concentrations of detectable trace elements. Other elements tested, but below detection limits (in parentheses) were: As, Be, Cd, Mo, Sb, Tl, V (0.2 μg l^{-1}); Cr, Pb (0.5 μg l^{-1}); Se (10 μg l^{-1}); Zn (5 μg l^{-1}). Only Fe and Mn displayed trends with depth.

Element	Average (μM)
Co	0.03
Cu	0.9
Fe	24.8
Mn	2.5
Ni	0.1
Sr	2.5
Ti	6.2

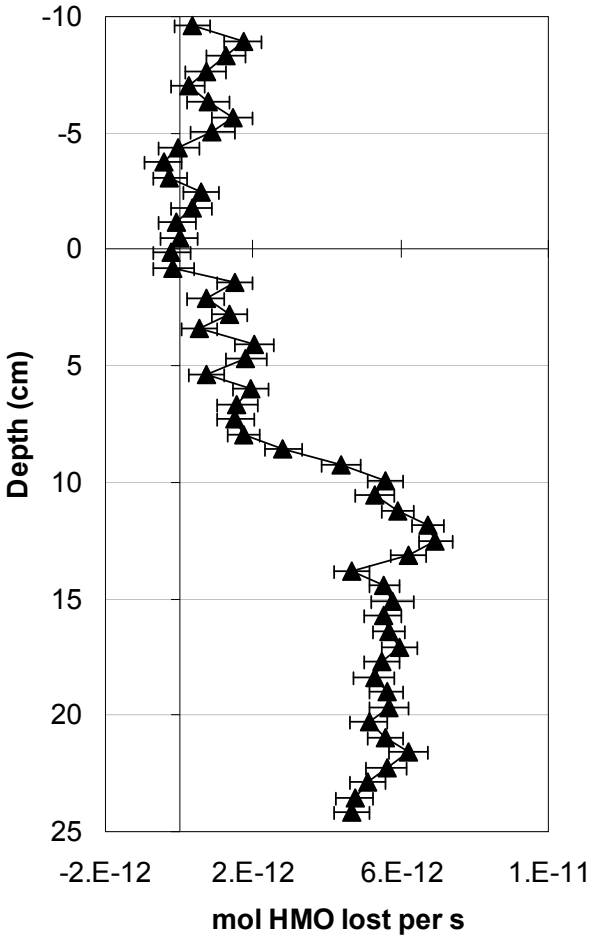

Figure B.1. Moles of HMO lost in each gel per s of deployment time. Error bars represent the variation from the 95% confidence interval in Mn_T. The R_{meas} data input to the MATLAB code is this data array divided by the mass of each gel.

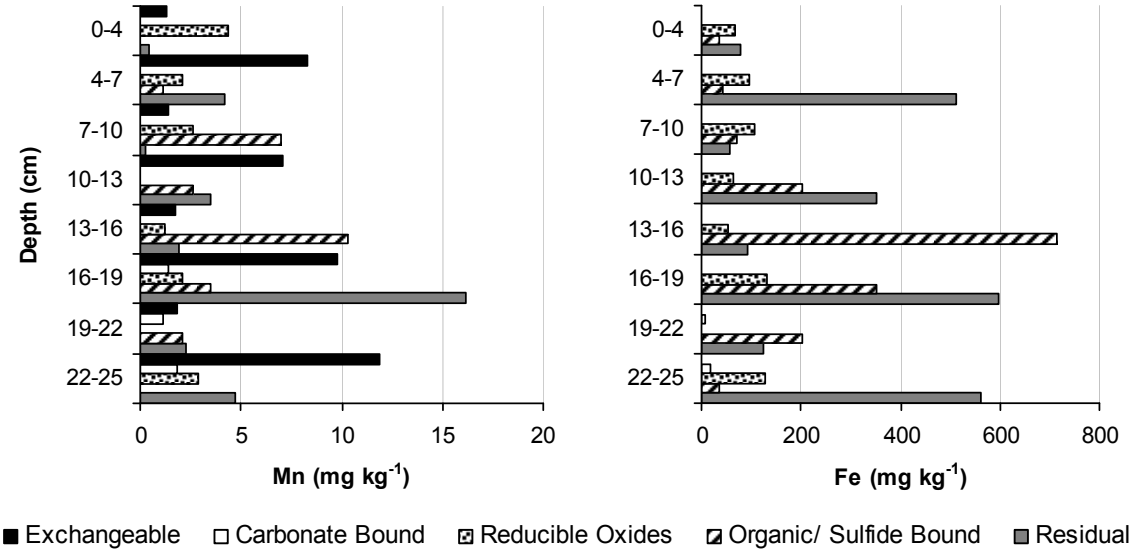

Figure B.2. Extracted manganese (left) and iron (right) concentrations per kg dry sediment, as determined by sequential extraction. Note the different scales of the two x-axes. Bars are averages of 3 subsamples for each core section.

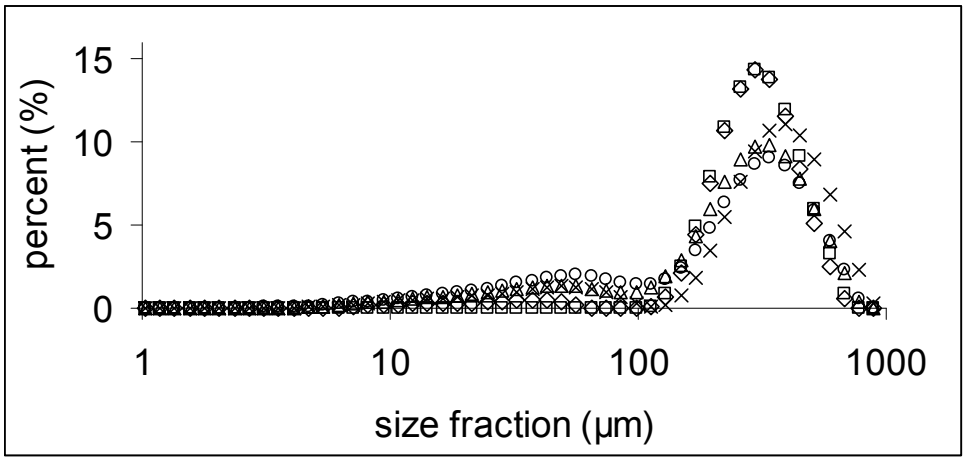

Figure B.3. Particle size in Lake Tegel shoreline sediment for 0–5 cm (◇), 5–10 cm (□), 10–15 cm (△), 15–20 cm (○), and 20–27.5 cm (×) core sections. Mode particle size values range from 301 to 382 µm (mean = 329 µm) and increase with depth.

Table B.3. Calculation of surface-area-normalized Mn reduction rates from field studies

Source	Location	Rate	Units	[MnOx] (M)	Notes
[1]	equatorial Atlantic Ocean	2.0×10^{-3}	yr^{-1}		a
	Chesapeake Bay	1.73×10^{-2}	yr^{-1}		a
	Long Island Sound	2.5×10^{1}	yr^{-1}		a
[2]	AMD wetland: shallow	5.2×10^{-10}	$M\ s^{-1}$	5.24×10^{-3}	a,b
	AMD wetland: maximum	1.04×10^{-9}	$M\ s^{-1}$	5.24×10^{-3}	a,b
[3]	Lake Michigan	7.0×10^{-6}	$g\ cm^{-2}\ yr^{-1}$		c
[4]	North Sea: Skagerrak Basin	$2.0\text{-}10\times10^{-4}$	$M\ d^{-1}$	6.14×10^{-4}	a,d
This	Lake Tegel: shallow	3.9×10^{-3}	h^{-1}		a
Study	Lake Tegel: deep	3.1×10^{-2}	h^{-1}		a
	Lake Tegel: maximum	1.0×10^{-1}	h^{-1}		a
[5]	eastern Danish coast	$3.6\text{-}11.7\times10^{-4}$	$mol\ m^{-2}\ d^{-1}$		e
[6]	Gulf of St. Lawrence	$3.1\text{-}46.2\times10^{-4}$	$mol\ m^{-2}\ d^{-1}$		e

[a] Rate divided by Mn oxide surface area of 49 $m^2\ g^{-1}$ and molecular weight of 86.94 g mol^{-1} (chemical formula MnO_2) for conversion

[b] Rate divided by the concentration of Mn oxide in the study's gel slabs, calculated from 1.1×10^{-6} mol Mn per unit length of gel and gel volume of 2.1×10^{-4} l per unit length

[c] Rate divided by Mn oxide molecular weight of 86.94 g mol^{-1} for conversion

[d] Rate divided by the concentration of Mn oxide in the sediment columns, 3×10^{-6} mol cm^{-3} of sediment, and $(1-\phi)\cdot\phi^{-1}$ (where ϕ is sediment porosity, 0.83) to convert the sediment volume to porewater volume (consistent with rate volume units)

[e] Only unit conversion needed

Sources: 1 Burdige and Gieskes (1983); 2 Edenborn and Brickett (2002); 3 Robbins and Callender (1975); 4 Canfield et al. (1993); 5 Balzer (1982); 6 Sundby and Silverberg (1985)

MATLAB m-file: “ksolver.m”

```
function [k,err,output] = ksolver(mn_f, MnT, var, Cpw, top, T)
% File ksolver.m
%  This function will solve the following partial differential equation
%  for k, the rate constant for Mn oxide reduction in sediments:
%    (dC/dt) = R_reductive_dissolution - R_diffusion
%    (dC/dt) = (k*(Mn_gel_total - C)) - (d/dx(dC/dx))
%   where C = C(t,x) and subject to boundary conditions:
%    C(0,x) = 0;
%    C(t,pw) = Cpw; pw = porewater outside of gel
%   The program will iterate upon various k values until (dC/dt)_gel at the
%   final t is equal to the dC/dt measured in the gel, within the
%   permissible error.
%   The rows in the mn_f matrix are considered separate "gels".  The
%   program will continue through each row until every gel has a k value.
%  The following variables must be entered:
%   mn_f = final amount of Mn recovered in each gel, given as mols
%    Mn/gel volume.  [vector; umol/mL]
%   MnT = total amount of Mn initially in gel, given as mols Mn/gel
%    volume.  Units must match mn_f. [single number; umol/mL]
%   var = 95% confidence interval bound for MnT batch.  Units must match
%    MnT. [single number; umol/mL]
%   Cpw = porewater Mn concentration for each depth, given as mols
%    Mn/porewater volume.  Assume porewater is an infinite sink for Mn,
%    with constant concentration Cpw. Units must match mn_f and MnT; size
%    must match mn_f. [vector; umol/mL]
%   top = distance from the top of the probe to the sediment-water
%    interface [cm]
%   T = total time of deployment [hrs]
%  The following output variables are possible:
%   k = rate coefficient for each gel, beginning at the top.  Columns list
%   k for MnT_lower, MnT, MnT_upper respectively. [1/hrs]
%   err = approximate relative error for each k [fractional]
%   output = code describing the solution of each k [0 = ok; 1 = error, k =
%    NaN; 2 = max iterations (100) reached before solution found]

%*****************************************************************
% First define parameters needed for calculations in all gels:
%
% Set dz step = vertical distance between gels = 0.65 cm.
dz = 0.65;
% Set number of gels = maximum number of z steps.
Z = max(size(mn_f));
% Define depth axis:
depth = top - dz*(0:(Z-1));
% Set dx step = gel thickness/5 "cells"
dx = 0.2/5;
% Set Dmn, the diffusion coefficient for Mn(2+) in gel [cm*cm/hr]. At 18C,
% Dmn = 5.75e-6 cm*cm/s (Li+Gregory 1974).
dmn = 0.0207;
B = dmn/dx/dx;
% Set initial dt step for stability: (1/(2B))>>dt
```

```
dt = dx*dx/(20*dmn);
% Define maximum number of time steps.
P = round(T/dt);
% Set limits of MnT; solving for k at each MnT gives an approximation of
% the k "error bounds".
Mn=[MnT-var;MnT;MnT+var];
% Begin at top of probe and run following code on each gel.
k=zeros(Z,3);
err=zeros(Z,3);
output=zeros(Z,3);
% Begin with MnT_lower, then MnT, finally MnT_upper.
for m=1:3
for z=1:Z
%*****************************************************************
% Next define parameters that apply only to one gel at a time:
%
% Set initial values of k equal to upper and lower guesses.
K=zeros(101,1);
K(1)=1e-4;
K(2)=2e-2;
% Calculate the measured dC/dt:
X=(Mn(m)-mn_f(z))/T;
% Acceptable error: [(k(i+1) - k(i))/k(i+1)] = 0.0005 = 0.05% for 3
% significant digits.
E=0.0005;
% Residual difference between X and X_t; solve for Resid(k)=0.
Resid=zeros(101,1);
Resid(1)=X;
%*****************************************************************
% Iterate on k until Resid is approximately 0.
%
for n=2:101
% Define concentration matrix: # columns = 5 cells.  Set boundary
% conditions: by default, C(0,x)=0 and C(t,pw)=Cpw.
% **Needs to be redefined for each iteration of code**
   C=zeros(P,5);
   HMO=Mn(m)*ones(P,1);
% Calculate C(t,x) for all t and x; keep track of HMO(t) [umols Mn/mL]
% for each time step.  HMO(t) is equivalent for all 5 cells.  When t = P (=
% approx. T), calculate dC [delta C (as in dC/dt); umols Mn/mL] and assess
% dC/T.
   for t=2:P
      HMO(t)=HMO(t-1)-dt*(K(n)*HMO(t-1));
      C(t,1)=C(t-1,1)+dt*(K(n)*(HMO(t-1))+B*(C(t-1,2)-C(t-1,1)));
      for x=2:4
         C(t,x)=C(t-1,x)+dt*(K(n)*HMO(t-1)+B*(C(t-1,x-1)-2*C(t-1,x)+C(t-1,x+1)));
      end
      C(t,5)=C(t-1,5)+dt*(K(n)*HMO(t-1)+B*((C(t-1,4)-C(t-1,5))+2*(Cpw(z)-C(t-1,5))));
   end
   dC=Mn(m)-HMO(P)-sum(C(P,1:5));
   X_t=dC/T;
   Resid(n)=X-X_t;
% Calculate new k value via the secant method.
   K(n+1)=K(n)-Resid(n)*(K(n)-K(n-1))/(Resid(n)-Resid(n-1));
% Compare k to previous k value; if less than acceptable error, return k.
   if abs((K(n+1)-K(n))/K(n+1))<=E
```

```
        k(z,m)=K(n+1);
        err(z,m)=abs((K(n+1)-K(n))/K(n+1));
        output(z,m)=0;
        break
    end
    % Break if k is not a number.
    if isnan(K(n+1))==1
        k(z,m)=K(n);
        err(z,m)=NaN;
        output(z,m)=1;
        break
    end
    % Maximum # of iterations is 100.
    if n+1==102
        k(z,m)=K(n);
        err(z,m)=NaN;
        output(z,m)=2;
    end
end
end
plot(k(1:Z,2),depth,'-ok')
hold on
plot(k(1:Z,1),depth,'>b')
plot(k(1:Z,3),depth,'<b')
xlabel('k [1/hrs]')
ylabel('Depth [cm]')
title('Apparent MnOxide rate coefficient vs. sediment depth')
hold off
end
```

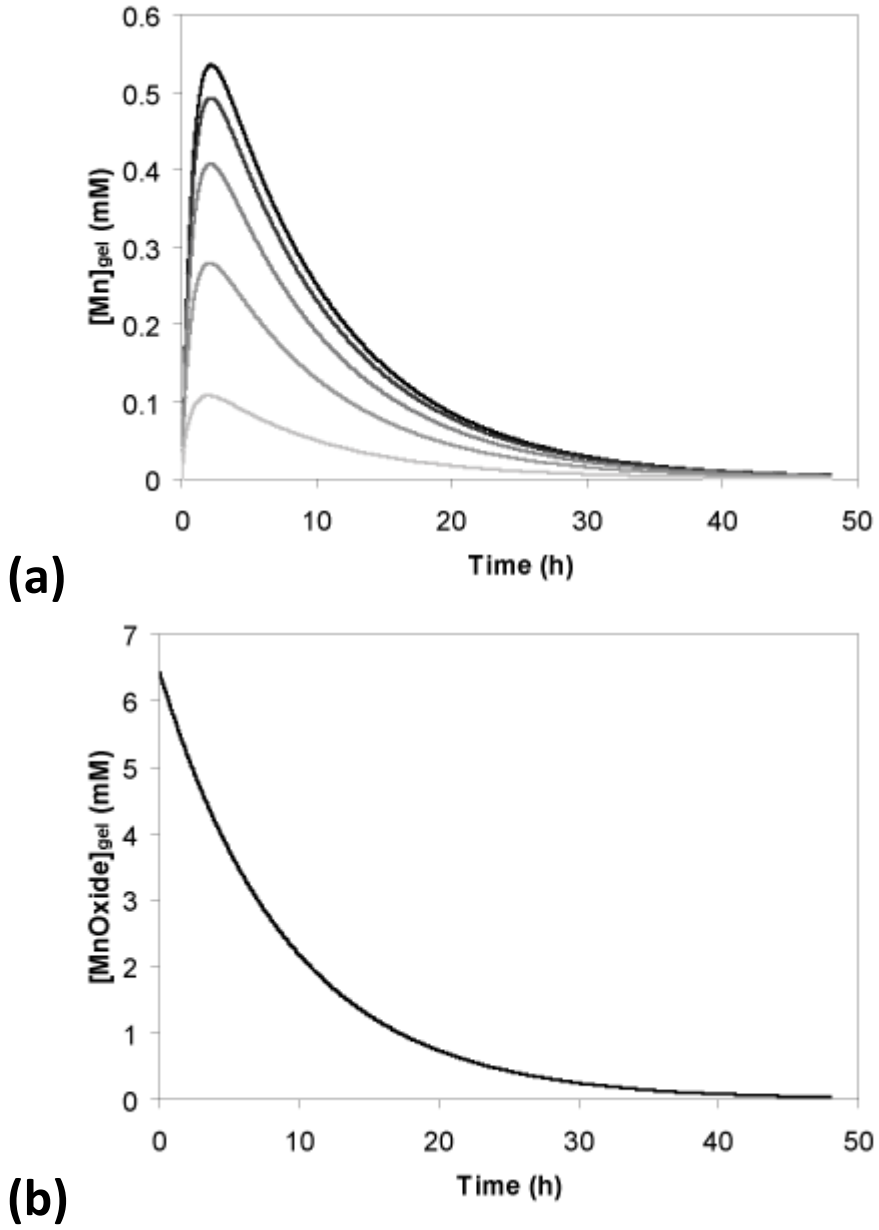

Figure B.4. Buildup of dissolved Mn ("C"; a) and decline of Mn oxide ("HMO"; b) inside of a gel, as calculated by the above Matlab m-file "ksolver". Dissolved Mn is plotted for each of the 5 cells, with darkest lines for the cells furthest from the porewater. This output was generated with the data for the maximum observed rate of Mn reduction in Figure 4.2b.

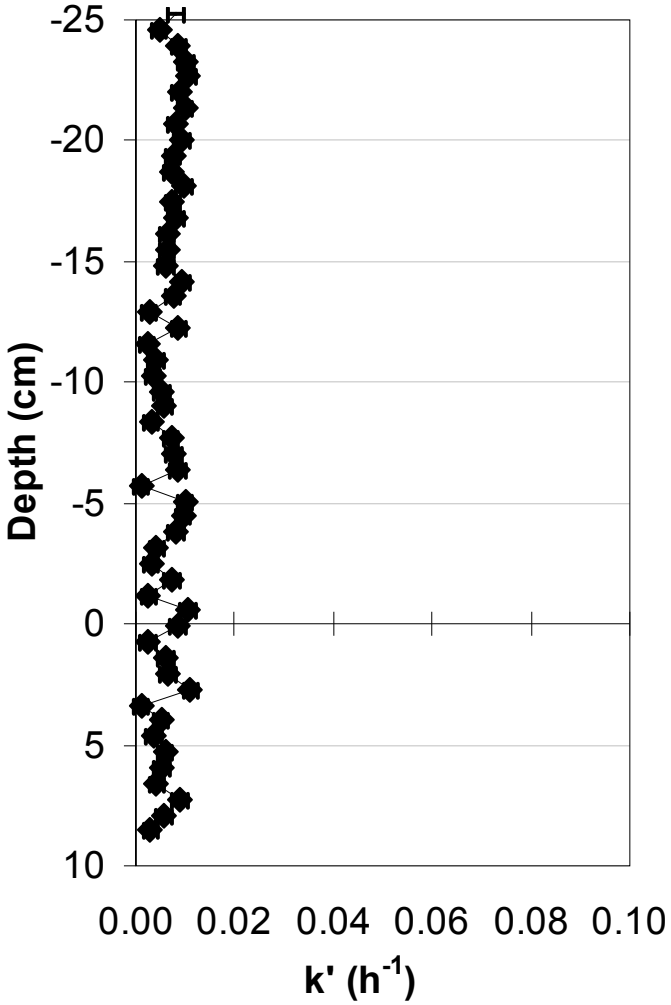

Figure B.5. Apparent pseudo-first-order rate coefficient k′ from HMO-doped gel probe deployed 20 m from the shoreline of Lake Tegel, Berlin, Germany (water depth = 89 cm). Porewater Mn was input as a constant 0.49 μM. This probe and a probe for clear gels were deployed, back-to-back, simultaneously with the probes presented in Chapter 4. However, sediments were quite hard, and both probes had to be hammered to reach just 10 cm depth (HMO-doped gel probe) and 20 cm depth (clear gel probe). The membrane of the clear gel probe ripped during deployment, so its data were suspect. Nevertheless, there was some evidence for a peak in dissolved Fe below 10 cm, which would be consistent with the probe deployed in more shallow water (Figure 4.2a). The rate coefficients for 0–9 cm depth in this figure (0.0056±0.0026 h^{-1}) are comparable with those for the same sediment depth in Figure 4.2b (0.0039±0.0025 h^{-1}).

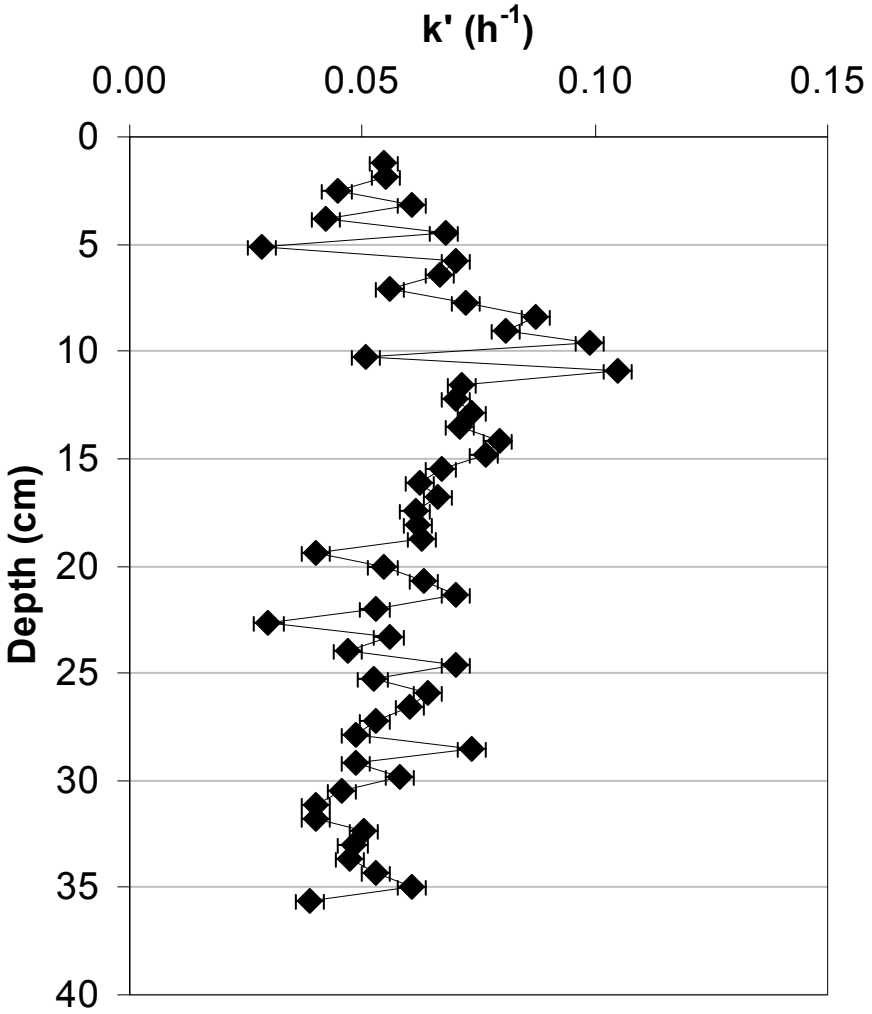

Figure B.6. Apparent pseudo-first-order rate coefficient k′ from HMO-doped gel probe deployed in the shallow sediments at Laguna Figueroa salt flats, Baja California, Mexico (12 h deployment; temperature 14–20°C). Porewater Mn was input as a constant 3.1 μM (average of porewater Mn from clear gel probe 85 cm away from HMO-doped gel probe), due to the contamination of many clear gels by sediment particles (Figure A8). The masses of the individual gels were not measured, and variation in these values may contribute significantly to the observed heterogeneities in the depth profile. Rate coefficients are comparable to the higher values in Figure 4.2b.

Table B.4. Gel probe data input to Matlab m-file "ksolver" and output k′ values. Total Mn for this batch was 6.03 ± 0.40 mM (95% confidence interval).

Sample:	Depth (cm)	C_{pw} (μM)	Mn recovered (mM)	k_lower	k (1/hr)	k_upper
a01	-10.25	2.445	5.61	8.80E-05	1.64E-03	3.09E-03
a02	-9.6	0.488	5.74	-4.48E-04	1.10E-03	2.55E-03
a03	-8.95	0.869	4.72	3.93E-03	5.48E-03	6.93E-03
a04	-8.3	0.007	5.09	2.23E-03	3.78E-03	5.23E-03
a05	-7.65	0.450	5.38	1.01E-03	2.56E-03	4.01E-03
a06	-7	1.252	5.85	-8.74E-04	6.76E-04	2.13E-03
a07	-6.35	0.358	5.44	7.58E-04	2.31E-03	3.76E-03
a08	-5.7	0.000	5.04	2.44E-03	3.99E-03	5.44E-03
a09	-5.05	0.000	5.36	1.05E-03	2.60E-03	4.05E-03
a10	-4.4	0.000	6.04	-1.60E-03	-4.95E-05	1.40E-03
a11	-3.75	0.000	6.42	-2.98E-03	-1.43E-03	1.96E-05
a12	-3.1	0.603	6.23	-2.30E-03	-7.51E-04	6.99E-04
a13	-2.45	0.000	5.59	1.29E-04	1.68E-03	3.13E-03
a14	-1.8	0.000	5.75	-5.21E-04	1.03E-03	2.48E-03
a15	-1.15	0.000	6.08	-1.75E-03	-2.01E-04	1.25E-03
a16	-0.5	0.791	6.03	-1.55E-03	5.03E-06	1.46E-03
a17	0.15	0.000	6.18	-2.11E-03	-5.60E-04	8.91E-04
a18	0.8	0.000	6.16	-2.04E-03	-4.94E-04	9.56E-04
a19	1.45	0.000	4.86	3.24E-03	4.79E-03	6.24E-03
a20	2.1	0.000	5.43	7.96E-04	2.35E-03	3.80E-03
a21	2.75	0.000	4.90	3.07E-03	4.62E-03	6.07E-03
a22	3.4	1.538	5.61	7.60E-05	1.63E-03	3.08E-03
a23	4.05	0.705	4.56	4.71E-03	6.26E-03	7.71E-03
a24	4.7	0.000	4.51	4.93E-03	6.48E-03	7.93E-03
a25	5.35	0.427	5.43	7.72E-04	2.32E-03	3.77E-03
a26	6	0.207	4.61	4.45E-03	6.00E-03	7.45E-03
a27	6.65	1.157	4.78	3.67E-03	5.22E-03	6.67E-03
a28	7.3	0.452	4.62	4.41E-03	5.96E-03	7.40E-03
a29	7.95	0.465	4.62	4.40E-03	5.94E-03	7.39E-03
a30	8.6	0.751	3.83	8.60E-03	1.01E-02	1.16E-02
a31	9.25	2.142	2.35	1.96E-02	2.11E-02	2.26E-02
a32	9.9	0.680	1.63	2.77E-02	2.93E-02	3.07E-02
a33	10.55	0.488	1.06	3.73E-02	3.89E-02	4.03E-02
a34	11.2	1.188	0.40	5.91E-02	6.06E-02	6.20E-02
a35	11.85	0.560	0.05	1.05E-01	1.07E-01	1.08E-01
a36	12.5	1.149	0.18	7.78E-02	7.94E-02	8.08E-02
a37	13.15	1.481	0.86	4.21E-02	4.36E-02	4.51E-02
a38	13.8	1.960	1.54	2.91E-02	3.06E-02	3.20E-02
a39	14.45	4.552	1.98	2.35E-02	2.51E-02	2.65E-02
a40	15.1	4.107	1.42	3.10E-02	3.25E-02	3.40E-02
a41	15.75	2.101	1.02	3.83E-02	3.99E-02	4.13E-02
a42	16.4	2.477	1.31	3.28E-02	3.43E-02	3.58E-02
a43	17.05	5.395	0.91	4.13E-02	4.28E-02	4.43E-02
a44	17.7	3.107	1.96	2.37E-02	2.53E-02	2.67E-02

Table B.4 (continued)

Sample:	Depth (cm)	C_{pw} (μM)	Mn recovered (mM)	k_lower	k (1/hr)	k_upper
a45	18.35	2.947	1.31	3.27E-02	3.43E-02	3.57E-02
a46	19	6.189	1.65	2.78E-02	2.94E-02	3.08E-02
a47	19.65	4.665	1.48	3.02E-02	3.18E-02	3.32E-02
a48	20.3	24.571	1.56	3.04E-02	3.20E-02	3.34E-02
a49	20.95	2.554	1.63	2.78E-02	2.94E-02	3.08E-02
a50	21.6	4.280	1.51	2.97E-02	3.12E-02	3.27E-02
a51	22.25	3.145	1.41	3.11E-02	3.26E-02	3.41E-02
a52	22.9	40.482	1.93	2.64E-02	2.80E-02	2.94E-02
a53	23.55	2.906	2.01	2.31E-02	2.46E-02	2.61E-02
a54	24.2	3.798	2.45	1.88E-02	2.03E-02	2.17E-02

Table B.5. Sequential extraction fractions of Mn (mg kg^{-1}). The detection limit was approximately 0.10 mg kg^{-1}.

	0-4 cm	4-7 cm	7-10 cm	10-13 cm	13-16 cm	16-19 cm	19-22 cm	22-25 cm
exchangeable	1.32	8.27	1.44	7.05	1.76	9.77	1.81	11.92
carbonate	>0.10	>0.10	>0.10	>0.10	0.10	1.42	1.16	1.80
reducible oxides	4.41	2.07	2.60	>0.10	1.22	2.13	>0.10	2.84
organics, sulfides	0.11	1.16	7.01	2.63	10.33	3.47	2.08	>0.10
residual (nonsilicate)	0.44	4.19	0.24	3.51	1.95	16.17	2.29	4.73

Table B.6. Sequential extraction fractions of Fe (mg kg^{-1}). The detection limit was approximately 0.10 mg kg^{-1}.

	0-4 cm	4-7 cm	7-10 cm	10-13 cm	13-16 cm	16-19 cm	19-22 cm	22-25 cm
exchangeable	1.1	>0.10	2.6	>0.10	>0.10	3.7	0.2	5.2
carbonate	>0.10	>0.10	>0.10	>0.10	>0.10	2.3	6.7	16.4
reducible oxides	67.9	97.5	105.6	62.4	53.8	131.7	3.5	128.0
organics, sulfides	33.8	41.8	71.7	201.6	714.5	353.4	201.4	36.4
residual (nonsilicate)	79.4	511.1	57.8	351.1	93.4	598.3	125.7	560.1

Appendix C

Supporting Information for

Chapter 5: Manganese Oxidation Induced by Water Table Fluctuations in a Sand Column.

Contents: 6 figures and 9 tables

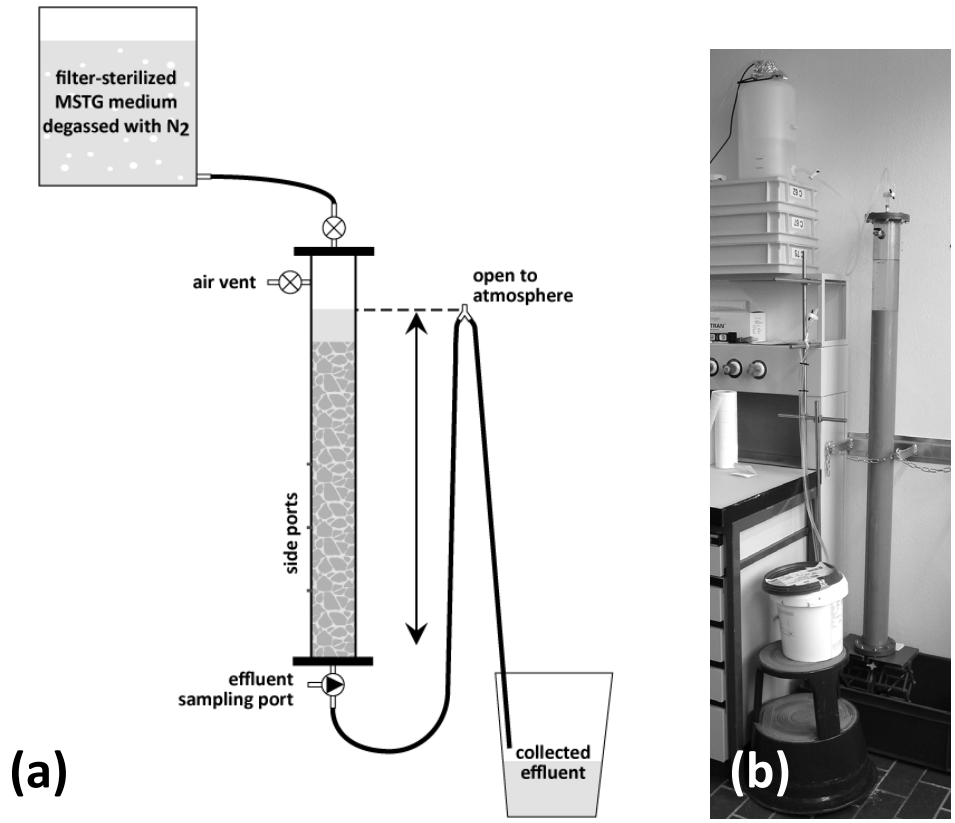

Figure C.1. Schematic (not to scale, a) and photo (b) of the column setup.

Table C.1. Results of oxidation assays at the end of the column experiment

sample #		OD_{600} t = 34 h	% Mn(II)	% Mn oxide
1	fresh MSTG, no cells	0.0529	100	0
2	fresh +plate, -Zn	0.1948	1	99
3a	fresh +effluent, -Zn	0.1948	1	99
3b	fresh +effluent, +Zn	0.3083	100	0
4	influent (+Zn)	0.3532	79	21

The first four batches used freshly prepared and filter-sterilized MSTG medium: (1) without inoculation, (2) inoculated from a plated GB-1 cell culture, and (3a) inoculated with the effluent at the end of the column experiment. One effluent-inoculated batch (3b) also contained 15 μM $ZnCl_2$. In addition, one batch used the column influent solution (4), which contained 15 μM $ZnCl_2$, collected at the end of the column experiment without deliberate inoculation; since that solution should have been sterile, some contamination

of the influent with cells able to travel upward along the column walls and through the 0.45 μm filter was suspected.

Lack of growth and oxidation in the fresh MSTG without cells (sample 1) confirms that the MSTG preparation was sterile. Remarkably, the OD_{600} and % oxidation were identical for the Zn-free batches inoculated with column effluent (3a) and directly from the refrigerated LB agar plate (2). Although no replicate assays were performed, this suggests strong similarity between the plated culture and the active culture in the column. The addition of Zn to a batch inoculated with column effluent (3b) resulted in complete inhibition of Mn oxidation, despite a slight growth enhancement. Intriguingly, the cells in the influent that included Zn (4) were able to grow even more and oxidized a fraction of the total Mn (N_2 degassing inhibited cell growth in the influent during the column experiment). This suggests that the pure culture eventually adjusted somewhat to the presence of Zn, or that a mixed culture developed inside the influent reservoir. On the other hand, this batch did not contain visible Mn oxides (+Zn batches had a greenish hue), so it is perhaps more likely that the nonzero Mn oxide fraction in this batch is an artifact of the extraction technique. Even if the column contained a mixed culture, the oxidation of significant amounts of Mn(II) during water table fluctuations does not detract from the end result of the paper.

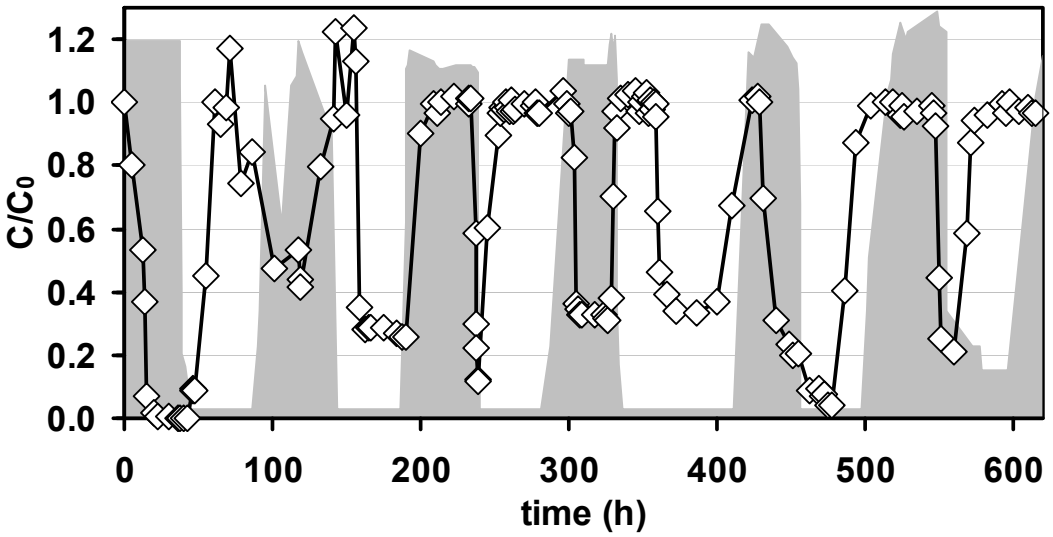

Figure C.2. Filtered relative effluent concentrations of Br (◇, C_0 = 10 μM). For reference, the water level in the column is shown in the shaded profile (note the vertical scale is different than Figure 5.1). Variation in Br derives from concentration differences in alternate batches of influent solution ("pulsed" inlet concentration). Up to 150 h, preferential flow paths and leaks through the column's side ports resulted in non-ideal flow behavior. Between concentration pulses, C/C_0 does not always approach 0 because 5-l batches of Br-free MSTG were added to the residual Br-containing MSTG in the influent reservoir, which was always > 0.5 l due to reservoir geometry.

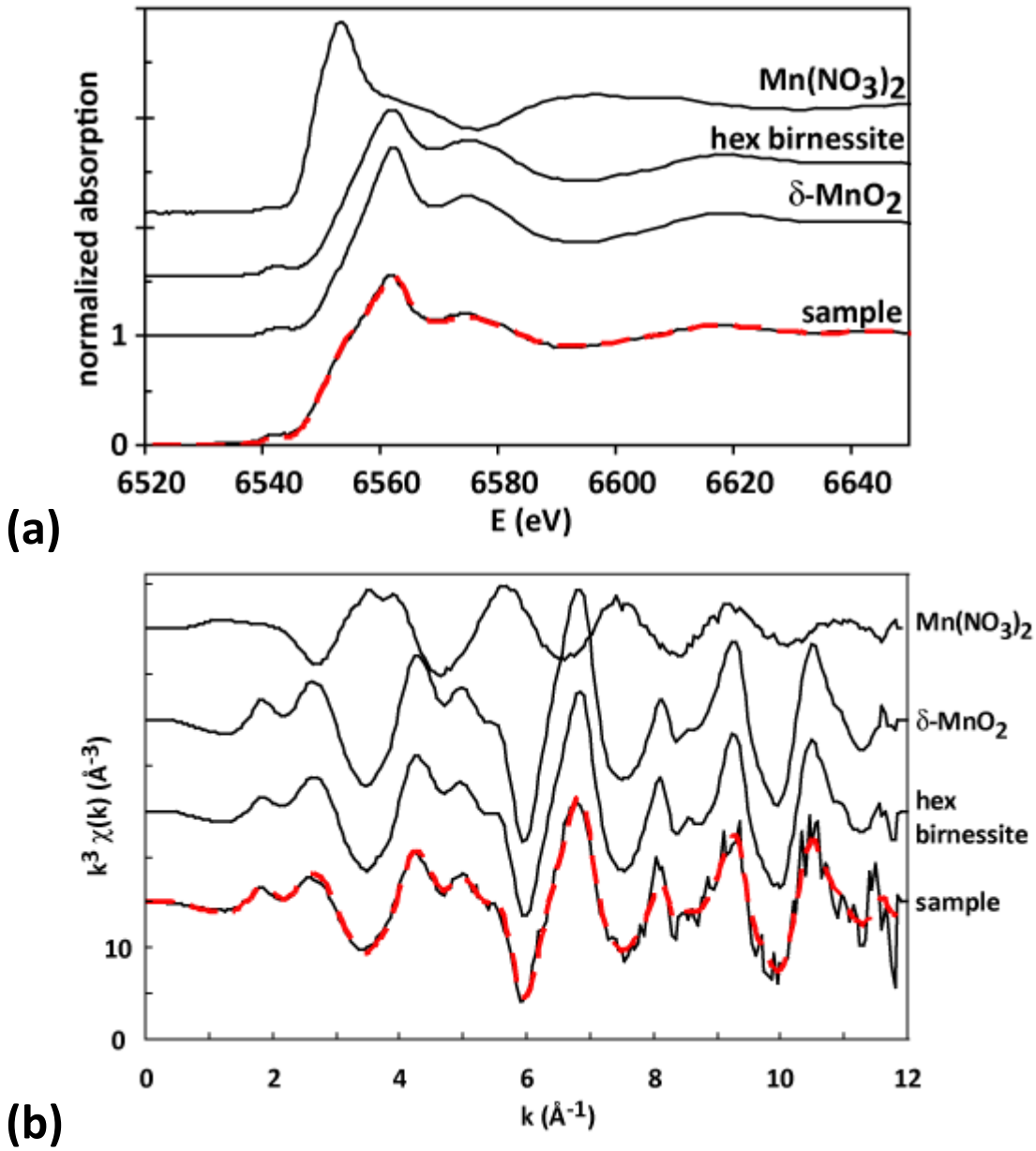

Figure C.3: (a) XANES and (b) EXAFS spectra of Mn at the top of the sand column, compared to linear combination fit (LCF) spectra based on reference spectra for aqueous Mn^{2+}, δ-MnO_2 (Webb et al. 2005), and hexagonal birnessite (Webb et al. 2005). LCF parameters are provided in Table C.2.

Comparison of the sample spectrum to the spectra of δ-MnO_2 (Mn oxidation state 3.8 (Villalobos et al. 2003)) and aqueous Mn^{2+} clearly indicates the presence of some Mn(II) in the sample spectrum. This Mn(II) fraction likely accounts for Mn^{2+} adsorbed to or inside bacteria, or sorbed to the Mn-precipitate or sand. Based on the LCF results for the

XANES region (considered more sensitive and reliable than the EXAFS region to quantify the Mn(II) fraction), this Mn(II) fraction was estimated to account for about 20% of the total Mn in the sand sample. Regarding the type of Mn oxide, the features in the EXAFS at 8 and 9.3 $Å^{-1}$ were characteristic for the phyllomanganates δ-MnO_2 and hexagonal birnessite but clearly distinct from the EXAFS of triclinic birnessite or the tectomanganate todorokite (Webb et al. 2005). This was confirmed by LCF analysis, which showed that the sample EXAFS spectrum could be reasonably reproduced by a combination of δ-MnO_2 and hexagonal birnessite.

Table C.2: Linear combination fit results for Mn XANES and EXAFS spectra at the top of the sand column

	δ-MnO_2	**hexagonal birnessite**	**aqueous Mn^{2+}**	**sum**	**NSSR[a]**
XANES	0.53 (0.04)[b]	0.28 (0.04)	0.20 (0.00)	1.01	4.6×10^{-4}
EXAFS	0.53 (0.13)	0.30 (0.14)	0.07 (0.00)	0.91	4.5×10^{-2}

[a]normalized sum of squared residuals = $\sum(data_i\text{-}fit_i)^2/\sum data_i^2$
[b]values in parentheses indicate fit uncertainty

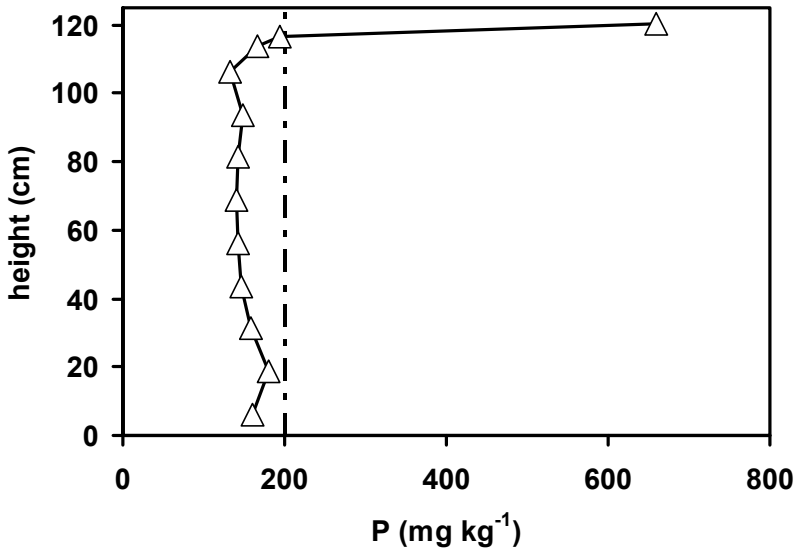

Figure C.4. XRF profile of P along the column at the end of the experiment. Dashed line indicates the background of unused sand. Other measured elements had no significant trend with height (not shown). Of note, the Fe concentration was below detection (1 mg kg^{-1}) in all samples.

Table C.3. Pseudo-first-order rate coefficients for Mn oxide reduction and OD_{600} during the reduction assay (averages of 3 replicate batches)

	k′ (h^{-1})	**OD_{600} t = 15 h**	**OD_{600} t = 64 h**
blank: MSTG only	0.0030 ± 0.0015	0.0531	0.0396
exponential: MSTG + *P. putida* GB-1[a]	0.0047 ± 0.0012	0.4328	0.2037
stationary: MSTG + *P. putida* GB-1[b]	0.0041 ± 0.0022	0.4441	0.2125

[a] Mn-doped gels were added at the beginning of exponential phase.
[b] Mn-doped gels were added at the beginning of stationary phase.

The rates for the two types of *P. putida* batches were not significantly different. Relatively large standard deviations for k′ (up to 50%) reflect the low amounts of Mn lost from the gels relative to the variation between individual gels. OD_{600} for the blank likely decreased due to colloidal components diffusing into the gels. The difference in OD_{600} at 15 h for exponential and stationary batches suggests a small inhibition of cell growth by the polyacrylamide gels doped with hydrous Mn oxide.

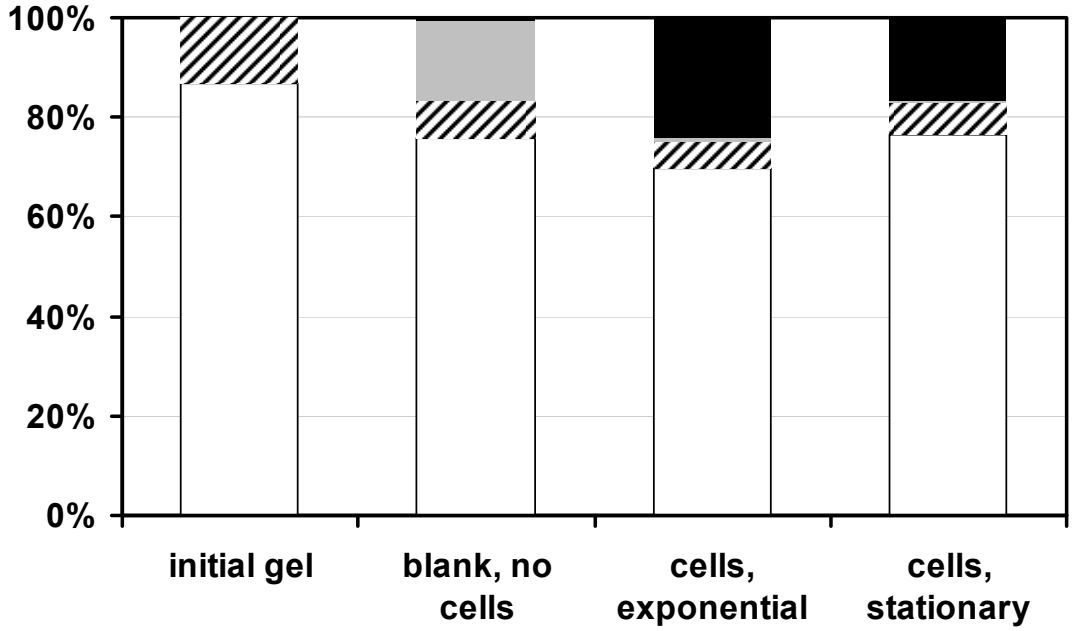

Figure C.5. Mass balance for unreacted gels ("initial gel") and batches at the end of the reduction assays (three replicates each), given as % of total mol Mn per batch. The white bar represents Mn oxide remaining in the gel, the striped bar represents Mn(II) remaining in the gel, the grey bar represents Mn(II) in solution, and the black bar represents Mn oxide in solution. Mn(II) was extracted with 0.05 M $Cu(NO_3)_2$ in 0.05 M $Ca(NO_3)_2$, while Mn oxide was calculated from the hydroxylamine-HCl-extracted total Mn minus the Mn(II). Total mass balance for each set of batches was closed within 4%. In the absence of cells, MSTG medium oxidized 4% of the solution-phase Mn (0.7% of the total Mn) in 64 h, which is negligible.

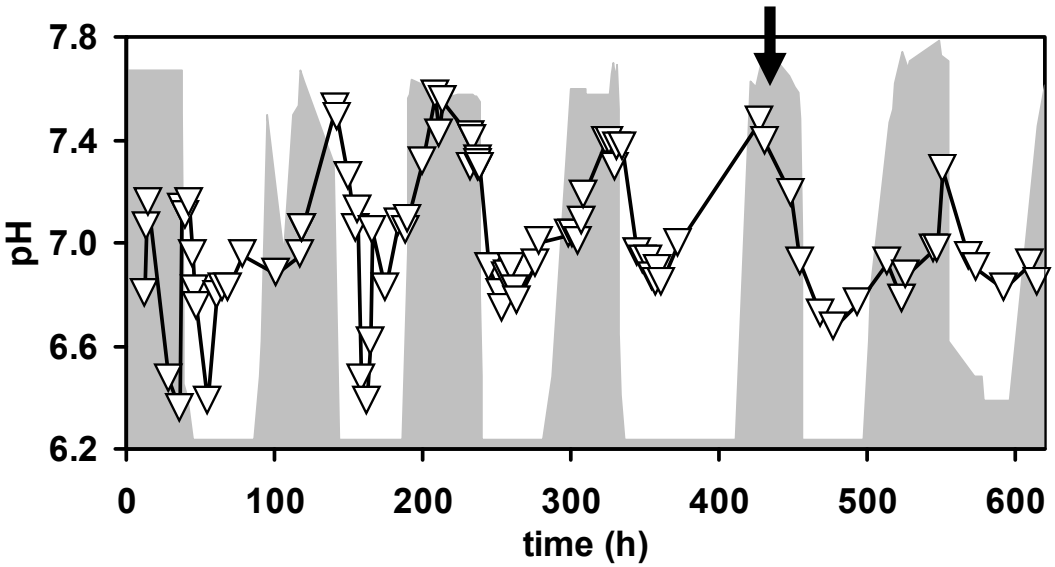

Figure C.6. Effluent pH (▽, influent pH = 7.5) measured directly at the base of the column. The arrow denotes the addition of 15 μM Zn to the influent. For reference, the water level in the column is shown in the shaded profile (note the vertical scale is different than Figure 5.1a). Low values in pH (< 6.6) before 60 h may indicate washout of residual amounts of Nanopure water (pH 5.5) trapped in the pore spaces.

Details of Mn Oxidation Rate Calculations

Abiotic Mn oxidation rate expressions are well-established in the literature.

Homogeneous Mn oxidation rate has been expressed (Morgan 2000):

$$-\frac{d[Mn^{2+}]}{dt} = k_1[O_2][OH^-]^2[Mn^{2+}] = k[Mn^{2+}] \qquad \text{(C-1)}$$

where k_1 is approximately 2×10^{12} M^{-3} d^{-1}, and k represents the pseudo-first-order rate constant. Heterogeneous Mn oxidation in this system is dependent on two different surfaces for catalysis: Mn oxides, here represented as MnO_2, and quartz sand, here represented as SiO_2. Mn adsorption to both surfaces has a reported (Davies and Morgan 1989) half-life of 5 min, so oxidation is assumed to be the only relevant step in the oxidation rate. Surface catalysis by Mn oxides was studied using hydrous Mn oxide (δ-

MnO_2) (Morgan and Stumm 1964), which is a high-surface-area analog of natural biogenic Mn oxides (Villalobos et al. 2003). Its ability to catalyze Mn oxidation has been expressed (Morgan 2000):

$$-\frac{d[Mn^{2+}]}{dt} = k_{Mn}[O_2][OH^-]^2[MnO_2][Mn^{2+}] = k_s[MnO_2][Mn^{2+}] \quad \text{(C-2)}$$

where k_{Mn} is approximately 5×10^{12} M^{-4} d^{-1}. The surface area and reactivity of δ-MnO_2 are assumed to be approximately equivalent to that of the Mn oxides in the column. Surface catalysis by SiO_2 was studied with nanoparticulate silica (Davies and Morgan 1989), a significantly different material than quartz sand. The rate expression for SiO_2-catalyzed Mn oxidation is:

$$-\frac{d[Mn^{2+}]}{dt} = k''a\{(>SO)_2Mn\}pO_2 = k''a\,{}^*\beta_2^s\{SOH\}[Mn^{2+}][H^+]^{-2}\,pO_2 \quad \text{(C-3)}$$

where k″ is 0.01 min^{-1} atm^{-1}, a is the mass loading (g l^{-1}), ${}^*\beta_2^s$ is $10^{-13.9}$ M, and {SOH} is 0.0015 mol g^{-1}, following Davies and Morgan (Davies and Morgan 1989). The surface area of nanoparticulate silica (182 m^2 g^{-1}) is orders of magnitude larger than that of the quartz sand, which was estimated to be 9.4×10^{-3} m^2 g^{-1} based on spherical particles with a diameter of 0.24 mm and a density of 2.65 g cm^{-3} (the surface area was too low to be measured by BET). The reactive surface sites and bidentate surface complexes are assumed to be the same for the two solids, and the reactivity is assumed to be proportional to the surface area. Thus, the rate constant k″ was scaled to the surface area of the quartz sand in the column.

To calculate the abiotic oxidation rates at the conditions inside the column, dissolved oxygen in equilibrium with air (or in the case of equation (C-3), pO_2 was 0.21 atm) and pH 7 were assumed. The maximum effluent dissolved oxygen was only 42%

saturation (Figure 5.2) and influent DO was always < 10%, so the calculated rates are faster than expected for the column's conditions. Although pH fluctuated between 6.35 and 7.55 (Figure C.6), the average was 7.01. The molar concentration of MnO_2 in equation (C-2) was estimated with the average XRF concentration across the column at the end of the experiment (20.5 mg kg^{-1}), the mass of Mn, and the mass of sand (~ 10 kg) in the column volume (~ 6 l). The mass of sand per liter was also used as "a" in equation (C-3). Finally, the influent [Mn^{2+}] of 100 μM was used in all three equations and the units converted to μM h^{-1}.

Table C.4. Observed levels of water table (WT; measured as cm above the base of the column) during experiment

time (h)	WT
0	135.5
4.63	135.5
12.75	135.5
13.50	135.5
14.50	135.5
16.92	135.5
20.58	135.5
22.50	135.5
29.25	135.5
36.17	135.5
37.50	135.5
37.67	123.9
38.67	65
39.50	48
41.25	44.5
45.33	32.5
46.60	32.5
47.83	32.5
54.60	32.5
61.33	32.5
65.33	32.5
69.33	32.5
71.83	32.5
79.30	32.5
86.75	32.5
89.17	50
90.67	60
94.17	121
94.83	123.5
106.83	84.5
111.58	123.5
115.33	126
117.58	135.5
119.00	132.5
139.58	110
142.58	32.5
150.00	32.5
155.17	32.5
156.75	32.5
159.33	32.5
162.67	32.5
164.50	32.5
166.33	32.5
175.25	32.5
184.16	32.5
185.08	32.5
188.58	85
189.83	128
190.24	128.7
191.21	133.2
207.96	130
208.41	129
211.08	128
213.75	128
222.92	129
232.08	129
233.08	128.5
234.08	128.5
237.50	127
237.67	100
237.83	73
238.00	50
238.50	32.5
239.00	32.5
252.17	32.5
254.67	32.5
259.50	32.5
262.17	32.5
263.17	32.5
276.67	32.5
279.08	32.5
285	50
298.17	130.4
301.83	130.4
304.67	130.4
307.42	130.4
308.67	129
323.67	129
325.50	134.5
326.75	137.5
327.92	133.5
329.08	136.5
329.83	137.3
330.54	125
330.70	95
330.92	62
331.08	45
334.83	32.5
345.25	32.5
348.92	32.5
352.75	32.5
355	32.5
357.58	32.5
359.08	32.5
360.83	32.5
372.33	32.5
399.5	32.5
408.08	32.5
418.58	132.5
421.20	130.8
426.92	140.3
431.58	140.1
444.33	134
448.83	130.8
450.21	129.4
451.83	122
452	90
452.2	50
453.58	32.5
454.5	32.5
469.25	32.5
472.5	32.5
477.75	32.5
494.33	32.5
497.67	60
498.67	75
511.83	121
513.33	125
515	132
519.67	140.6
523.58	136
525.75	138.2
544.58	144
544.83	144
546.83	140
550	138.2
550.17	135.5
550.38	130.4
550.52	128
550.92	100
551.33	75
551.7	60
568.58	50
569.08	50
573.83	50
574.67	43.3
590	43.3
592.16	43.3
610.5	120
615.25	131.3

Table C.5. Dissolved oxygen concentrations in the column effluent

time (h)	DO%	mg/L
0.00	1.5	0.13
37.50	5.8	0.47
39.50	9	0.7
45.33	21.3	1.81
47.83	24	2.05
61.33	27.1	2.32
69.33	19.2	1.65
71.83	23.9	2.05
86.75	25	2.14
118.25	5	0.43
119.00	3.3	0.28
141.83	14	1.20
142.33	16.3	1.40
155.17	34.3	2.94
156.25	35.6	3.05
159.33	36	3.08
162.67	36	3.08
166.33	37.9	3.26
184.16	36	3.09
187.30	1.5	0.13
190.41	2.1	0.18
208.41	1.6	0.14
213.75	1.4	0.12
232.08	1.6	0.14
234.08	12.5	1.07
237.33	8.6	0.73
237.67	13.3	1.13
238.00	16.4	1.40
238.50	14.8	1.26
239.00	15	1.28
252.17	18.7	1.61
257.83	29.6	2.54
259.50	24.5	2.10
262.17	27.8	2.38
263.17	30.6	2.61
276.67	32.3	2.76
279.08	23.3	2.00
298.42	12	1.02
301.83	2.3	0.20
304.67	3.2	0.27
307.42	2.3	0.20
308.67	2	0.17
323.67	9.1	0.78
326.75	15.5	1.33
329.92	9.8	0.83
331	14.1	1.19
334.83	16.1	1.38
345.25	34.7	2.97
348.92	36.1	3.09
352.75	41.7	3.56
355	36.6	3.13
357.58	40	3.42
359.08	35.7	3.05
360.83	39.2	3.35
372.33	38.5	3.30
399.5	32.9	2.82
426.92	16.3	1.39
431.58	12.6	1.08
448.83	10.6	0.90
454.5	33.1	2.82
469.25	33.5	2.88
472.5	37.7	3.22
477.75	30.3	2.59
494.33	32.9	2.81
513.33	2.2	0.19
523.58	2.1	0.18
525.75	2.7	0.23
544.83	11.6	0.99
547.9	12.3	1.05
551.4	19.8	1.68
569.08	34.1	2.92
573.83	31.4	2.69
592.16	24	2.05
610.5	14.5	1.24
615.25	13.2	1.12

Table C.6. pH values in the column effluent

time (h)	pH
12.75	6.80
13.50	7.06
14.50	7.15
29.25	6.47
36.17	6.35
37.50	7.13
39.50	7.10
42.50	7.15
45.33	6.95
46.60	6.81
47.83	6.75
54.60	6.38
61.33	6.79
65.33	6.82
69.33	6.82
79.30	6.95
100.83	6.88
117.92	6.95
118.25	7.05
119.00	7.05
141.83	7.52
142.33	7.48
150.00	7.25
155.17	7.05
156.75	7.12
159.33	6.47
162.67	6.38
164.50	6.61
166.33	7.04
175.25	6.82
184.16	7.07
188.30	7.04
190.41	7.09
199.41	7.31
208.41	7.57
211.08	7.42
213.75	7.55
232.08	7.41
233.08	7.29
234.08	7.40
237.33	7.32
237.67	7.30
238.00	7.29
238.50	7.29
239.00	7.29
245.60	6.90
252.17	6.80
253.40	6.74
256.25	6.86
257.83	6.87
259.50	6.90
262.17	6.81
263.17	6.77
276.67	6.91
279.08	7.00
298.42	7.03
301.83	7.03
304.67	7.00
307.42	7.08
308.67	7.18
323.67	7.39
326.75	7.39
329.92	7.29
331	7.37
334.83	7.37
345.25	6.96
348.92	6.93
352.75	6.93
355	6.86
357.58	6.84
359.08	6.89
360.83	6.84
372.33	6.99
426.92	7.47
431.58	7.39
448.83	7.19
454.5	6.92
469.25	6.72
477.75	6.67
494.33	6.76
513.33	6.92
523.58	6.78
525.75	6.87
544.83	6.97
547.9	6.97
551.4	7.28
569.08	6.94
573.83	6.90
592.16	6.82
610.5	6.91
615.25	6.84

Table C.7. Mn C/C_0 values in the column effluent

time (h)	C/C_0	time (h)	C/C_0	time (h)	C/C_0	time (h)	C/C_0
13.5	0.00	237.67	0.94	356.29	0.00	597.75	0.07
14.5	0.00	238	0.93	357.58	0.00	604.1	0.32
20.5	0.04	238.5	0.94	358.33	0.00	610.5	0.74
22.5	0.70	239	0.84	359.08	0.00	612.9	0.89
29.5	0.73	245.6	0.79	360	0.00	615.25	1.02
36	0.77	252.17	0.37	360.83	0.00		
37.5	0.80	253.4	0.31	366.58	0.00		
39.5	0.85	254.67	0.19	372.33	0.00		
42.5	0.87	256.25	0.10	385.92	0.00		
45.83	0.93	257.83	0.04	399.5	0.01		
46.6	0.93	258.67	0.02	410.5	0.01		
47.83	0.94	259.5	0.02	424.17	0.04		
54.6	0.97	260.83	0.01	426.92	0.09		
61.33	0.90	262.17	0.01	429.25	0.34		
65.33	0.92	263.17	0.01	431.58	0.58		
69.33	0.91	269.42	0.35	440.2	0.77		
71.83	0.92	276.67	1.11	448.83	0.90		
79.3	0.92	277.9	1.20	451.67	0.97		
86.75	0.80	279.08	1.03	454.5	0.96		
100.83	0.81	280.33	1.21	461.9	0.69		
117.92	0.90	295.92	1.22	469.25	0.75		
118.25	0.82	298.4	1.18	470.9	0.80		
119	0.87	300.1	1.25	472.5	0.73		
132	0.89	301.83	1.24	475.1	0.87		
141.83	0.88	303.25	1.27	477.75	0.89		
142.33	0.90	304.67	1.23	486	0.71		
150	0.96	306	1.23	494.33	0.69		
155.17	0.93	307.42	1.10	503.83	0.91		
156.75	0.85	308.67	0.93	513.33	0.99		
159.33	0.55	317	0.83	518.5	1.05		
162.67	0.31	323.67	0.86	523.58	0.99		
164.5	0.58	325.2	0.90	524.7	1.01		
166.33	0.83	326.75	0.89	525.75	0.93		
175.25	0.97	328.33	0.91	535.3	1.00		
184.16	0.90	329.92	0.92	544.83	1.03		
187.3	1.00	331	0.84	546.4	1.06		
190.41	1.00	332.56	0.87	547.9	1.01		
199.41	0.82	334.83	0.88	549.6	1.05		
208.41	0.87	340	0.40	551.4	0.98		
211.08	0.79	345.25	0.03	560.25	1.07		
213.75	0.86	347.08	0.01	569.08	1.03		
222.92	0.85	348.92	0.02	571.5	0.72		
232.08	0.86	350.83	0.01	573.83	0.30		
233.08	0.89	352.75	0.01	583	0.05		
234.08	0.87	353.9	0.00	592.16	0.02		
237.33	0.93	355	0.00	595	0.01		

Table C.8. Zn C/C_0 values in the column effluent

time (h)	C/C_0
440.2	0.02
448.83	0.02
451.67	0.02
454.5	0.02
461.9	0.18
469.25	0.22
470.9	0.31
472.5	0.27
475.1	0.28
477.75	0.29
486	0.36
494.33	0.30
503.83	0.30
513.33	0.32
518.5	0.34
523.58	0.38
524.7	0.33
525.75	0.32
535.3	0.32
544.83	0.35
546.4	0.34
547.9	0.35
549.6	0.35
551.4	0.36
560.25	0.39
569.08	0.51
571.5	0.56
573.83	0.60
583	0.60
592.16	0.62
595	0.60
597.75	0.63
604.1	0.51
610.5	0.42
612.9	0.43
615.25	0.46

Table C.9. XRF concentrations of Mn and Zn in the column at the end of the experiment

height above column base	**Mn ($mg\ kg^{-1}$)**	**Zn ($mg\ kg^{-1}$)**
118-122 cm	212.9	8.2
115-118 cm	87.3	2.9
113-115 cm	39.1	2
100-113 cm	21.7	1.8
88-100 cm	17.9	1.6
75-88 cm	10.6	1.8
63-75 cm	8.7	1.4
50-63 cm	8.2	1.6
38-50 cm	7.9	1.4
25-35 cm	8.7	1.3
13-25 cm	8.8	1.3
0-13 cm	9.2	1.2
unreacted sand	6.3	1.5

References

MINTEQA2/PRODEFA2, Geochemical assessment model for environmental systems, Version 4.03, 4.03; U.S. Environmental Protection Agency, National Exposure Research Laboratory, Ecosystems Research Division: Athens, GA, 2006.

Abboud, R.; Popa, R.; Souza-Egipsy, V.; Giometti, C.S.; Tollaksen, S.; Mosher, J.J.; Findlay, R.H.; Nealson, K.H., Low-Temperature Growth of *Shewanella oneidensis* MR-1. *Appl. Environ. Microbiol.* **2005,** *71*, 811–816.

Abiye, T.; Sulieman, H.; Ayalew, M., Use of treated wastewater for managed aquifer recharge in highly populated urban centers: a case study in Addis Ababa, Ethiopia. *Environ. Geol.* **2009,** *58*, 55–59.

Appelo, C.A.J.; Drijver, B.; Hekkenberg, R.; de Jonge, M., Modeling *In Situ* Iron Removal from Ground Water. *Ground Water* **1999,** *37*, 811–817.

Axe, L.; Trivedi, P., Intraparticle surface diffusion of metal contaminants and their attenuation in microporous amorphous Al, Fe, and Mn oxides. *J. Colloid Interf. Sci.* **2002,** *247*, 259–265.

Balcke, G.U.; Turunen, L.P.; Geyer, R.; Wenderoth, D.F.; Schlosser, D., Chlorobenzene biodegradation under consecutive aerobic–anaerobic conditions. *FEMS Microbiol. Ecol.* **2004,** *49*, 109–120.

Balzer, W., On the distribution of iron and manganese at the sediment/water interface: thermodynamic versus kinetic control. *Geochim. Cosmochim. Ac.* **1982,** *46*, 1153–1161.

Bandstra, J.Z.; Ross, D.E.; Brantley, S.L.; Burgos, W.D., Compendium and synthesis of bacterial manganese reduction rates. *Geochim. Cosmochim. Ac.* **2011,** *75*, 337–351.

Barnett, T.P.; Pierce, D.W., When will Lake Mead go dry? *Water Resour. Res.* **2008,** *44*, W03201.

Barnett, T.P.; Pierce, D.W.; Hidalgo, H.G.; Bonfils, C.; Santer, B.D.; Das, T.; Bala, G.; Wood, A.W.; Nozawa, T.; Mirin, A.A.; Cayan, D.R.; Dettinger, M.D., Human-Induced Changes in the Hydrology of the Western United States. *Science* **2008,** *319*, 1080–1083.

Battersby, S.; Teixeira, P.W.; Beltramini, J.; Duke, M.C.; Rudolph, V.; Diniz da Costa, J.C., An analysis of the Peclet and Damkohler numbers for dehydrogenation reactions using molecular sieve silica (MSS) membrane reactors. *Catalysis Today* **2006,** *116*, 12–17.

Bauer, R.D.; Rolle, M.; Kürzinger, P.; Grathwohl, P.; Meckenstock, R.U.; Griebler, C., Two-dimensional flow-through microcosms—Versatile test systems to study biodegradation processes in porous aquifers. *J. Hydrol.* **2009,** *369*, 284–295.

Bear, J., *Dynamics of Fluids in Porous Media*. Dover Publications, Inc.: Mineola, NY, 1972.

Beliaev, A.S.; Saffarini, D.A., *Shewanella putrefaciens* mtrB Encodes an Outer Membrane Protein Required for Fe(III) and Mn(IV) Reduction. *J. Bacteriol.* **1998,** *180*, 6292–6297.

Berner, R.A., *Early Diagenesis: A Theoretical Approach*. Princeton University Press: Princeton, NJ, 1980.

Berner, R.A., A new geochemical classification of sedimentary environments. *J. Sediment. Res.* **1981,** *51*, 359–365.

Beyerle, U.; Aeschbach-Hertig, W.; Hofer, M.; Imboden, D.M.; Baur, H.; Kipfer, R., Infiltration of river water to a shallow aquifer investigated with 3H/3He, noble gases and CFCs. *J. Hydrol.* **1999,** *220*, 169–185.

Blakeney, M.D.; Moulaei, T.; DiChristina, T.J., Fe(III) reduction activity and cytochrome content of *Shewanella putrefaciens* grown on ten compounds as sole terminal electron acceptor. *Microbiol. Res.* **2000,** *155*, 87–94.

Boogerd, F.C.; de Vrind, J.P., Manganese oxidation by *Leptothrix discophora*. *J. Bacteriol.* **1987,** *169*, 489–494.

Borch, T.; Kretzschmar, R.; Kappler, A.; Cappellen, P.V.; Ginder-Vogel, M.; Voegelin, A.; Campbell, K., Biogeochemical Redox Processes and their Impact on Contaminant Dynamics. *Environ. Sci. Technol.* **2010,** *44*, 15–23.

Bourg, A.C.M.; Darmendrail, D., Effect of Dissolved Organic-Matter and pH on the Migration of Zinc through River Bank Sediments. *Environ. Technol.* **1992,** *13*, 695–700.

Bourg, A.C.M.; Bertin, C., Biogeochemical Processes During the Infiltration of River Water into an Alluvial Aquifer. *Environ. Sci. Technol.* **1993,** *27*, 661–666.

Bourg, A.C.M.; Richard-Raymond, F., Spatial and temporal variability in the water redox chemistry of the M27 experimental site in the Drac River calcareous alluvial aquifer (Grenoble, France). *J. Contam. Hydrol.* **1994,** *15*, 93–105.

Bourg, A.C.M.; Bertin, C., Seasonal and Spatial Trends in Manganese Solubility in an Alluvial Aquifer. *Environ. Sci. Technol.* **2002,** *28*, 868–876.

Bouwer, H., Artificial recharge of groundwater: hydrogeology and engineering. *Hydrogeol. J.* **2002,** *10*, 121–142.

Brikowski, T.H., Doomed reservoirs in Kansas, USA? Climate change and groundwater mining on the Great Plains lead to unsustainable surface water storage. *J. Hydrol.* **2008,** *354*, 90–101.

Brown, C.J.; Misut, P.E., Aquifer geochemistry at potential aquifer storage and recovery sites in coastal plain aquifers in the New York city area, USA. *Appl. Geochem.* **2010,** *25*, 1431–1452.

Burdige, D.J.; Gieskes, J.M., A pore water/solid phase diagenetic model for manganese in marine sediments. *Am. J. Sci.* **1983,** *283*, 29–47.

Burdige, D.J.; Nealson, K.H., Chemical and Microbiological Studies of Sulfide-Mediated Manganese Reduction. *Geomicrobiol. J.* **1986,** *4*, 361–387.

Burdige, D.J.; Dhakar, S.P.; Nealson, K.H., Effects of Manganese Oxide Mineralogy on Microbial and Chemical Manganese Reduction. *Geomicrobiol. J.* **1992,** *10*, 27–48.

Buros, O.K.; Pyne, R.D.G., Extending Water-Supplies in Water Short Areas. *Desalination* **1994,** *98*, 437–442.

Campbell, K.M.; Root, R.; O'Day, P.A.; Hering, J.G., A Gel Probe Equilibrium Sampler for Measuring Arsenic Porewater Profiles and Sorption Gradients in Sediments: I. Laboratory Development. *Environ. Sci. Technol.* **2008a,** *42*, 497–503.

Campbell, K.M.; Root, R.; O'Day, P.A.; Hering, J.G., A Gel Probe Equilibrium Sampler for Measuring Arsenic Porewater Profiles and Sorption Gradients in Sediments: II. Field Application to Haiwee Reservoir Sediment. *Environ. Sci. Technol.* **2008b,** *42*, 504–510.

Canfield, D.E.; Thamdrup, B.; Hansen, J.W., The anaerobic degradation of organic matter in Danish coastal sediments: Iron reduction, manganese reduction, and sulfate reduction. *Geochim. Cosmochim. Ac.* **1993,** *57*, 3867–3883.

Capone, D.G.; Kiene, R.P., Comparison of Microbial Dynamics in Marine and Freshwater Sediments: Contrasts in Anaerobic Carbon Catabolism. *Limnol. Oceanogr.* **1988,** *33*, 725–749.

Carpenter, J.H., The Chesapeake Bay Institute Technique for the Winkler Dissolved Oxygen Method. *Limnol. Oceanogr.* **1965,** *10*, 141.

Caspi, R.; Tebo, B.M.; Haygood, M.G., c-Type Cytochromes and Manganese Oxidation in *Pseudomonas putida* MnB1. *Appl. Environ. Microbiol.* **1998,** *64*, 3549–3555.

Castro, F.D.; Tufenkji, N., Role of Oxygen Tension on the Transport and Retention of Two Pathogenic Bacteria in Saturated Porous Media. *Environ. Sci. Technol.* **2008,** *42*, 9178–9183.

Cey, B.D.; Hudson, G.B.; Moran, J.E.; Scanlon, B.R., Impact of Artificial Recharge on Dissolved Noble Gases in Groundwater in California. *Environ. Sci. Technol.* **2008**.

Chrambach, A.; Rodbard, D., Polyacrylamide Gel Electrophoresis. *Science* **1971,** *172*, 440–451.

Chrambach, A., *The Practice of Quantitative Gel Electrophoresis*. VCH: Weinheim, 1985.

Clark, J.F.; Hudson, G.B.; Davisson, M.L.; Woodside, G.; Herndon, R., Geochemical imaging of flow near an artificial recharge facility, Orange County, California. *Ground Water* **2004,** *42*, 167–174.

Corstjens, P.L.; de Vrind, J.P.; Westbroek, P.; de Vrind-de Jong, E.W., Enzymatic iron oxidation by *Leptothrix discophora*: identification of an iron-oxidizing protein. *Appl. Environ. Microbiol.* **1992,** *58*, 450–454.

Davies, S.H.R.; Morgan, J.J., Manganese(II) oxidation kinetics on metal oxide surfaces. *J. Colloid Interf. Sci.* **1989,** *129*, 63–77.

Davison, W.; Zhang, H.; Grime, G.W., Performance-Characteristics of Gel Probes Used for Measuring the Chemistry of Pore Waters. *Environ. Sci. Technol.* **1994,** *28*, 1623–1632.

Davranche, M.; Bollinger, J.-C., Heavy Metals Desorption from Synthesized and Natural Iron and Manganese Oxyhydroxides: Effect of Reductive Conditions. *J. Colloid Interf. Sci.* **2000,** *227*, 531–539.

de Vet, W.W.J.M.; van Genuchten, C.C.A.; van Loosdrecht, M.C.M.; van Dijk, J.C., Water quality and treatment of river bank filtrate. *Drink. Water Eng. Sci.* **2010,** *3*, 79–90.

de Vitre, R.R.; Buffle, J.; Perret, D.; Baudat, R., A study of iron and manganese transformations at the O_2/S(-II) transition layer in a eutrophic lake (Lake Bret, Switzerland): A multimethod approach. *Geochim. Cosmochim. Ac.* **1988,** *52*, 1601–1613.

DePalma, S.R. Ph.D. Thesis. Manganese Oxidation by *Pseudomonas putida*. Harvard University, 1993.

Descourvières, C.; Hartog, N.; Patterson, B.M.; Oldham, C.; Prommer, H., Geochemical controls on sediment reactivity and buffering processes in a heterogeneous aquifer. *Appl. Geochem.* **2009,** *25*, 261–275.

Dillon, P., Future management of aquifer recharge. *Hydrogeol. J.* **2005,** *13*, 313–316.

Dillon, P.; Pavelic, P.; Toze, S.; Rinck-Pfeiffer, S.; Martin, R.; Knapton, A.; Pidsley, D., Role of aquifer storage in water reuse. *Desalination* **2006,** *188*, 123–134.

Doussan, C.; Poitevin, G.; Ledoux, E.; Detay, M., River bank filtration: modelling of the changes in water chemistry with emphasis on nitrogen species. *J. Contam. Hydrol.* **1997,** *25*, 129–156.

Doussan, C.; Ledoux, E.; Detay, M., River-groundwater exchanges, bank filtration, and groundwater quality: Ammonium behavior. *J. Environ. Qual.* **1998,** *27*, 1418–1427.

Eckert, P.; Irmscher, R., Over 130 years of experience with Riverbank filtration in Düsseldorf, Germany. *J. Water Supply Res. T.* **2006,** *55*, 283–291.

Eckhardt, K.; Ulbrich, U., Potential impacts of climate change on groundwater recharge and streamflow in a central European low mountain range. *J. Hydrol.* **2003,** *284*, 244–252.

Edenborn, H.M.; Brickett, L.A., Determination of manganese stability in a constructed wetland sediment using redox gel probes. *Geomicrobiol. J.* **2002,** *19*, 485–504.

Edenborn, H.M.; Brickett, L.A.; Chaiken, R.F., Determination of trace element stability in sediments using redox gel probes: Probe construction and theoretical performance. *Geomicrobiol. J.* **2002,** *19*, 465–483.

Eusuff, M.M.; Lansey, K.E., Optimal operation of artificial groundwater recharge systems considering water quality transformations. *Water Resour. Manage.* **2004,** *18*, 379–405.

Farnsworth, C.E.; Hering, J.G., Hydrous Manganese Oxide Doped Gel Probe Sampler for Measuring *In Situ* Reductive Dissolution Rates. 1. Laboratory Development. *Environ. Sci. Technol.* **2010,** *44*, 34–40.

Farnsworth, C.E.; Griffis, S.D.; Wildman, J.R.A.; Hering, J.G., Hydrous Manganese Oxide Doped Gel Probe Sampler for Measuring *In Situ* Reductive Dissolution Rates. 2. Field Deployment. *Environ. Sci. Technol.* **2010,** *44*, 41–46.

Fones, G.R.; Davison, W.; Grime, G.W., Development of constrained DET for measurements of dissolved iron in surface sediments at sub-mm resolution. *Sci. Total Environ.* **1998,** *221*, 127–137.

Francis, C.A.; Tebo, B.M., *cumA* Multicopper Oxidase Genes from Diverse Mn(II)-Oxidizing and Non-Mn(II)-Oxidizing *Pseudomonas* Strains. *Appl. Environ. Microbiol.* **2001,** *67*, 4272–4278.

Frischherz, H.; Zibuschka, F.; Jung, H.; Zerobin, W., Biological elimination of iron and manganese. *Water Supply* **1985,** *3, Berlin 'B'*, 125–136.

Fuller, C.C.; Harvey, J.W., Reactive Uptake of Trace Metals in the Hyporheic Zone of a Mining-Contaminated Stream, Pinal Creek, Arizona. *Environ. Sci. Technol.* **2000,** *34*, 1150–1155.

Gadde, R.R.; Laitinen, H.A., Heavy metal adsorption by hydrous iron and manganese oxides. *Anal. Chem.* **1974,** *46*, 2022–2026.

Gandy, C.J.; Smith, J.W.N.; Jarvis, A.P., Attenuation of mining-derived pollutants in the hyporheic zone: A review. *Sci. Total Environ.* **2007,** *373*, 435–446.

Gaus, I.; Shand, P.; Gale, I.N.; Williams, A.T.; Eastwood, J.C., Geochemical modelling of fluoride concentration changes during Aquifer Storage and Recovery (ASR) in

the Chalk aquifer in Wessex, England. *Q. J. Eng. Geol. Hydroge.* **2002,** *35*, 203–208.

Gino, E.; Starosvetsky, J.; Kurzbaum, E.; Armon, R., Combined Chemical-Biological Treatment for Prevention/Rehabilitation of Clogged Wells by an Iron-Oxidizing Bacterium. *Environ. Sci. Technol.* **2010,** *44*, 3123–3129.

Gleick, P.H., Water management: Soft water paths. *Nature* **2002,** *418*, 373–373.

Greskowiak, J.; Prommer, H.; Massmann, G.; Johnston, C.D.; Nutzmann, G.; Pekdeger, A., The impact of variably saturated conditions on hydrogeochemical changes during artificial recharge of groundwater. *Appl. Geochem.* **2005,** *20*, 1409–1426.

Greskowiak, J.; Prommer, H.; Massmann, G.; Nutzmann, G., Modeling seasonal redox dynamics and the corresponding fate of the pharmaceutical residue phenazone during artificial recharge of groundwater. *Environ. Sci. Technol.* **2006,** *40*, 6615–6621.

Gunkel, G.; Hoffmann, A. In *Clogging processes in a bank filtration system in the littoral zone of Lake Tegel (Germany)*, 5th International Symposium on Managed Aquifer Recharge, Berlin, 2005; 599–604.

Gupta, V.; Johnson, W.P.; Shafieian, P.; Ryu, H.; Alum, A.; Abbaszadegan, M.; Hubbs, S.A.; Rauch-Williams, T., Riverbank Filtration: Comparison of Pilot Scale Transport with Theory. *Environ. Sci. Technol.* **2009,** *43*, 669–676.

Haberer, C.M.; Rolle, M.; Liu, S.; Cirpka, O.A.; Grathwohl, P., A high-resolution non-invasive approach to quantify oxygen transport across the capillary fringe and within the underlying groundwater. *J. Contam. Hydrol.* **2011,** *122*, 26–39.

Hallberg, R.O.; Martinell, R., Vyredox—*In Situ* Purification of Ground Water. *Ground Water* **1976,** *14*, 88–93.

Harper, M.P.; Davison, W.; Tych, W., Temporal, spatial, and resolution constraints for *in situ* sampling devices using diffusional equilibration: Dialysis and DET. *Environ. Sci. Technol.* **1997,** *31*, 3110–3119.

Hässelbarth, U.; Lüdemann, D., Biological Incrustation of Wells Due to Mass Development of Iron and Manganese Bacteria. *Water Treatment and Examination* **1972,** *21*, 20–29.

Hastings, D.; Emerson, S., Oxidation of manganese by spores of a marine *Bacillus*: Kinetic and thermodynamic considerations. *Geochim. Cosmochim. Ac.* **1986,** *50*, 1819–1824.

Herczeg, A.L.; Rattray, K.J.; Dillon, P.J.; Pavelic, P.; Barry, K.E., Geochemical processes during five years of aquifer storage recovery. *Ground Water* **2004,** *42*, 438–445.

Hiscock, K.M.; Grischek, T., Attenuation of groundwater pollution by bank filtration. *J. Hydrol.* **2002,** *266*, 139–144.

Hoffmann, A.; Gunkel, G., Carbon input, production and turnover in the interstices of a Lake Tegel bank filtration site, Berlin, Germany. *Limnologica* **2011a,** *In Press, Corrected Proof.*

Hoffmann, A.; Gunkel, G., Bank filtration in the sandy littoral zone of Lake Tegel (Berlin): Structure and dynamics of the biological active filter zone and clogging processes. *Limnologica* **2011b,** *41*, 10–19.

Hoppe-Jones, C.; Oldham, G.; Drewes, J.E., Attenuation of total organic carbon and unregulated trace organic chemicals in U.S. riverbank filtration systems. *Water Res.* **2010,** *44*, 4643–4659.

Immerzeel, W.W.; van Beek, L.P.H.; Bierkens, M.F.P., Climate Change Will Affect the Asian Water Towers. *Science* **2010,** *328*, 1382–1385.

Jacobs, L.A.; von Gunten, H.R.; Keil, R.; Kuslys, M., Geochemical Changes Along a River-Groundwater Infiltration Flow Path—Glattfelden, Switzerland. *Geochim. Cosmochim. Ac.* **1988,** *52*, 2693–2706.

Jensen, D.L.; Boddum, J.K.; Tjell, J.C.; Christensen, T.H., The solubility of rhodochrosite (MnCO3) and siderite (FeCO3) in anaerobic aquatic environments. *Appl. Geochem.* **2002,** *17*, 503–511.

Jha, M.K.; Peiffer, S. In *Simulation modeling of salient artificial recharge techniques for sustainable groundwater management*, 5th International Symposium on Managed Aquifer Recharge, Berlin, 2005; 388–394.

Jimenez, B.; Chavez, A., Quality assessment of an aquifer recharged with wastewater for its potential use as drinking source: "El Mezquital Valley" case. *Water Sci. Technol.* **2004,** *50*, 269–276.

Johnson, J.S.; Baker, L.A.; Fox, P., Geochemical transformations during artificial groundwater recharge: soil-water interactions of inorganic constituents. *Water Res.* **1999,** *33*, 196–206.

Jurgensen, A.; Widmeyer, J.R.; Gordon, R.A.; Bendell-Young, L.I.; Moore, M.M.; Crozier, E.D., The structure of the manganese oxide on the sheath of the

bacterium *Leptothrix discophora*: An XAFS study. *Am. Mineral.* **2004,** *89*, 1110–1118.

Katsoyiannis, I.A.; Zouboulis, A.I., Biological treatment of Mn(II) and Fe(II) containing groundwater: kinetic considerations and product characterization. *Water Res.* **2004,** *38*, 1922–1932.

Kay, J.T.; Conklin, M.H.; Fuller, C.C.; O'Day, P.A., Processes of Nickel and Cobalt Uptake by a Manganese Oxide Forming Sediment in Pinal Creek, Globe Mining District, Arizona. *Environ. Sci. Technol.* **2001,** *35*, 4719–4725.

Kedziorek, M.A.M.; Geoffriau, S.; Bourg, A.C.M., Organic Matter and Modeling Redox Reactions during River Bank Filtration in an Alluvial Aquifer of the Lot River, France. *Environ. Sci. Technol.* **2008,** *42*, 2793–2798.

Kedziorek, M.A.M.; Bourg, A.C.M., Electron trapping capacity of dissolved oxygen and nitrate to evaluate Mn and Fe reductive dissolution in alluvial aquifers during riverbank filtration. *J. Hydrol.* **2009,** *365*, 74–78.

Kennedy, C.; Smith, D.S.; Warren, L.A., Surface chemistry and relative Ni sorptive capacities of synthetic hydrous Mn oxyhydroxides under variable wetting and drying regimes. *Geochim. Cosmochim. Ac.* **2004,** *68*, 443–454.

Klump, S.; Cirpka, O.A.; Surbeck, H.; Kipfer, R., Experimental and numerical studies on excess-air formation in quasi-saturated porous media. *Water Resour. Res.* **2008,** *44*.

Kneebone, P.E.; O'Day, P.A.; Jones, N.; Hering, J.G., Deposition and fate of arsenic in iron- and arsenic-enriched reservoir sediments. *Environ. Sci. Technol.* **2002,** *36*, 381–386.

Kohfahl, C.; Massmann, G.; Pekdeger, A., Sources of oxygen flux in groundwater during induced bank filtration at a site in Berlin, Germany. *Hydrogeol. J.* **2009,** *17*, 571–578.

Konikow, L.F.; August, L.L.; Voss, C.I., Effects of clay dispersion on aquifer storage and recovery in coastal aquifers. *Transport Porous Med.* **2001,** *43*, 45–64.

Krom, M.D.; Davison, P.; Zhang, H.; Davison, W., High-Resolution Pore-Water Sampling with a Gel Sampler. *Limnol. Oceanogr.* **1994,** *39*, 1967–1972.

Kübeck, C.; Hansen, C.; Bergmann, A.; Kamphausen, S.; König, C.; van Berk, W., Model Based Raw Water Quality Management—Manganese Mobilization Induced by Bank Filtration. *Clean* **2009,** *37*, 945–954.

Lee, G.; Bigham, J.M.; Faure, G., Removal of trace metals by coprecipitation with Fe, Al and Mn from natural waters contaminated with acid mine drainage in the Ducktown Mining District, Tennessee. *Appl. Geochem.* **2002,** *17*, 569–581.

Lienert, C.; Short, S.A.; von Gunten, H.R., Uranium Infiltration from a River to Shallow Groundwater. *Geochim. Cosmochim. Ac.* **1994,** *58*, 5455–5463.

Lloyd, J.R., Microbial reduction of metals and radionuclides. *FEMS Microbiol. Rev.* **2003,** *27*, 411–425.

Lohman, S.W. *Ground-Water Hydraulics*; Professional Paper 708; U.S. Geological Survey: Washington D.C., 1972.

Lorenzen, G.; Sprenger, C.; Taute, T.; Pekdeger, A.; Mittal, A.; Massmann, G., Assessment of the potential for bank filtration in a water-stressed megacity (Delhi, India). *Environ. Earth Sci.* **2010,** *61*, 1419–1434.

Lovley, D.R., Dissimilatory Fe(III) and Mn(IV) reduction. *Microbiol. Mol. Biol. R.* **1991,** *55,* 259–287.

Luther, G.W., Manganese(II) Oxidation and Mn(IV) Reduction in the Environment—Two One-Electron Transfer Steps Versus a Single Two-Electron Step. *Geomicrobiol. J.* **2005,** *22,* 195–203.

Manning, B.A.; Fendorf, S.E.; Bostick, B.; Suarez, D.L., Arsenic(III) Oxidation and Arsenic(V) Adsorption Reactions on Synthetic Birnessite. *Environ. Sci. Technol.* **2002,** *36,* 976–981.

Marsili, E.; Baron, D.B.; Shikhare, I.D.; Coursolle, D.; Gralnick, J.A.; Bond, D.R., *Shewanella* secretes flavins that mediate extracellular electron transfer. *Proceedings of the National Academy of Sciences* **2008,** *105,* 3968–3973.

Martinez-Lavanchy, P.M.; Muller, C.; Nijenhuis, I.; Kappelmeyer, U.; Buffing, M.; McPherson, K.; Heipieper, H.J., High Stability and Fast Recovery of Expression of the TOL Plasmid-Carried Toluene Catabolism Genes of *Pseudomonas putida* mt-2 under Conditions of Oxygen Limitation and Oscillation. *Appl. Environ. Microbiol.* **2010,** *76,* 6715–6723.

Massmann, G.; Tichomirowa, M.; Merz, C.; Pekdeger, A., Sulfide oxidation and sulfate reduction in a shallow groundwater system (Oderbruch Aquifer, Germany). *J. Hydrol.* **2003,** *278,* 231–243.

Massmann, G.; Pekdeger, A.; Merz, C., Redox processes in the Oderbruch polder groundwater flow system in Germany. *Appl. Geochem.* **2004,** *19,* 863–886.

Massmann, G.; Greskowiak, J.; Dünnbier, U.; Zuehlke, S.; Knappe, A.; Pekdeger, A., The impact of variable temperatures on the redox conditions and the behaviour of pharmaceutical residues during artificial recharge. *J. Hydrol.* **2006,** *328*, 141–156.

Massmann, G.; Sültenfuß, J.; Dünnbier, U.; Knappe, A.; Taute, T.; Pekdeger, A., Investigation of groundwater residence times during bank filtration in Berlin: a multi-tracer approach. *Hydrol. Process.* **2007,** *22*, 788–801.

Massmann, G.; Dünnbier, U.; Heberer, T.; Taute, T., Behaviour and redox sensitivity of pharmaceutical residues during bank filtration—Investigation of residues of phenazone-type analgesics. *Chemosphere* **2008a,** *71*, 1476–1485.

Massmann, G.; Nogeitzig, A.; Taute, T.; Pekdeger, A., Seasonal and spatial distribution of redox zones during lake bank filtration in Berlin, Germany. *Environ. Geol.* **2008b,** *54*, 53–65.

Massmann, G.; Sültenfuß, J., Identification of processes affecting excess air formation during natural bank filtration and managed aquifer recharge. *J. Hydrol.* **2008,** *359*, 235–246.

Metge, D.W.; Harvey, R.W.; Aiken, G.R.; Anders, R.; Lincoln, G.; Jasperse, J., Influence of organic carbon loading, sediment associated metal oxide content and sediment grain size distributions upon Cryptosporidium parvum removal during riverbank filtration operations, Sonoma County, CA. *Water Res.* **2010,** *44*, 1126–1137.

Mettler, S.; Abdelmoula, M.; Hoehn, E.; Schoenenberger, R.; Weidler, P.; Gunten, U., Characterization of Iron and Manganese Precipitates from an *In Situ* Ground Water Treatment Plant. *Ground Water* **2001,** *39*, 921–930.

Mirecki, J.E.; Campbell, B.G.; Conlon, K.J.; Petkewich, M.D., Solute changes during aquifer storage recovery testing in a limestone clastic aquifer. *Ground Water* **1998,** *36*, 394–403.

Monbet, P.; McKelvie, I.D.; Worsfold, P.J., Combined Gel Probes for the *In Situ* Determination of Dissolved Reactive Phosphorus in Porewaters and Characterization of Sediment Reactivity. *Environ. Sci. Technol.* **2008,** *42,* 5112–5117.

Morel, F.M.M.; Hering, J.G., *Principles and Applications of Aquatic Chemistry*. Wiley-Interscience: New York, 1993.

Moreno, G.; Pariente, F.; Lorenzo, E., Electrocatalytic oxidation of ascorbate at glassy carbon electrodes modified with electrodeposited films derived from dihydroxybenzaldehyde isomers. *Anal. Chim. Acta* **2000,** *420*, 29–37.

Morgan, J.J.; Stumm, W., Colloid-chemical properties of manganese dioxide. *J. Colloid Sci.* **1964,** *19*, 347–359.

Morgan, J.J., Manganese in natural waters and earth's crust: its availability to organisms. In *Manganese and its role in biological processes*, Sigel, A.S., Ed. Marcel Dekker, Inc.: New York, 2000.

Morgan, J.J., Kinetics of reaction between O_2 and Mn(II) species in aqueous solutions. *Geochim. Cosmochim. Ac.* **2005,** *69*, 35–48.

Mouchet, P., From Conventional to Biological Removal of Iron and Manganese in France. *J. Am. Water Works As.* **1992,** *84*, 158–167.

Murray, J.W., Surface Chemistry of Hydrous Manganese-Dioxide. *J. Colloid Interf. Sci.* **1974,** *46*, 357–371.

Murray, J.W., The interaction of metal ions at the manganese dioxide-solution interface. *Geochim. Cosmochim. Ac.* **1975,** *39*, 505–519.

Murray, K.J.; Webb, S.M.; Bargar, J.R.; Tebo, B.M., Indirect Oxidation of Co(II) in the Presence of the Marine Mn(II)-Oxidizing Bacterium *Bacillus* sp. Strain SG-1. *Appl. Environ. Microbiol.* **2007,** *73*, 6905–6909.

Myers, C.R.; Nealson, K.H., Microbial reduction of manganese oxides: Interactions with iron and sulfur. *Geochim. Cosmochim. Acta* **1988a,** *52*, 2727–2732.

Myers, C.R.; Nealson, K.H., Bacterial Manganese Reduction and Growth with Manganese Oxide as the Sole Electron Acceptor. *Science* **1988b,** *240*, 1319–1321.

Nassef, H.M.; Radi, A.-E.; O'Sullivan, C., Simultaneous detection of ascorbate and uric acid using a selectively catalytic surface. *Anal. Chim. Acta* **2007,** *583*, 182–189.

Ng, G.-H.C.; McLaughlin, D.; Entekhabi, D.; Scanlon, B.R., Probabilistic analysis of the effects of climate change on groundwater recharge. *Water Resour. Res.* **2010,** *46*, W07502.

Ngiam, L.-S.; Lim, P.-E., Speciation patterns of heavy metals in tropical estuarine anoxic and oxidized sediments by different sequential extraction schemes. *Sci. Total Environ.* **2001,** *275*, 53–61.

Nielsen, L.P.; Risgaard-Petersen, N.; Fossing, H.; Christensen, P.B.; Sayama, M., Electric currents couple spatially separated biogeochemical processes in marine sediment. *Nature* **2010,** *463*, 1071–1074.

NRC, *Prospects for Managed Underground Storage of Recoverable Water*. National Academies Press: Washington D.C., 2008.

O'Loughlin, E.J., Effects of Electron Transfer Mediators on the Bioreduction of Lepidocrocite (γ-FeOOH) by *Shewanella putrefaciens* CN32. *Environ. Sci. Technol.* **2008,** *42*, 6876–6882.

Okazaki, M.; Sugita, T.; Shimizu, M.; Ohode, Y.; Iwamoto, K.; de Vrind-de Jong, E.W.; de Vrind, J.P.; Corstjens, P.L., Partial purification and characterization of manganese-oxidizing factors of *Pseudomonas fluorescens* GB-1. *Appl. Environ. Microbiol.* **1997,** *63*, 4793–4799.

Oren, O.; Gavrieli, I.; Burg, A.; Guttman, J.; Lazar, B., Manganese Mobilization and Enrichment during Soil Aquifer Treatment (SAT) of Effluents, the Dan Region Sewage Reclamation Project (Shafdan), Israel. *Environ. Sci. Technol.* **2007,** *41*, 766–772.

Parikh, S.J.; Chorover, J., FTIR Spectroscopic Study of Biogenic Mn-Oxide Formation by *Pseudomonas putida* GB-1. *Geomicrobiol. J.* **2005,** *22*, 207–218.

Parkhurst, D.L.; Petkewich, M.D. In *Geochemical Modeling of an Aquifer Storage Recovery Experiment, Charleston, South Carolina*, U.S. Geological Survey Artifical Recharge Workshop Proceedings, Sacramento, CA, April 2–4, 2002; Aiken, G.R.; Kuniansky, E.L., Eds. U.S. Geological Survey: 2002.

Patras, G.; Qiao, G.G.; Solomon, D.H., Novel cross-linked homogeneous polyacrylamide gels with improved separation properties: Investigation of the cross-linker functionality. *Electrophoresis* **2000,** *21*, 3843–3850.

Patterson, B.M.; Shackleton, M.; Furness, A.J.; Pearce, J.; Descourvieres, C.; Linge, K.L.; Busetti, F.; Spadek, T., Fate of nine recycled water trace organic contaminants

and metal(loid)s during managed aquifer recharge into a anaerobic aquifer: Column studies. *Water Res.* **2010,** *44*, 1471–1481.

Peltier, E.; Dahl, A.L.; Gaillard, J.-F., Metal Speciation in Anoxic Sediments: When Sulfides Can Be Construed as Oxides. *Environ. Sci. Technol.* **2005,** *39*, 311–316.

Petkewich, M.D.; Parkhurst, D.L.; Conlon, K.J.; Campbell, B.G.; Mirecki, J.E. *Hydrologic and Geochemical Evaluation of Aquifer Storage Recovery in the Santee Limestone/Black Mingo Aquifer, Charleston, South Carolina, 1998–2002.*; SIR 2004-5046; U.S. Geological Survey: Reston, VA, 2004.

Petrunic, B.M.; MacQuarrie, K.T.B.; Al, T.A., Reductive dissolution of Mn oxides in river-recharged aquifers: a laboratory column study. *J. Hydrol.* **2005,** *301*, 163–181.

Piao, S.; Ciais, P.; Huang, Y.; Shen, Z.; Peng, S.; Li, J.; Zhou, L.; Liu, H.; Ma, Y.; Ding, Y.; Friedlingstein, P.; Liu, C.; Tan, K.; Yu, Y.; Zhang, T.; Fang, J., The impacts of climate change on water resources and agriculture in China. *Nature* **2010,** *467*, 43–51.

Post, J.E., Manganese oxide minerals: Crystal structures and economic and environmental significance. *P. Natl. Acad. Sci. USA* **1999,** *96*, 3447–3454.

Postma, D.; Appelo, C.A.J., Reduction of Mn-oxides by ferrous iron in a flow system: Column experiment and reactive transport modeling. *Geochim. Cosmochim. Ac.* **2000,** *64*, 1237–1247.

Price, R.E.; Pichler, T., Abundance and mineralogical association of arsenic in the Suwannee Limestone (Florida): Implications for arsenic release during water-rock interaction. *Chem. Geol.* **2006,** *228*, 44–56.

Ravel, B.; Newville, M., ATHENA, ARTEMIS, HEPHAESTUS: data analysis for X-ray absorption spectroscopy using IFEFFIT. *J. Synchrotron Rad.* **2005,** *12*, 537–541.

Reichert, P., AQUASIM—a tool for simulation and data analysis of aquatic systems. *Water Sci. Technol.* **1994,** *30*, 21–30.

Rimstidt, J.D.; Balog, A.; Webb, J., Distribution of trace elements between carbonate minerals and aqueous solutions. *Geochim. Cosmochim. Ac.* **1998,** *62*, 1851–1863.

Rinck-Pfeiffer, S.; Ragusa, S.; Sztajnbok, P.; Vandevelde, T., Interrelationships between biological, chemical, and physical processes as an analog to clogging in aquifer storage and recovery (ASR) wells. *Water Res.* **2000,** *34*, 2110–2118.

Robbins, J.A.; Callender, E., Diagenesis of manganese in Lake Michigan sediments. *Am. J. Sci.* **1975,** *275*, 512–533.

Roberts, L.C.; Hug, S.J.; Dittmar, J.; Voegelin, A.; Kretzschmar, R.; Wehrli, B.; Cirpka, O.A.; Saha, G.C.; Ashraf Ali, M.; Badruzzaman, A.B.M., Arsenic release from paddy soils during monsoon flooding. *Nature Geosci.* **2010,** *3*, 53–59.

Rockström, J.; Falkenmark, M.; Karlberg, L.; Hoff, H.; Rost, S.; Gerten, D., Future water availability for global food production: The potential of green water for increasing resilience to global change. *Water Resour. Res.* **2009,** *45*, W00A12.

Ross, D.E.; Brantley, S.L.; Tien, M., Kinetic Characterization of OmcA and MtrC, Terminal Reductases Involved in Respiratory Electron Transfer for Dissimilatory Iron Reduction in *Shewanella oneidensis* MR-1. *Appl. Environ. Microbiol.* **2009,** *75*, 5218–5226.

Rüchel, R.; Brager, M.D., Scanning electron microscopic observations of polyacrylamide gels. *Anal. Biochem.* **1975,** *68*, 415–428.

Ruebush, S.S.; Icopini, G.A.; Brantley, S.L.; Tien, M., In vitro enzymatic reduction kinetics of mineral oxides by membrane fractions from *Shewanella oneidensis* MR-1. *Geochim. Cosmochim. Ac.* **2006,** *70*, 56–70.

Schauser, I.; Chorus, I.; Lewandowski, J., Effects of nitrate on phosphorus release: comparison of two Berlin lakes. *Acta Hydroch. Hydrob.* **2006,** *34*, 325–332.

Schauser, I.; Chorus, I., Assessment of internal and external lake restoration measures for two Berlin lakes. *Lake Reservoir Manage.* **2007,** *23*, 366–376.

Schauser, I.; Chorus, I., Water and phosphorus mass balance of Lake Tegel and Schlachtensee—A modelling approach. *Water Res.* **2009,** *43*, 1788–1800.

Schmidt, C.K.; Lange, F.T.; Brauch, H.-J.; Kühn, W. *Experiences with riverbank filtration and infiltration in Germany*; DVGW-Water Technology Center (TZW): Karlsruhe, Germany, 2003; 17 p.

Schubert, J., Hydraulic aspects of riverbank filtration--field studies. *J. Hydrol.* **2002,** *266*, 145–161.

Schwarzenbach, R.P.; Giger, W.; Hoehn, E.; Schneider, J.K., Behavior of organic compounds during infiltration of river water to groundwater. Field studies. *Environ. Sci. Technol.* **1983,** *17*, 472–479.

Senn, D.B.; Hemond, H.F., Nitrate Controls on Iron and Arsenic in an Urban Lake. *Science* **2002,** *296*, 2373–2376.

Shen, L.; Chen, Z., Critical review of the impact of tortuosity on diffusion. *Chem. Eng. Sci.* **2007,** *62*, 3748–3755.

Singh, P.; Kumar, P.; Mehrotra, I.; Grischek, T., Impact of riverbank filtration on treatment of polluted river water. *J. Environ. Manage.* **2010,** *91*, 1055–1062.

Sontheimer, H., Experience with riverbank filtration along the Rhine river. *J. Am. Water Works As.* **1980,** *72,* 386–390.

Sperazza, M.; Moore, J.N.; Hendrix, M.S., High-Resolution Particle Size Analysis of Naturally Occurring Very Fine-Grained Sediment Through Laser Diffractometry. *J. Sediment. Res.* **2004,** *74,* 736–743.

Spiteri, C.; Slomp, C.P.; Regnier, P.; Meile, C.; Van Cappellen, P., Modelling the geochemical fate and transport of wastewater-derived phosphorus in contrasting groundwater systems. *J. Contam. Hydrol.* **2007,** *92*, 85–106.

Sprenger, C.; Lorenzen, G.; Hülshoff, I.; Grützmacher, G.; Ronghang, M.; Pekdeger, A., Vulnerability of bank filtration systems to climate change. *Sci. Total Environ.* **2010,** *409,* 655–663.

Starostina, N.G.; Lusta, K.A.; Fikhte, B.A., Morphological and physiological changes in bacterial cells treated with acrylamide. *Eur. J. Appl. Microbiol.* **1983,** *18*, 264–270.

Stone, A.T.; Morgan, J.J., Reduction and Dissolution of Manganese(III) and Manganese(IV) Oxides by Organics .2. Survey of the Reactivity of Organics. *Environ. Sci. Technol.* **1984,** *18,* 617–624.

Stone, A.T.; Morgan, J.J., Reductive Dissolution of Metal Oxides. In *Aquatic Surface Chemistry: Chemical processes at the particle-water interface*, Stumm, W., Ed. Wiley-Interscience: New York, 1987; 221–254.

Stuyfzand, P.J.; Juhàsz-Holterman, M.H.A.; Lange, W.J., Riverbank Filtration in the Netherlands: Well Fields, Clogging and Geochemical Reactions. In *Riverbank*

Filtration Hydrology, Hubbs, S.A., Ed. Springer Netherlands: 2006; Vol. 60, 119–153.

Sunda, W.G.; Huntsman, S.A.; Harvey, G.R., Photoreduction of manganese oxides in seawater and its geochemical and biological implications. *Nature* **1983,** *301*, 234–236.

Sundby, B.; Silverberg, N., Manganese Fluxes in the Benthic Boundary Layer. *Limnol. Oceanogr.* **1985,** *30*, 372–381.

Tebo, B.M.; Bargar, J.R.; Clement, B.G.; Dick, G.J.; Murray, K.J.; Parker, D.; Verity, R.; Webb, S.M., Biogenic Manganese Oxides: Properties and Mechanisms of Formation. *Annu. Rev. Earth Pl. Sc.* **2004,** *32*, 287–328.

Tessier, A.; Campbell, P.G.C.; Bisson, M., Sequential extraction procedure for the speciation of particulate trace metals. *Anal. Chem.* **1979,** *51*, 844–851.

Thomas, N.E.; Kan, K.T.; Bray, D.I.; MacQuarrie, K.T.B., Temporal Changes in Manganese Concentrations in Water from the Fredericton Aquifer, New Brunswick. *Ground Water* **1994,** *32*, 650–656.

Toner, B.; Sposito, G., Reductive dissolution of biogenic manganese oxides in the presence of a hydrated biofilm. *Geomicrobiol. J.* **2005,** *22*, 171–180.

Toride, N.; Leij, F.J.; van Genuchten, M. *The CXTFIT code for estimating transport parameters from laboratory or field tracer experiments—Version 2.0*; U.S. Salinity Laboratory Report No. 137; Riverside, CA, 1995.

Toze, S.; Bekele, E.; Page, D.; Sidhu, J.; Shackleton, M., Use of static Quantitative Microbial Risk Assessment to determine pathogen risks in an unconfined

carbonate aquifer used for Managed Aquifer Recharge. *Water Res.* **2010,** *44*, 1038–1049.

Tufenkji, N.; Ryan, J.N.; Elimelech, M., The promise of bank filtration. *Environ. Sci. Technol.* **2002,** *36*, 422A–428A.

van Beek, C., Restoring Well Yield in the Netherlands. *J. Am. Water Works As.* **1984,** *76*, 66–72.

van Beek, C., Experiences with underground water treatment in the Netherlands. *Water Supply* **1985,** *3, Berlin "B"*, 1–11.

van Beek, C.; Breedveld, R.; Stuyfzand, P., Preventing two types of well clogging. *J. Am. Water Works As.* **2009,** *101*, 125–134.

van Breukelen, B.M.; Appelo, C.A.J.; Olsthoorn, T.N., Hydrogeochemical transport modeling of 24 years of Rhine water infiltration in the dunes of the Amsterdam Water Supply. *J. Hydrol.* **1998,** *209*, 281–296.

van Halem, D.; de Vet, W.; Verberk, J.; Amy, G.; vanDijk, H., Characterization of accumulated precipitates during subsurface iron removal. *Appl. Geochem.* **2011,** *26*, 116–124.

Villalobos, M.; Toner, B.; Bargar, J.; Sposito, G., Characterization of the manganese oxide produced by *Pseudomonas putida* strain MnB1. *Geochim. Cosmochim. Ac.* **2003,** *67*, 2649–2662.

Villinski, J.E.; O'Day, P.A.; Corley, T.L.; Conklin, M.H., *In Situ* Spectroscopic and Solution Analyses of the Reductive Dissolution of MnO2 by Fe(II). *Environ. Sci. Technol.* **2001,** *35*, 1157–1163.

Villinski, J.E.; Saiers, J.E.; Conklin, M.H., The Effects of Reaction-Product Formation on the Reductive Dissolution of MnO_2 by Fe(II). *Environ. Sci. Technol.* **2003,** *37,* 5589–5596.

von Canstein, H.; Ogawa, J.; Shimizu, S.; Lloyd, J.R., Secretion of Flavins by *Shewanella* Species and Their Role in Extracellular Electron Transfer. *Appl. Environ. Microbiol.* **2008,** *74*, 615–623.

von Gunten, H.R.; Kull, T.P., Infiltration of Inorganic-Compounds from the Glatt River, Switzerland, into a Groundwater Aquifer. *Water Air Soil Poll.* **1986,** *29*, 333–346.

von Gunten, H.R.; Karametaxas, G.; Krahenbuhl, U.; Kuslys, M.; Giovanoli, R.; Hoehn, E.; Keil, R., Seasonal Biogeochemical Cycles in Riverborne Groundwater. *Geochim. Cosmochim. Ac.* **1991,** *55*, 3597–3609.

von Gunten, H.R.; Karametaxas, G.; Keil, R., Chemical Processes in Infiltrated Riverbed Sediments. *Environ. Sci. Technol.* **1994,** *28*, 2087–2093.

von Gunten, U.; Zobrist, J., Biogeochemical Changes in Groundwater-Infiltration Systems - Column Studies. *Geochim. Cosmochim. Acta* **1993,** *57*, 3895–3906.

Vorosmarty, C.J.; McIntyre, P.B.; Gessner, M.O.; Dudgeon, D.; Prusevich, A.; Green, P.; Glidden, S.; Bunn, S.E.; Sullivan, C.A.; Liermann, C.R.; Davies, P.M., Global threats to human water security and river biodiversity. *Nature* **2010,** *467*, 555–561.

Wada, Y.; van Beek, L.P.H.; van Kempen, C.M.; Reckman, J.W.T.M.; Vasak, S.; Bierkens, M.F.P., Global depletion of groundwater resources. *Geophys. Res. Lett.* **2010,** *37*, L20402.

Waite, T.D.; Wrigley, I.C.; Szymczak, R., Photoassisted dissolution of a colloidal manganese oxide in the presence of fulvic acid. *Environ. Sci. Technol.* **1988,** *22,* 778–785.

Wallis, I.; Prommer, H.; Simmons, C.T.; Post, V.; Stuyfzand, P.J., Evaluation of Conceptual and Numerical Models for Arsenic Mobilization and Attenuation during Managed Aquifer Recharge. *Environ. Sci. Technol.* **2010,** *44,* 5035–5041.

Wang, Y.; Stone, A.T., Reaction of $Mn^{III,IV}$ (hydr)oxides with oxalic acid, glyoxylic acid, phosphonoformic acid, and structurally-related organic compounds. *Geochim. Cosmochim. Ac.* **2006a,** *70,* 4477–4490.

Wang, Y.; Stone, A.T., The citric acid-$Mn^{III,IV}O_2$(birnessite) reaction. Electron transfer, complex formation, and autocatalytic feedback. *Geochim. Cosmochim. Ac.* **2006b,** *70,* 4463–4476.

Warden, B.T.; Reisenauer, H.M., Fractionation of Soil Manganese Forms Important to Plant Availability. *Soil Sci. Soc. Am. J.* **1991,** *55,* 345–349.

Webb, S.M.; Tebo, B.M.; Bargar, J.R., Structural characterization of biogenic Mn oxides produced in seawater by the marine *Bacillus* sp. strain SG-1. *Am. Mineral.* **2005,** *90,* 1342–1357.

Wehrli, B.; Stumm, W., Vanadyl in natural waters: Adsorption and hydrolysis promote oxygenation. *Geochim. Cosmochim. Ac.* **1989,** *53,* 69–77.

Wellsbury, P.; Herbert, R.A.; Parkes, R.J., Bacterial activity and production in near-surface estuarine and freshwater sediments. *FEMS Microbiol. Ecol.* **1996,** *19,* 203–214.

Wiese, B.; Nützmann, G., Transient Leakance and Infiltration Characteristics during Lake Bank Filtration. *Ground Water* **2009,** *47*, 57–68.

Wildman, R.A. Biogeochemical Implications of Changing Groundwater and Surface Water Hydrology at Lake Powell, Utah and Arizona, and the Merced River, California, USA. Ph.D. Thesis, California Institute of Technology, Pasadena, CA, 2009.

Williams, M.D.; Oostrom, M., Oxygenation of anoxic water in a fluctuating water table system: an experimental and numerical study. *J. Hydrol.* **2000,** *230*, 70–85.

Xyla, A.G.; Sulzberger, B.; Luther, G.W.; Hering, J.G.; Van Cappellen, P.; Stumm, W., Reductive dissolution of manganese(III, IV) (hydr)oxides by oxalate: the effect of pH and light. *Langmuir* **1992,** *8*, 95–103.

Yezek, L.P.; van Leeuwen, H.P., Donnan Effects in the Steady-State Diffusion of Metal Ions through Charged Thin Films. *Langmuir* **2005,** *21*, 10342–10347.

Yuan-Hui, L.; Gregory, S., Diffusion of ions in sea water and in deep-sea sediments. *Geochim. Cosmochim. Ac.* **1974,** *38*, 703–714.

Zhang, J.; Lion, L.W.; Nelson, Y.M.; Shuler, M.L.; Ghiorse, W.C., Kinetics of Mn(II) oxidation by *Leptothrix discophora* SS1. *Geochim. Cosmochim. Ac.* **2002,** *66*, 773–781.

Ziegler, D.H. Untersuchungen zur nachhaltigen Wirkung der Uferfiltration im Wasserkreislauf Berlins. Dr.-Ing. Thesis, Technical University of Berlin, Berlin, Germany, 2001.